UVSOR-13
February 1986

UVSOR
ACTIVITY REPORT
1984/85

Ultraviolet Synchrotron Orbital Radiation Facility
Institute for Molecular Science

CONTENTS

4.Research Activities

PREFACE

It was in 1975 that researchers of molecular science first proposed UVSOR (synchrotron orbital radiation) project. It is my great pleasure to report to you that the UVSOR Facility is now operational. Regular operation has been made since April 1985. The maximum current of the light source so far attained is 330 mA and the lifetime at 100 mA is two hours. The increase of electron energy from 600 MeV to 750 MeV was successfully done. The understanding of beam behavior, such as ion trapping effect has progressed. Single bunch operations were performed several times for time-resolved spectroscopy. Ten measurement systems have been opened to users and 49 research programs are accepted in this fiscal year of 1985. The research fields of the users extend from molecular science to the related fields, such as radiometry, lithograpy, topography and so on. From this year on, we publish annual Activity Report, which includes the status of UVSOR Facility, the development of the light source and measurement systems, and research activities. I would like to express my sincere thanks to the staffs of ISSP and INS, University of Tokyo, and Photon Factory for their kind support. I also appreciate the efforts of the members of the UVSOR Facility, who have participated in the construction, operation, maintenance and development of the light source and measurement systems. Finally I hope that many in-house staff of IMS as well as the researchers outside of IMS will make full use of UVSOR.

February, 1985

Hiroo INOKUCHI

Director,
UVSOR Facility

OVERVIEW

OVERVIEW OF THE UVSOR FACILITY

T. Kasuga and M. Watanabe
UVSOR Facility, Institute for Molecular Science,
Myodaiji, Okazaki 444, Japan

1. General Description

Institute for Molecular Science (IMS) is inter-university research institute, established in 1975. It has six departments and six research facilities working organically. Departments are Departments of Theoretical Studies, Molecular Structure, Electronic Structure, Molecular Assemblies and Applied Molecular Science, and Coordination Chemistry Laboratories. Research Facilities are Computer Center, Low-Temperature Center, Instrument Center, Chemical Materials Center, Equipment Development Center and Ultraviolet Synchrotron Orbital Radiation (UVSOR) Facility. In IMS, there are 85 scientific staffs including 16 guest staffs, 42 technical staffs and administrative staffs. Lodging facilities for visitors are provided.

The UVSOR is a dedicated VUV source for molecular science and related fields. It is a 600 MeV (max. 750 MeV) electron storage ring, of which injector is a 600 MeV synchrotron with a 15 MeV linac.[1-3] They are located underground for radiation safety as shown in Fig.1. Synchrotron radiation from ordinary bending sections is mainly utilized. Three insertion devices can be installed. The UVSOR Facility had been proposed since 1975. The construction started in 1980 with fabrication of measurement systems. In 1981, the construction of the light source started and its commissioning was succeeded on the 10th November, 1983. The number of beam lines at the first stage is 14,[4] but eventually more than 20 beam lines can be attached to the ring. Experiments have been made since September, 1984. The total cost of the light source and the measurement systems is about 2.2×10^9 yen, the cost of building is 1.7×10^9 yen and the annual running cost is about 4×10^8 yen. These values do not include salaries of IMS staffs.

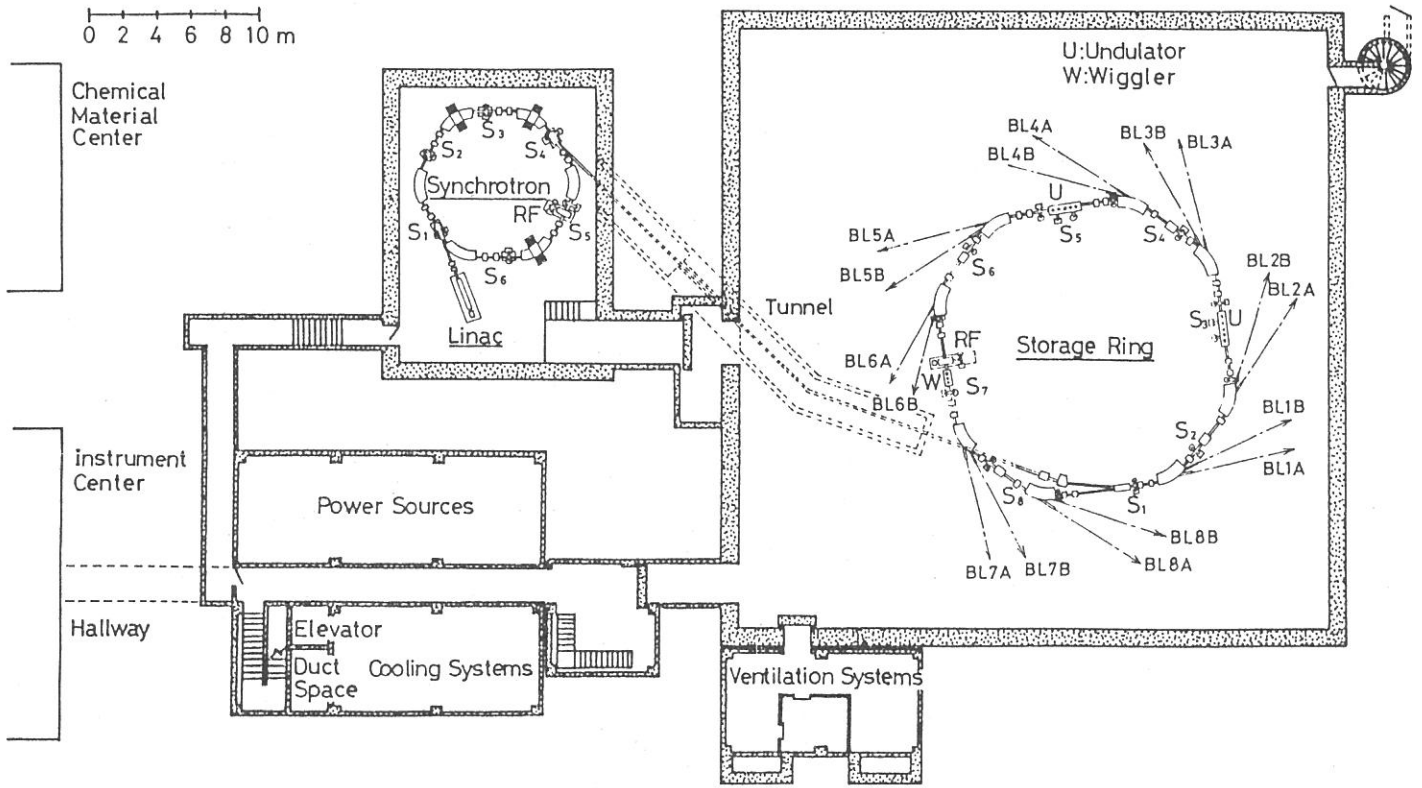

Fig. 1 Plane view of the basement of the UVSOR Facility.

Staffs of the UVSOR Facility are a director (Prof. H. Inokuchi), two associate professors, two research associates, six technical staffs and an adjunct associate professor. Associate Professors T. Kasuga and M. Watanabe are responsible for the light source and measurement systems, respectively. Staffs of Department of Molecular Assemblies are main users in IMS as well as the promoters of the UVSOR project. The UVSOR Facility is responsible for the operation of the light source and beam lines for users outside IMS.

Proposals can be applied twice per year, which are judged by a steering committee. Items of proposals are Joint Studies, Cooperative Research and Use of Facility. In 1984, 4 proposals of Use of Facility were approved. In 1985, for the first item, 3 proposals are approved, for the second, 14 proposals and for the third, 32 proposals. Experimentalists should be registered as radiation worker. Monday is a day for machine study and days from Tuesday to Friday are for users. Users' time is 9:30-13:00 and 13:30-18:00. The injection is twice per day. 37 weeks will be delivered to users in this fiscal year. During the injection, experimentalists should keep out from the storage ring room. (Shield blocks against the radiation due to the decay of stored current are put around the ring.) Users' meeting is usually held once per year and activity report will be published.

2. Light Source

2.1 Overview

Plane view of the light source is shown in Fig.1 and design parameters are given in Table 1. The booster synchrotron consists of 6 bending magnets, 6 doublets of quadrupoles and 6 long straight sections. These magnets are lamination type (thickness of lamination is 0.35 mm). The waveform of power supplies for the magnets is trianglar whose repetition time is 380 ms. Electron beam from the 15 MeV linac is injected by means of an electro-static septum (inflector) and 3 bump magnets (perturbator). The beam is accelerated by a usual re-entrant type RF cavity, which is excited by a 5 kW power amplifier. Accelerated beam is extracted by means of a fast kicker and a septum magnet (deflector).

Table 1 Parameters of UVSOR

	Designed		Achieved	
Linac				
Energy	15	MeV	15	MeV
Frequency	2.856	GHz		
Synchrotron				
Energy	600	MeV	600	MeV
Current	50	mA	15	mA
Circumference	26.6	m		
Periodicity	6			
Bending Radius	1.8	m		
Tune (Q_H, Q_V)	(2.25, 1.25)			
Harmonic Number	8			
Radio Frequency	90.1	MHz		
Repetition Rate	1-3	Hz	2.5	Hz
Storage Ring				
Energy	600	MeV	750	MeV
	(max. 750	MeV)		
Critical Wavelength	56.9	Å		
Current	500	mA	330	mA
Lifetime	1	hr	2	hr
	(500	mA)	(100	mA)
Circumference	53.2	m		
Periodicity	4			
Bending Radius	2.2	m		
Bending Field	0.91	T		
Tune (Q_H, Q_V)	(3.25, 2.75)			
Harmonic Number	16			
Radio Frequency	90.1	MHz		
RF Voltage	75	kV		
Radiation Damping Time				
Horizontal	45.4	ms		
Vertical	40.9	ms		
Longitudinal	19.5	ms		
Emittance				
Horizontal	$8\pi \times 10^{-8}$	m rad	$16\pi \times 10^{-8}$	m rad
Vertical	$8\pi \times 10^{-9}$	m rad*		
Beam Size (at the Center of Bending Section)				
Horizontal ($2\sigma_H$)	0.64	mm		
Vertical ($2\sigma_V$)	0.46	mm*		
Bunch Length (2σ)	0.17	ns		

*10% coupling is assumed.

The storage ring is composd of eight bending magnets, and four long and four short straight sections as shown in Fig.2. The beam is injected into the storage ring by means of a septum magnet (inflector) and 3 bump magnets (perturbator). The vacuum systems of the beam transport line and the storage ring are separated by a thin polyimide film (thickness of 50 μm) at the exit of the inflector. An RF cavity of the ring is excited by a 20 kW power amplifier. The RF power amplifier of the synchrotron and that of the storage ring are driven by the same master oscillator, therefore the synchronized transfer of the bunched beam is quite easy.

Button type position monitors are set around the ring to measure closed orbit distortions. The orbit distortions are corrected by trim coils wound on bending magnets and vertical steering magnets. An electrode for an RF knockout system to measure tunes of both horizontal and vertical directions is situated in a short straight section. The electrode is excited by a wideband power amplifier (0.3 - 35 MHz, 300 W). Another RF knockout electrode and 21 DC electrodes for ion-clearing are installed.

The beam current can be measured by a DC current transformer. It is monitored every one minute by a micro-computer and the e-folding lifetime is calculated. The profile of the beam is observed using a television camera, and beam size is estimated from the video signal from the camera.

Two outlets of synchrotron radiation are available for each bending section. A permanent magnet undulator and a super-conducting wiggler are installed at S_3 and S_7 long straight sections, respectively. [5] Fig. 3 shows the intensity distribution from ordinary bending sections and the superconducting wiggler. Fig. 4 shows that from the undulator. (Units of intensity in these figures are different.)

2.2 Construction and Commissioning

The construction of the light source was started in 1981. The magnet system, the RF system and the vacuum system of the booster synchrotron and the pre-injector linac were completed in March 1982. These components were installed in the building for the synchrotron and aligned precisely by the autumn. The

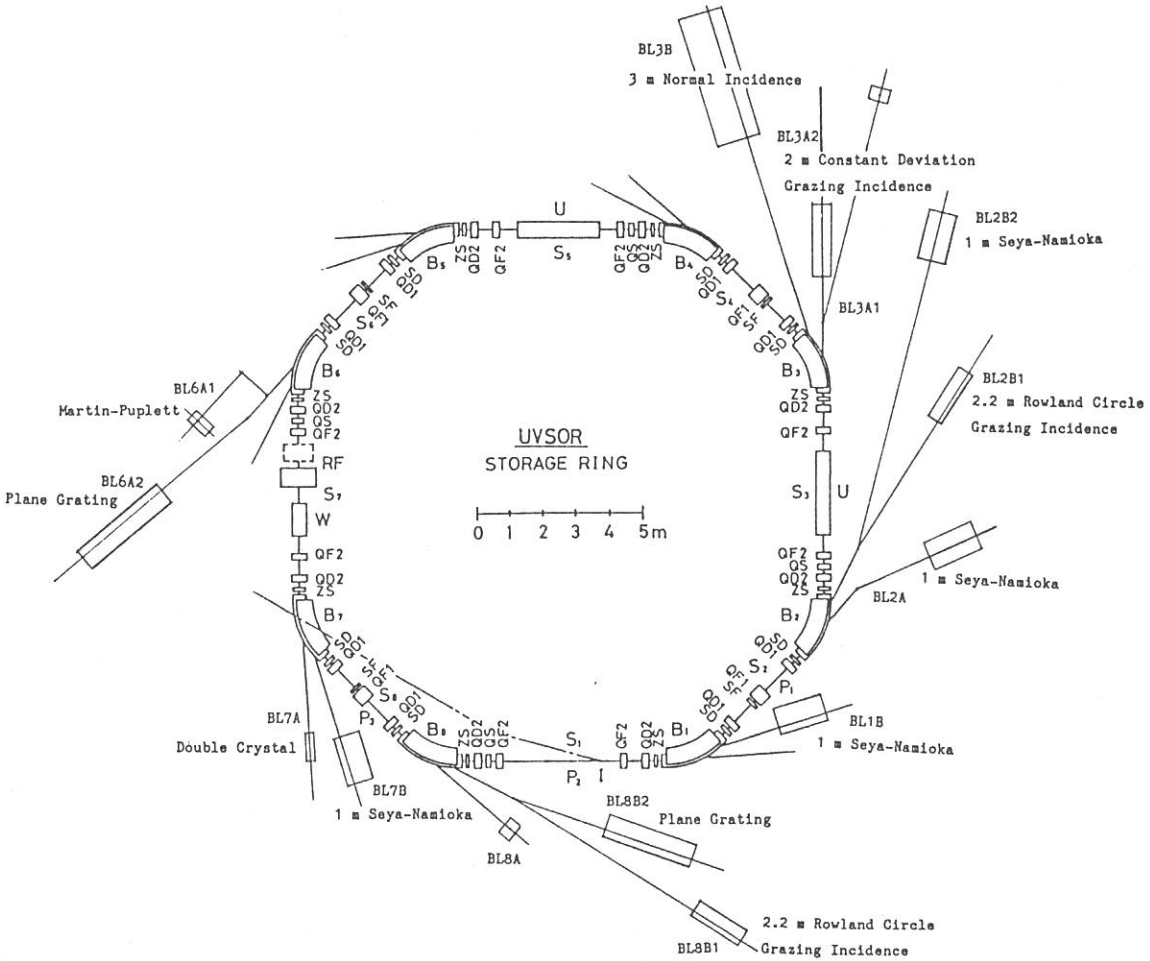

Fig. 2 Plane view of the UVSOR storage ring.

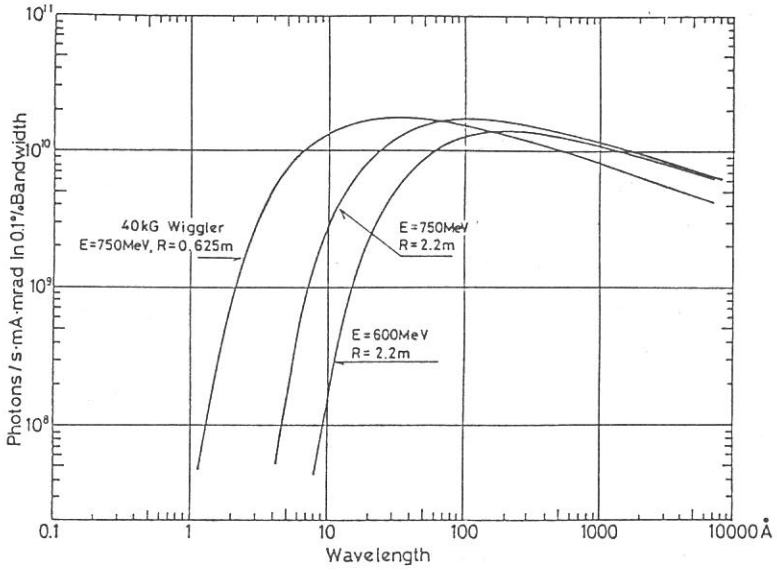

Fig. 3 Intensity distribution of the radiation from ordinary bending sections and the superconducting wiggler.

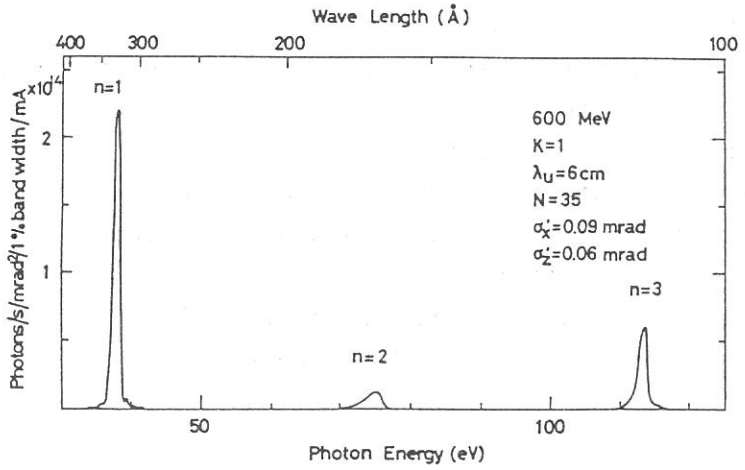

Fig. 4 Intensity distribution of the radiation from the undulator at the S_3 straight section (courtesy H. Kitamura).

test of the linac was successfully done at the end of 1982. As the pulse power supplies for synchrotron magnets were not finished at that time, small DC power supplies were connected to the magnets to test the injection scheme of the synchrotron. It was a serious problem encountered in the test that the injected beam was lost in several turns after injection. The cause of this problem was the mismatch between the vertical closed orbit and the vertical aperture of a beam monitor in front of the inflector, and it was solved by widening the beam monitor. The pulse power supplies for the magnets were finished in July 1983. The injected beam was accelerated without any difficulty. A fast kicker and a septum magnet for the beam extraction were installed in September 1983. After the installation of the fast kicker, the injection of the electron beam into the synchrotron became impossible. This problem was caused by remanent field of the kicker, and DC bias current is superposed upon the high voltage pulse to solve the problem. In succession, the beam extraction from the synchrotron and the transport of the extracted beam were tried.

Almost all components of the storage ring were delivered in March 1983, and basic parameters of these components were measured and installed in the ring by August. The injection of the electron beam into the storage ring was begun on the 10th of November, and the first electron beam was stored on that evening. Since then, efforts were devoted to measurements of important parameters of the ring, search for the optimum operating point, and studies of the behavior of the stored beam.

2.3 Performance and Beam Characteristics

The design parameters with achieved ones are tabulated in Table 1. The design energy of the synchrotron is easily achieved. Though the final beam current of the synchrotron is 1/3 of the designed value, time required to accumulate the electron beam in the storage ring is short enough. It takes only several minutes to accumulate the beam current of 100mA. The maximum stored current of the storage ring up to now is 330 mA, and at this current, a window glass for an optical beam monitor cracked. An attempt to increase the maximum stored

current was not made after that time. The e-folding lifetime of the beam at 100 mA is about 2 hrs. This figure is very close to the lifetime estimated considering the Touschek effect and the effect of the vacuum pressure (3×10^{-9} Torr at 100 mA). The beam size is estimated from the video signal from the television camera used to monitor the beam profile, and the emittance is estimated from the measured beam size and the beta functions at the radiant point. The measured emittance is twice the designed value. This disagreement must be due to inaccuracy in estimating the beam size. Injected beam (600 MeV) can be accelerated up to 750 MeV without appreciable beam loss.

Single bunch operation of the storage ring was tried successfully.[6] The maximum beam current in a single bunch up to now is 25 mA, and a ratio of number of electrons in an adjacent bucket to that in the aimed bucket is about 0.1 %. The first experiment using the single bunch mode was done in September 1985.

Since the first beam was stored, efforts have been devoted to improving the performance of the ring. Some inconvenient phenomena have been found during the accelerator studies. One of the most serious problems was the growth of the vertical size of the electron beam.[7] This phenomenon is explained by the ion-trapping effect. DC clearing electrodes and an RF knockout electrode were installed to clear ions. These two ion-clearing techniques are used together to improve the beam size. The improvement of the beam profile is shown in Fig.5. Fig. 5 (a) and (b) are pictures of the beam profile without and

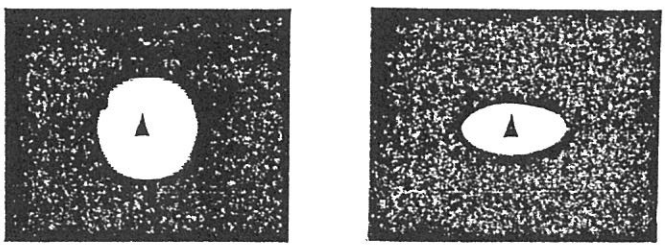

a) b)

Fig. 5 Improvement of Profile (a) Ion-Cleaning OFF, b) Ion-Cleaning ON)

with the ion clearing by these two methods, respectively. The second problem is the longitudinal coupled-bunch instability induced by the parasitic resonances of the RF cavity. We have no way except the temperature control of the cavity to avoid the parasitic resonances for the present.

2.4 Undulator and Wiggler

An undulator with 35 periods and a superconducting wiggler were installed in the storage ring in March 1984. The undulator is planer type and the gap is movable between 27 and 80 mm. One period in 35 periods is composed of 8 blocks of permanent magnets made of $SmCo_5$ and the length of the period is 60 mm. The maximum magnetic field of the undulator is 0.3 T at the minimum gap. Though the horizontal closed orbit was deformed slightly (max. 3 mm at 32 mm gap), appreciable tune shifts were not observed and the lifetime of the beam was not affected.

A horizontal orbit bump is formed by the wiggler, which is composed of 3 sets of superconducting coils. The inner and outer size of the middle coil (main coil) are 30 mm W x 110 mm L x 55.8 mm H and 118.4 mm W x 198.4 mm L x 55.8 mm H. Those of the outer coils (auxiliary coils) are 30 mm W x 136 mm L x 40.8 mm H and 97.4 mm W x 203.4 mm L x 40.8 mm H. The space between the center of the upper coil and that of the lower coil is 140 mm. The maximum field produced by the main coils is 4 T. The tune shifts and the vertical closed orbit distortion due to the excitation of the wiggler is not negligible. A quadrupole magnet and a vertical steering magnet were installed near the wiggler to correct the influence of the wiggler.

3. Measurement Systems

3.1 Beam Lines

Schematic diagram of the beam line is shown in Fig. 6. Horizontal acceptance angle of the front end is 80 mrad. It is composed of a manual valve (V_0), a beam shutter, a pneumatic valve (V_1) and a fast closing valve (V_F). After the front end, a pre-mirror chamber, beam pipes and a pneumatic valve (V_2)are connected. V_0, V_1 and V_2 use viton O-rings, while V_F is an all metal valve. Closing time of V_F is 10 ms and leak rate is 1 Torr l/s. When accidental leakage occurs, the combination of V_F and V_1 can prevent the leakage so that the pressure deterioration at the outlet of synchrotron radiation is below 1 x 10^{-3} Torr. In July 1985, an accidental leakage occurred from a sample chamber at BL7B. At that time the beam current decreased by amount of 10 mA, but the lifetime soon recovered.

Between a pre-mirror chamber and a monochromator, an acoustic delay line is inserted. The acoustic delay line can delay propagation time of the front of leakage by 10 ms. However in our case, even if the fast closing valve shuts before the front arrives, the leak from the fast closing valve is dominant on the vacuum deterioration of the ring. If the effect of leakage should be neglected, it is recommended that one should use

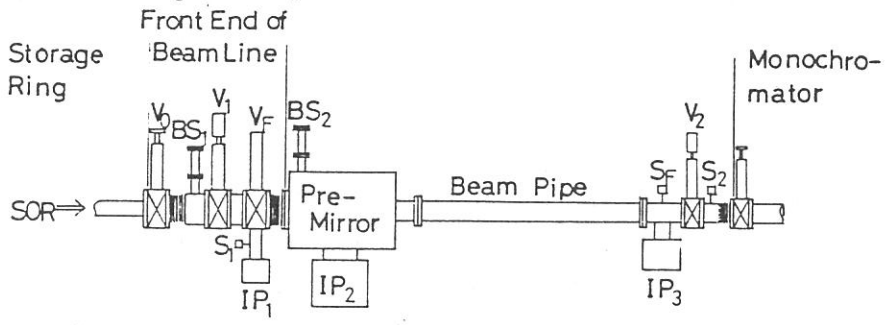

Fig. 6 Schematic diagram of beam line. V_0: manual valve. V_1 and V_2: pneumatic valves. V_F: fast closing valve. BS_1 and BS_2: beam shutters. S_1, S_2 and S_F: vacuum gauges which control V_1, V_2 and V_F, respectively. IP_1 - IP_3: sputter ion pumps.

combination of a fast closing valve with a negligibly small leak rate and the acoustic deley line.

The first pre-mirrors are made of quartz and their surfaces are coated with platinum or gold. At present, they are not cooled.

3.2 Experimental Equipments

Monochromators listed in Table 2 are located as shown in Fig. 2 . They cover wavelength region from far infrared to soft X-ray. The beam lines and monochromators of BL2A, BL2B2, BL3B and BL8B2 are mainly used by staffs of Department of Molecular Assemblies in IMS. The others are for users outside IMS. The UVSOR Facility is responsible for the maintainance of these lines. A monochromator of BL7B was made by Equipment Development Center, equipped with time resolving instrument made by Instrument Center. BL6A2 and BL7A were made in cooperation with adjunct associate professors of UVSOR. BL1B, BL2B1, BL3A1, BL3A2, BL6A1 and BL8B1 were made or are under construction in cooperation with visiting scientists. BL8A is opened to users who bring their own optical instruments and to those who make irradiation experiments, such as lithography. A double crystal monochromator (BL7A) usually used at the ordinary bending section, can be used in combination with the wiggler radiation a few or several weeks per year. BL3A2 and BL3A1 are undulator radiation ports with and without a monochromator, respectively. The use of oil diffusion pumps is allowed only in the case of evacuating molecular beam sources. Standard DC detecting systems and counting systems are provided. Micro-computors are used individually. The date buses are both IEEE-488 and CAMAC.

4. Building

The UVSOR building is a four-storied building, whose whole area is 2750 m^2. It has rooms to accomodate the storage ring, the synchrotron, power supplies, chillers, heat exchangers, air conditioners and the control system. It has also small rooms such as an electronics shop, a machine shop, a dark room, a computer room and offices. Both the synchrotron and the storage ring rooms have x-y cranes. As the synchrotron room inclined when the storage ring room was completed, the magnet system of the synchrotron had to be aligned precisely again. Each beam line has its own pit for cabling and piping cooling water, compressed air and helium gas. The amount of toxic gas as for the sample is limited and it should be handled in drafts. Ordinary and emergency ventilation systems are provided.

Table 2 Monochromators at UVSOR

Beam Line	Monochromator, Spectrometer	Wavelength Region	Acceptance Angle(mrad) Horiz.	Vert.	Experiment
BL1B*	1 m Seya-Namioka	6500-300 Å	60	6	Gas & Solid
BL2A	1 m Seya-Namioka	4000-300 Å	40	6	Gas
BL2B1*	2.2 m Rowland Circle Grazing Incidence	440-20 Å	10	2	Gas
BL2B2	1 m Seya-Namioka	2000-300 Å	20	6	Gas
BL3A1	None (Filter, Mirror)		(U) 0.3	0.3	Gas & Solid
BL3A2*	2 m Constant Deviation Grazing Incidence	1000-100 Å	10	4	Gas & Solid
			(U) 0.3	0.3	
BL3B	3 m Normal Incidence	4000-300 Å	20	6	Gas
BL6A1	Martin-Puplett	5 mm-50μ m	80	60	Solid
BL6A2	Plane Grating	6500-80 Å	10	6	Solid
BL7A	Double Crystal	15-8 Å	2	0.3	Solid
		15-2 Å	(W) 1	0.15	
BL7B	1 m Seya-Namioka	6500-300 Å	40	8	Solid
BL8A	None		25	8	Irradiation, User's Instrum.
BL8B1*	2.2 m Rowland Circle Grazing Incidence	440-20 Å	10	2	Solid
BL8B2	Plane Grating	6500-80 Å	10	6	Solid

* : under construction. U : with an undulator. W : with a wiggler.

5. Future Plan

A second undulator will be installed in spring of 1986. Some fundamental experiments of FEL using the undulator will be done. We will start to make a plan of the second stage of the measurement systems, using six unused outlets of synchrotron radiation.

Acknowledgements

We are heavily indebted to all of the scientists who supported our UVSOR project, especially to the staffs of the Institute for Solid State Physics and the Institute for Nuclear Study, the University of Tokyo, and to the staff of Photon Factory, KEK in giving us a lot of useful information and helpful suggestions concerning both the light source and measurement systems.

References

1) M. Watanabe et al., IEEE Trans. Nucl. Sci. NS-28 (1981) 3175.
2) I. Koyano et al., Nucl. Instr. Meth. 195 (1982) 273.
3) T. Kasuga et al., IEEE Trans. Nucl. Sci. NS-32 (1985) 3409.
4) M. Watanabe, Nucl. Instr. Meth. to be published.
5) H. Yonehara et al., IEEE Trans. Nucl. Sci. NS-32 (1985) 3412.
6) T. Kasuga et al., Proc. 5th Symp. Accelerator Sci. & Tech. (Ionics, Tokyo,1984) p.295.
7) T. Kasuga et al., Jpn. J. Appl. Phys. 24 (1985) 1212.

LIGHT SOURCE

VACUUM SYSTEM OF UVSOR STORAGE RING

Masami HASUMOTO, Toshio KASUGA, Toshio KINOSHITA
and Hiroto YONEHARA

Institute for Molecular Science Myodaiji, Okazaki 444

After all beam ducts were connected, leak test by a helium leak detector was finished for the whole ring on April 12 and there was nothing wrong. We baked the vacuum system of the whole ring for seventy two hours from April 15. On April 19, cooling water leaked into the vacuum system from one of two tuners of the rf cavity. We took out the tuner from the cavity and evacuated the ring. We found small leak from a welding part of ceramics and stainless steel pipe at a DCCT chamber and fixed it by "VAC seal". After the repair we could not detect leak from it. Average vacuum pressure was 1.3×10^{-8} Torr in the morning on April 23 and we began to store the electron beam and the maximum stored current was 50 mA on the day. Average vacuum pressure at the beam current of 30 mA was 3.9×10^{-8} Torr and the beam lifetime was only 7.4 minutes. The maximum stored current was 150 mA on the second day, 190 mA on the third day and 250 mA on the fourth day. Before injection, average vacuum pressure was 3.4×10^{-9} Torr on May 7. When stored beam current was 30 mA, average vacuum pressure was 4.7×10^{-9} Torr and the beam lifetime was 68 minutes. After about 30 minutes from start of injection, a glass of view port on a 70 mm flange was cracked and air leaked when stored bream current became 330 mA.

We exchanged the view port and evacuated the ring again on that day. On May 8, average vacuum pressure was 2.7×10^{-8} Torr before injection and 4.4×10^{-8} Torr at the stored current of 30 mA and the lifetime was 6.9 minutes. We decided that beam current kept below 150 mA. For seven days after the vacuum accident, the beam current of 150 mA was kept in the ring about seven hours per day in order to improve the vacuum pressure by synchrotron radiation. Average vacuum pressure was 3.6×10^{-9} Torr before injection and beam lifetime at 30 mA became 100 minutes. So we began to use synchrotron radiation for experiments. Injection was two times in a day at nine and

thirteen o'clock. The beam was kept in the ring from nine o'clock till eighteen o'clock. Figure shows average vacuum pressure before injection and lifetime at 30 mA from May 8 to December 20. According to improvement of the vacuum pressure, we increased stored beam current gradually. It was 35 mA in May, 50～60 mA in June, 70 mA in July, 110 mA in October. During August 20 and September 6, beam was accelerated up to 750 MeV. As average vacuum pressure did not become good after September, we exchange filaments of titanium getter pumps in December and average vacuum pressure improved about 10 persents.

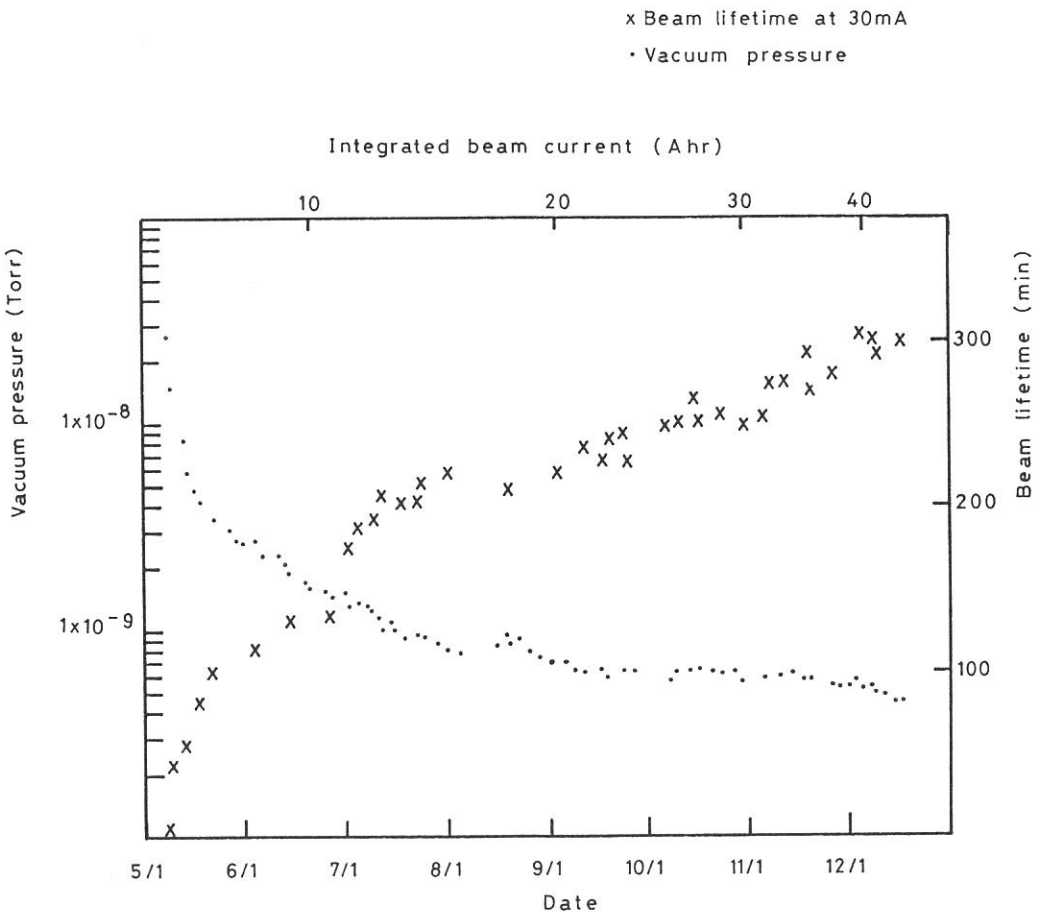

ION-TRAPPING EFFECT IN STORAGE RING

Toshio KASUGA, Hiroto YONEHARA, Toshio KINOSHITA
and Masami HASUMOTO

Institute for Molecular Science, Myodaiji, Okazaki 444

When the storage ring was first put into operation, the most serious problem was the enlargement of the vertical beam size. This effect was investigated in detail, and it was found that the enlargement was accompanied by positive tune shifts in both the horizontal and vertical planes. The positive tune shifts in both planes suggest a focusing force acting on the electron beam due to positive ions. It is another remarkable aspect in the tune diagram that no stabe area except for a few small areas exists above the sum resonance line $Q_H+Q_V=6$, and the lifetime of the stored beam is long in the region below the sum resonance line except along the third resonance line $Q_V=8/3$, but the vertical beam size grows at the high beam current in almost every part of the region. These aspects are explained by the tune shifts due to ions trapped in the beam and the coupling of horizontal and vertical oscillations near the sum resonance line. If the operating point (Q_H, Q_V) is located below the sum resonance line, i.e. $Q_H+Q_V<6$, then the operating point moves toward the resonance line, as the tune shifts in both planes are positive. When the operating point approaches the resonance line, the coefficient of coupling grows larger, and the vertical beam size becomes large. The growth of the vertical beam size decrease the focusing force

due to ions and the tune shift becomes small. Thus, if the operating point is located below the resonance line the tune shift is suppressed by the negative feedback mechanism at the cost of the beam size. In contrast to this, if the operating point is positioned above the sum resonance line, the tune shift is energized by the positive feedback effect.

Various attempts were made to clear ions. First, a DC clering voltage was applied to the electrodes. Though the vertical beam size was reduced slightly, the improvement was not satisfactory. The excitation of the transverse oscillation of the electron beam was also tried. When the frequency and amplitude of the excitation were appropriate, the beam size became almost perfect. These two ion-clearing techniques are used together in the routine operation of the ring. (Improvement of the beam profile by the ion-cleraring is shown in Fig.5 of p. 9 .)

LOW ENERGY OPERATION

Hiroto YONEHARA, Toshio KASUGA, Masami HASUMOTO
and Toshio KINOSHITA

Institute for Molecular Science, Myodaiji, Okazaki 444

The wavelength range of quasi-monochromatic light from the undulator is between 500 Å and 230 Å at the electron energy of 600 MeV. When quasi-monochromatic light of about 1000 Å is necessary, the storage ring must be operated at lower energy than the ordinary energy.

The currents of the magnet system can be changed keeping trackings between the quadrupoles and the bending magnets constant. Electron beam is injected and stored at the 600 MeV and decelerated down to an required value. Down to 300 MeV, survival ratio of the stored beam was about 70 %, when the initial stored current was 50 mA. However, as the control system of the power supplies is not suitable to search the best operating points along the deceleration, the injection at required electron energy must be tried.

The electron energy influences on beam characteristics. Variations of some nominal parameters are roughly estimated as to those of the 600 MeV electron beam as shown in Fig. 1. In this figure integers and half-integers are the powers which show the energy dependence of the beam characteristics. With this figure it is apparent that the lifetime of the stored beam is rigorously restricted with the Touschek effect, which depends strongly on the electron beam energy.

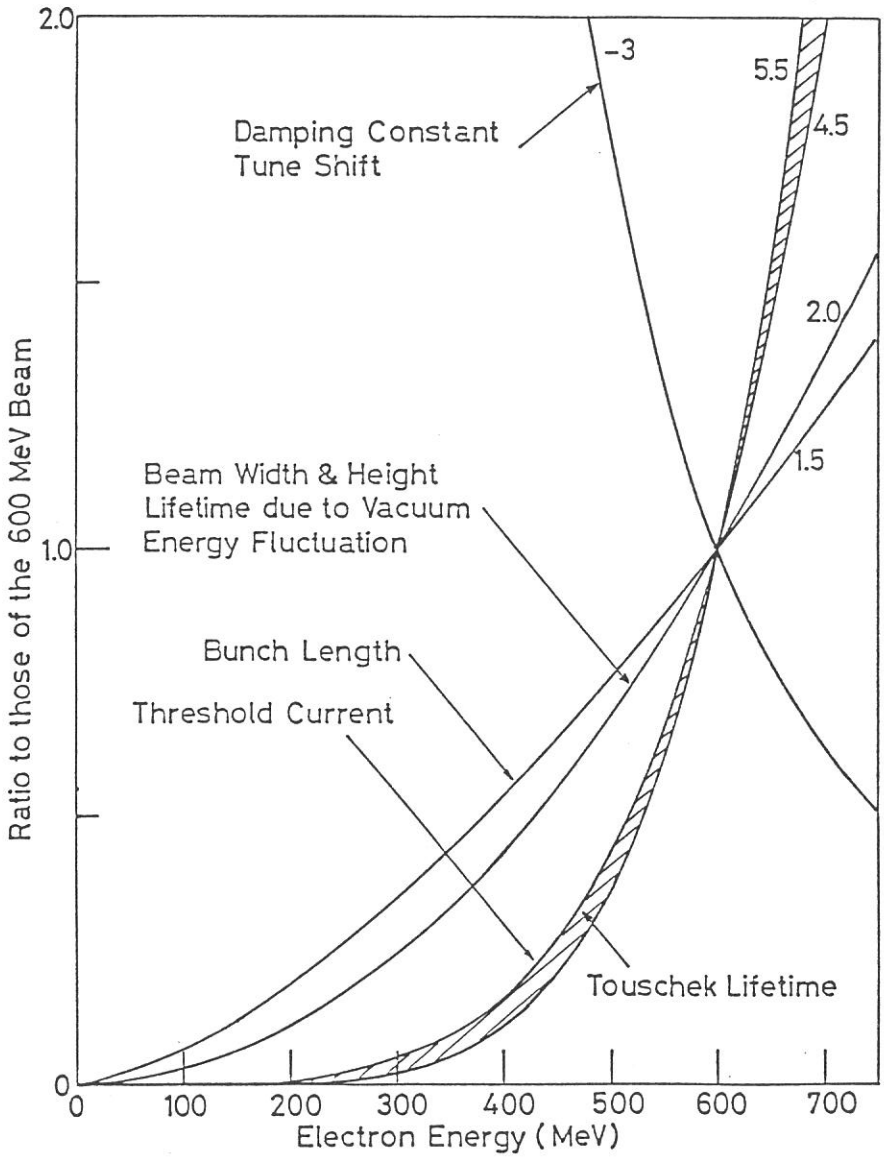

Fig.1 Variations of Beam Characteristics due to Electron Energy

UNDULATOR

Hiroto YONEHARA, Toshio KASUGA, Toshio KINOSHITA,
Masami HASUMOTO and Tatsuhisa KATO[#]

Institute for Molecular Science, Myodaiji, Okazaki 444
[#]) Faculty of Science, Kyoto University

A permanent magnet undulator was installed at the long straight section S3 of the storage ring, which produces a quasi-monochromatic light between 500 Å and 230 Å with the 600 MeV electron. The wavelength of the light is usually selected with varing the undulator gap. When the electron is accelerated up to the maximum energy of 750 MeV, the undulator light is expected to be available down to 150 Å. The bandwidth of the quasi-monochromatic light from the undulator was measured at about 2000 Å with the 300 MeV electron as shown in Fig. 1. The light was extracted through a sapphire window into atmosphere and taken into a monochromator. In this figure undulator gap was chosen between 32.0 mm and 29.0 mm, and shorter wavelength region the light was absorbed. The gap is narrower, the parameter K is bigger and wavelength of undulator light is longer. The bandwidth of the light, $\Delta\lambda / \lambda$, was gained as 6 % in FWHM. Moreover the electron energy was decelerated down to 180 MeV, and a coloured ring which is expected as following equation

$$\lambda = \frac{\lambda_0}{2\gamma^2}\left(1 + \frac{K^2}{2} + \gamma^2\theta^2\right)$$

was observed in the visible wavelength range.

The closed orbit distortion due to the undulator was corrected with the orbit correction systems in the almost all gaps and the experiment with the undulator light can be utilized at the same time with some experiments using synchrotron radiation from ordinary bending sections.

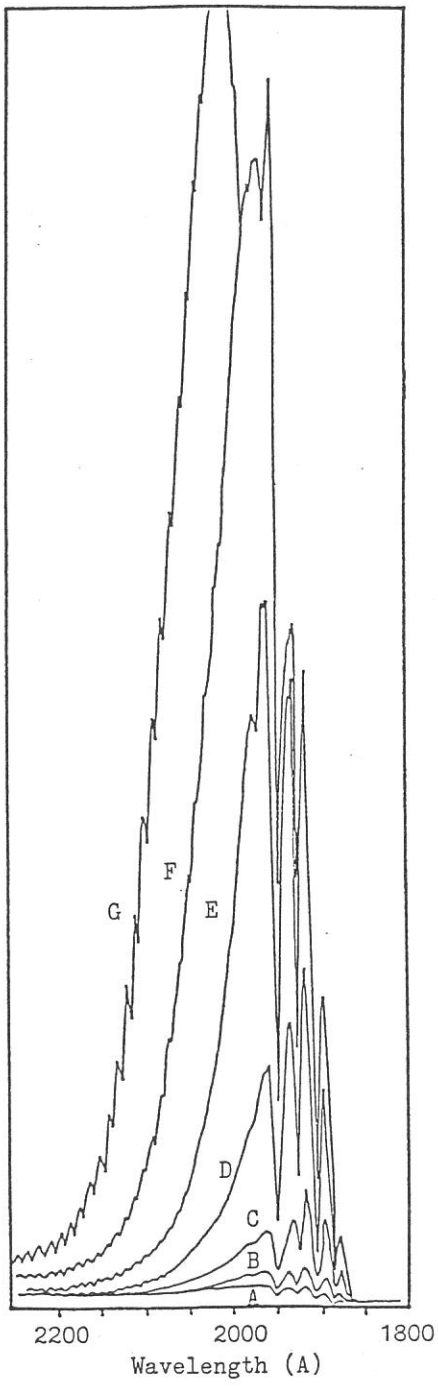

Electron Energy 300 MeV

Gap A ; 32.0 mm

B ; 31.5 mm

C ; 31.0 mm

D ; 30.5 mm

E ; 30.0 mm

F ; 29.5 mm

G ; 29.0 mm

$$\frac{\Delta\lambda}{\lambda} = 5.4\ \%$$

Fig. 1 Spectra of the Undulator Light

WIGGLER

Hiroto YONEHARA, Toshio KASUGA, Toshio KINOSHITA
and Masami HASUMOTO

Institute for Molecular Science, Myodaiji, Okazaki 444

A superconducting wiggler was installed at the long straight section S7 of the storage ring, which can supply synchrotron radiation to the BL-7A. Its maximum magnetic field strength is 4 Tesla. With exciting the wiggler field up to about 3 Tesla, the 600 MeV beam from the synchrotron can be injected in the ring easily. To make possible to store the beam at the 4 Tesla operation, a quadrupole and a z-steering magnet are installed to suppress the effects of the wiggler field on the beam, and appropriate currents of the sub-coils and these correction magnets were measured at some excitation levels between 2 Tesla and 3.9 Tesla operation of the wiggler field. These are shown in Fig. 1. These parameters were chosen to keep the position and shape of the beam profile which is monitored with an ITV system. With this figure, the increasing rate of correction magnets for the wiggler are recognized to be not the same behaviours of the sub-coils of the wiggler. Moreover the vertical and horizontal tune shifts, and the closed orbit distortions due to the wiggler magnetic field were measured, and the results are shown in Fig. 2. The vertical closed orbit distortion was steeply grown to be more than 3 mm at some points of the ring at about 3.2 Tesla.

Some efforts will be paied to suppress these tune shifts more precisely and COD with the normal quadrupole magnet system and with the vertical and horizontal orbit correction magnet systems.

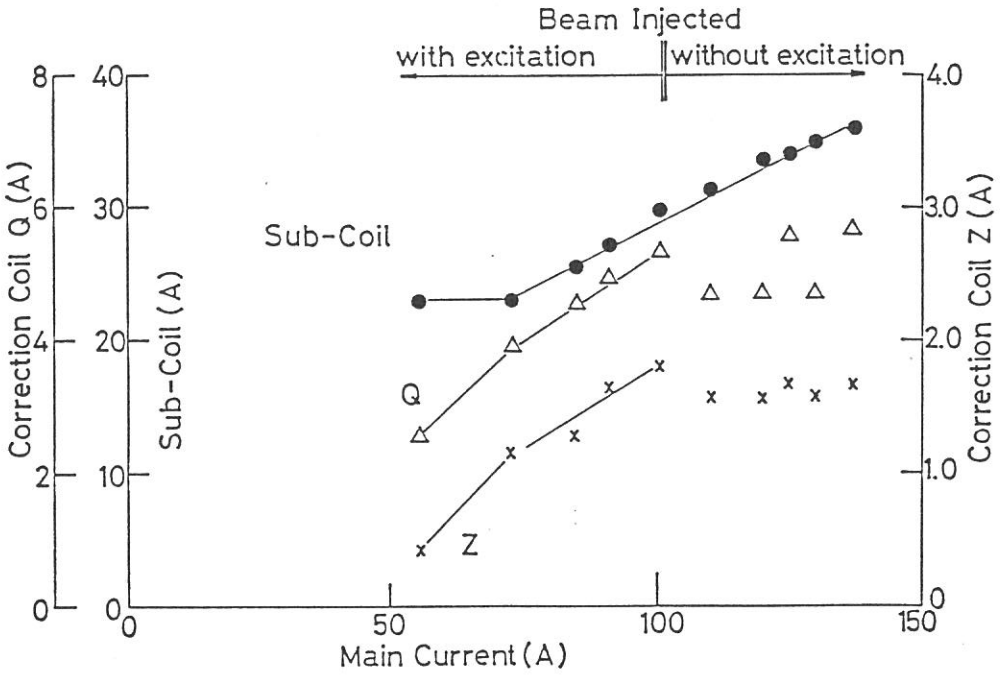

Fig. 1 Parameters of Wiggler Excitation

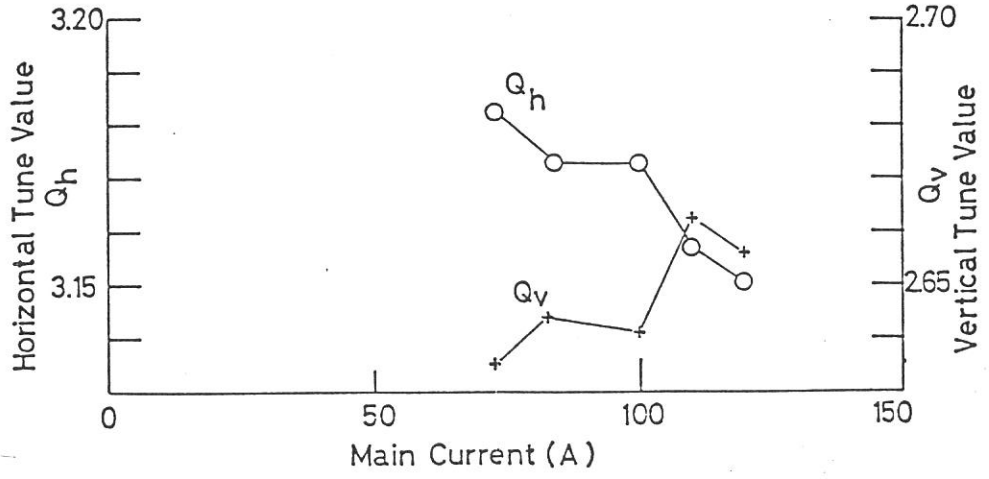

Fig. 2 Vertical and Horizontal Tune Shifts

MEASUREMENT SYSTEMS

BL2A Fluorescence Apparatus for Studies of Vapor Phase Photochemistry

K. SHOBATAKE, S. OHSHIMA*, A. HIRAYA, and K. TABAYASHI
Institute for Molecular Science, Myodaiji, Okazaki 444, JAPAN
* Dept. of Chem., Toho Univ., Funabashi, Chiba, 274, JAPAN

An apparatus for studies of photochemical processes in the vapor phase using fluorescence spectroscopy has been constructed on the beam line BL2A. Figure 1 shows a schematic of the apparatus. The optical system was designed such that (i) synchrotron radiation with a horizontal divergence of 40 m radians can be accepted by a 1 m Seya-Namioka monochromator (Hitachi SN2), and (ii) final dispersed synchrotron radiation

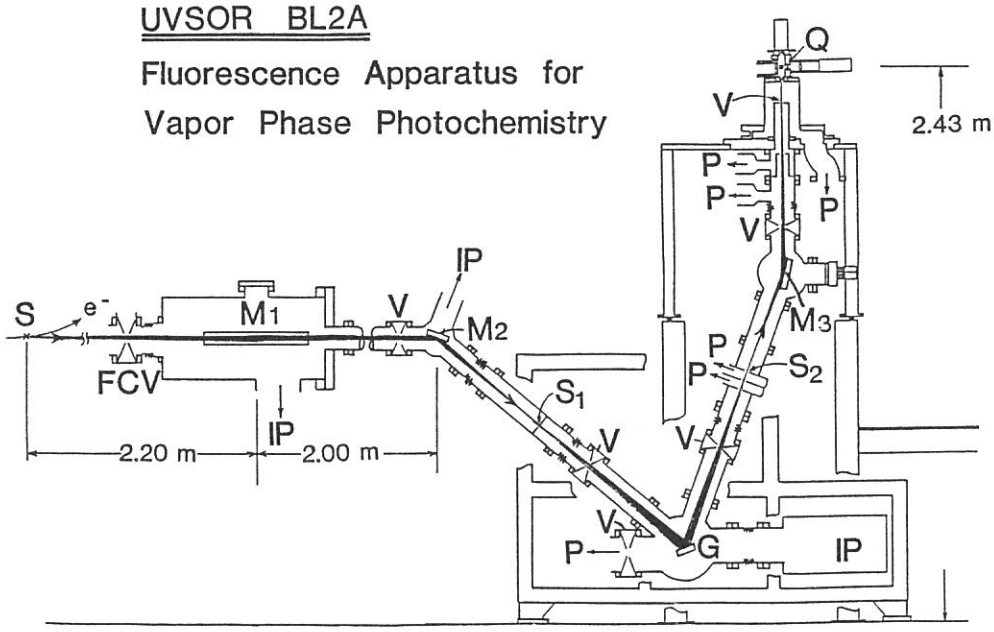

Fig. 1. Schematic side view of the fluorescence apparatus for vapor phase photochemistry. From left to right, S: source point of synchrotron radiation; FCV: fast closing valve; M1: first focusing mirror; M2: second focusing mirror; S1: entrance slit into 1 m Seya-Namioka monochromator; G: grating; S2: exit slit; M3: post focusing mirror; Q: synchrotron radiation- molecule interaction region (spot position). IP: ion pump; V: shutoff valve; P: turbomolecular pump.

goes upward. This apparatus was designed to use both samples in a gas cell and supercooled molecules or molecular complexes in a free jet. So far gas cell experiments have been done. Dispersed SR, after being focused by a toroidal mirror(M3), enters through a LiF window into a gas cell with a 10.9 cm pass length. Photon flux was monitored by a combination of sodium salicilate converter and photomultiplier (Hamamatsu R585). Fluorescence was detected perpendicularly to the incident light by a photomulti-plier tube (Hamamatsu R585). Intensities of the transparent light and fragment fluorescence, the sample pressure, and the electron beam current in the storage ring were concurrently monitored for every stepwise scan of the monochromator wave length, and were inter-faced into a microcomputer (NEC PC9801) via GP-IB interface (see Fig. 2). The photoabsorption and the relative fluorescence cross section were determined vs wave length.

Dispersed fluorescence spectra have been measured by using a Nikon P250 monochromator, installed between the gass cell and HP R585 photomultipier tube for emission detection. With purging N_2 gas flow emission above 180 nm was recorded. Fluorescence polarization measurement and studies of photochemical processes by means of molecuar beam vacuum UV spectroscopy of molecular complexes are under way.

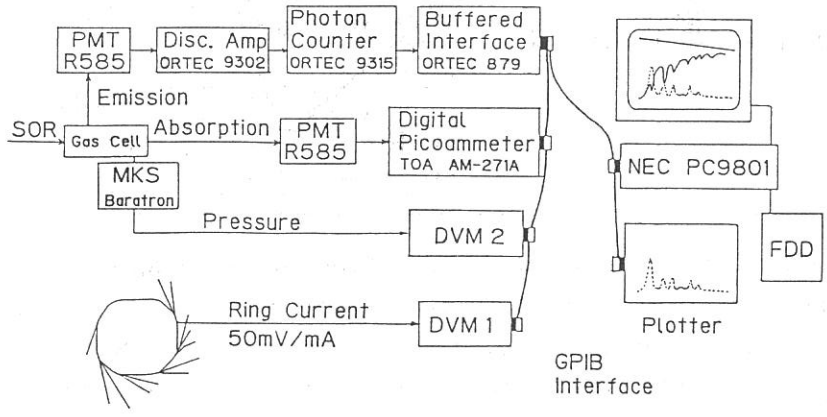

Fig. 2 Block diagram for absorption and fluorescence measurements. Data was transfered via IEEE 488 (GP-IB) interface from and to NEC PC-9801 microcomputer.

CONSTRUCTION OF A SUPERSONIC MOLECULAR BEAM APPARATUS FOR BEAM LINE BL2B2

Yohji ACHIBA, Haruo SHIROMARU, Kenji SATO, and Katsumi KIMURA
Institute for Molecular Science, Myodaiji, Okazaki 444

A supersonic molecular beam apparatus for the beam line BL2B2 has almost been completed. A technique of supersonic beam is apparently suitable and desirable for spectroscopic studies of molecular clusters as well as free molecules. Particularly a combination of this technique with a synchrotron radiation light source would undoubtedly open new aspects in the fields of vacuum UV photophysics and photochemistry.

As shown in Figure 1, in the BL2B2 the synchrotron radiation light beam is focused on the entrance slit of a 1 m seya monochromator by three pre-focusing mirrors, and then after passing through the monochromator, the light beam is further focused by a toroidal mirror.

Schematic side view of our molecular beam apparatus is shown in Figure 2. The photon-molecular beam collision chamber is separated from a beam-source chamber with a skimmer, and each chamber is evacuated by two turbo molecular pumps (1500 l/s, 1000 l/s) or an oil diffusion pump (5000 l/s). There is a two-stage differential pumping system between the molecular beam apparatus and a monochromator exit slit to keep the vacuum in the monochromator below 2×10^{-9} Torr under operation. This apparatus would enable us to study; 1) vacuum UV absorption spectra of ultracold free molecules, 2) half collisional reaction processes of superexcited or ionic molecular clusters using a mass selected photoionization technique, and 3) photoelectron energy and angular dependence spectra of molecules and molecular clusters.

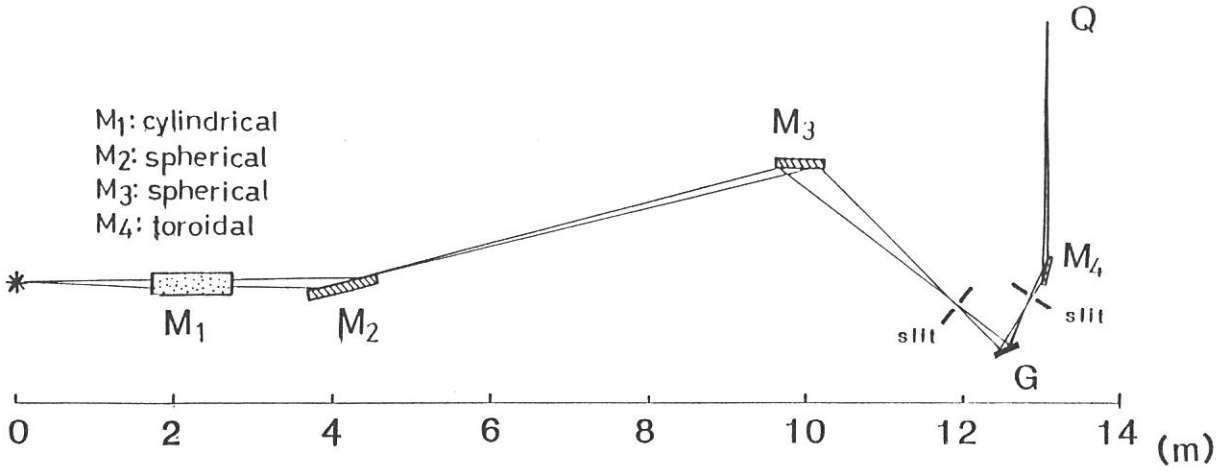

Figure 1 An optical system for beam line BL2B2.

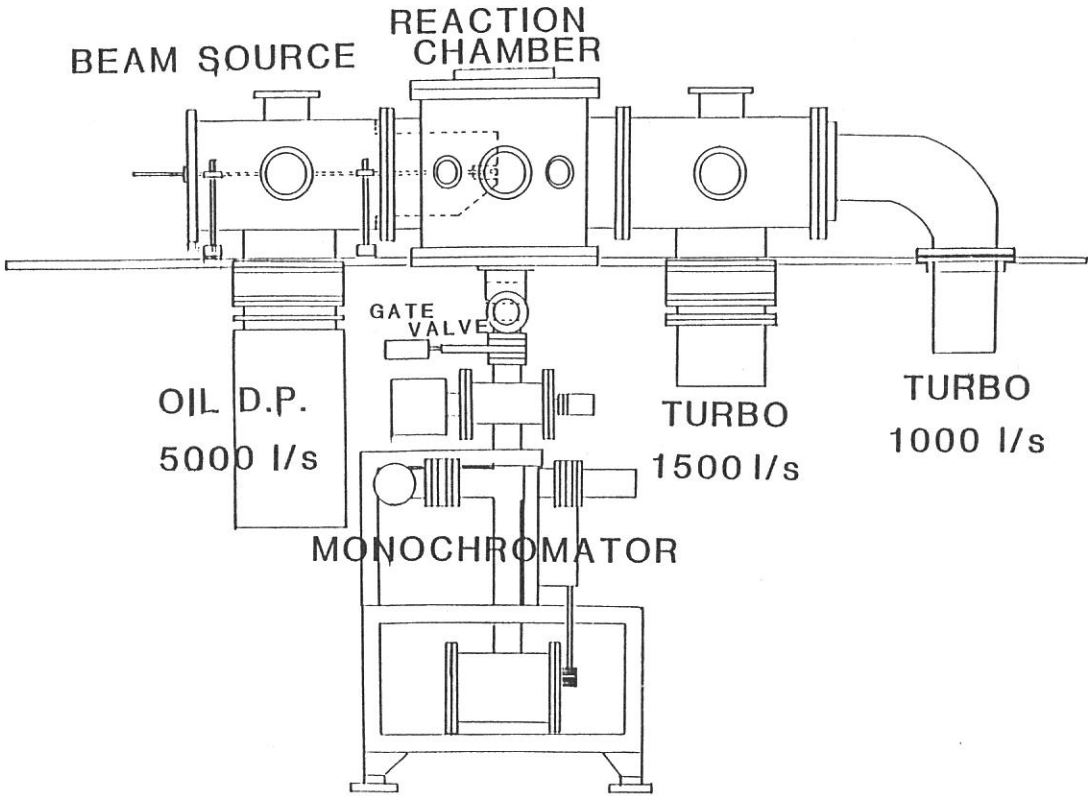

Figure 2 A schematic side view of a supersonic nozzle beam apparatus.

STATUS OF BL3A1

Makoto WATANABE, Tatsuhisa KATO* and Kusuo SAKAI

Institute for Molecular Science, Myodaiji, Okazaki 444
*Department of Chemistry, Kyoto University, Sakyoku, Kyoto 606

BL3A is a beam line for the undulator radiation. At a pre-mirror chamber of BL3A the beam line is split into two, which are BL3A1 without a monochromator and BL3A2 with a monochromator (2 m constant deviation grazing incidence) under construction. Fig. 1 shows the cross sectional view of the pre-mirror chamber. At the entrance of the pre-mirror chamber, movable diaphragms are located to limit acceptance angle of the undulator radiation for both horizontal and vertical directions. Mirrors M_{-1}, M_0 and M_1 introduce the synchrotron radiation from B_3 bending section to the monochromator. At BL3A1, one can use the undulater radiation as the quasi-monochromatic light between 500-230 Å (at 600 MeV) by the use of filters. Before the sample chamber an ion-chamber and a photo-electron spectrometer of gases will be attached with a differential pumping section to measure the intensity and the line shape of the undulator radiation, respectively. An Al photo-cathode beam monitor is also mounted before the sample chamber. The plan view of the S_3 straight section and BL3A1 is given in Fig. 2.

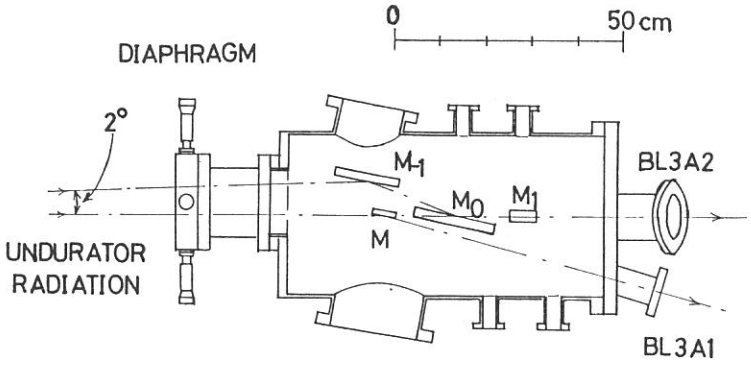

Fig.1 Cross sectional view of BL3A pre-mirror chamber. M, M_{-1}, M_0 and M_1 are pre-mirrors.

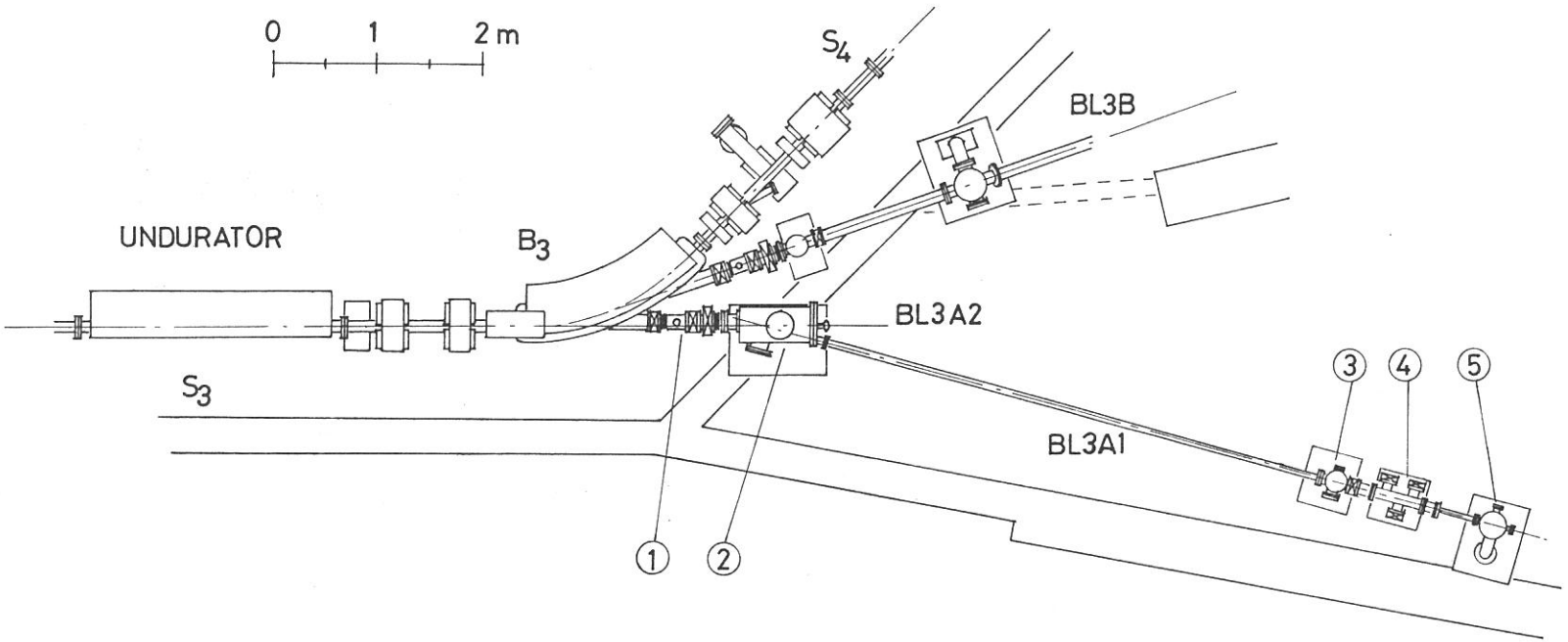

Fig.2 Plan view of the S_3 straight section and BL3A1.
1: front end, 2: pre-mirror chamber, 3: pumping station,
4: differential pumping section and 5: sample chamber.

THE TEPSICO-II APPARATUS AT BL3B FOR GAS PHASE PHOTOIONIZATION STUDIES

I. Koyano, K. Tanaka, T. Kato, and E. Ishiguro*

Institute for Molecular Science, Myodaiji, Okazaki 444
* Department of Applied Physics, Osaka City University
Sumiyoshi-ku, Osaka 558

At the UVSOR facility, several experimental stations for the study of elementary atomic and molecular processes in the gas phase have been constructed intensively over the last few years. Here, we report a system which has been designed for the study of secondary reactions of molecular ions produced by synchrotron radiation. The main objective is the state selection of the reactant ions, and for this purpose a novel coincidence technique TESICO[1] (threshold electron - secondary ion coincidence) is incorporated.

A schematic drawing of the apparatus, nicknamed TEPSICO-II, is shown in Fig. 1. The monochromator is a vertically dispersed normal incidence type (McPherson Type) with 3 m focal length and 10° angle between incidence and diffracted beam. It has a mechanically ruled aberration-corrected concave grating[2] with 1200 lines/mm groves. A cylindrical mirror M_1 and two spherical mirrors M_2 and M_3 focus SR of 20 mrad horizontally and 6 mrad vertically onto the entrance slit S_1, as shown in Fig. 2. The monochromatized light is ultimately directed upward and focused at a point Q in the interaction region by a toroidal mirror M_4.

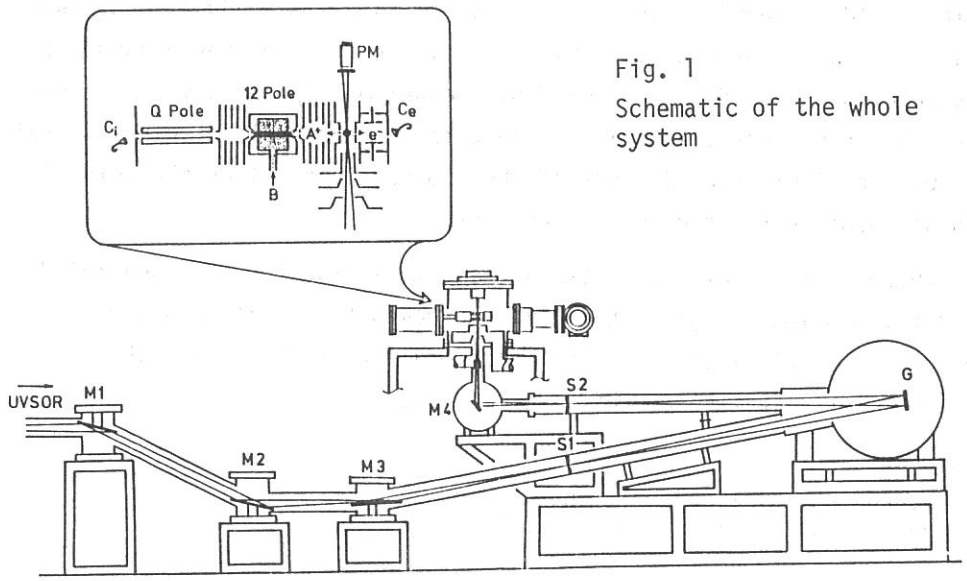

Fig. 1
Schematic of the whole system

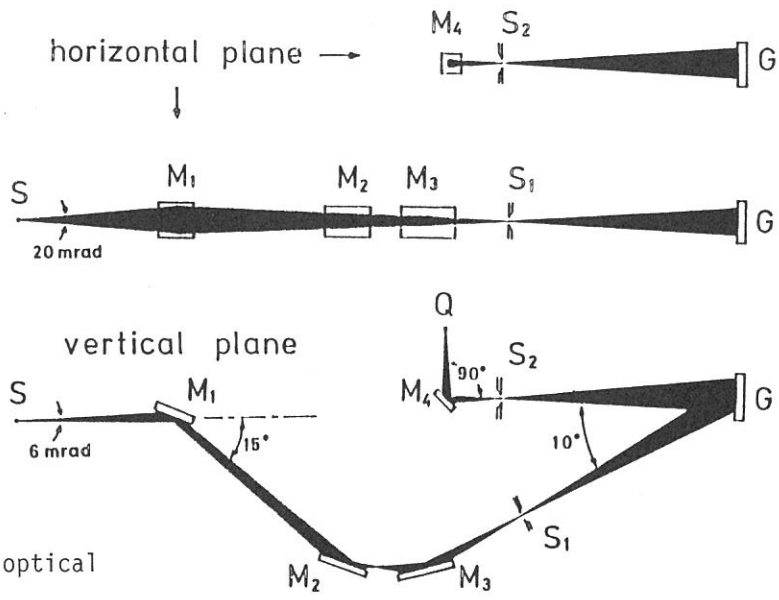

Fig. 2
Scheme of the optical layout

Sample gas A is introduced into the interaction region as a free jet and photoionized therein. Ions A^+ and photoelectrons e^- produced are expelled from the ionization region by a weak field in the directions opposite to each other and perpendicular to the photon beam. Threshold electrons are selected from the photoelectrons with finite kinetic energies by means of a non-line-of-sight steradiancy analyzer of our own design. Ions, on the other hand, are led into the reaction zone filled with neutral reactant B and surrounded by 12 poles on which RF voltages of opposite signs are applied alternately. Reaction takes place in this confining field produced by these 12 poles, so that all product ions, as well as all reactant ions entering this region, pass through the quadrupole mass spectrometer and are detected by channel multiplier C_i. This ion signal is then counted in coincidence with the threshold electron signal. The 100 % collection efficiency of the product ions allows the determination of absolute reaction cross sections.

These sections of the system are assembled together via several differential pumping systems. Experiments showed that, with a stagnation pressure of sample A of 2 atm, no deterioration of the ultrahigh vacuum (1×10^{-8} torr) in the monochromator is caused at all.

References

1 I. Koyano and K. Tanaka, J. Chem. Phys. 72 (1980) 4858.
2 T. Harada and T. Kita, Appl. Opt. 19 (1980) 3987.

FAR-INFRARED SPECTROSCOPY OF SOLID AT BL6A1

Takao NANBA, Yasuhito URASHIMA, Mikihiko IKEZAWA,
Makoto WATANABE[+], Eiken NAKAMURA[+], Kazutoshi Fukui[+],
and
Hiroo INOKUCHI[+]

Department of Physics, Faculty of Science, Tohoku University,
Sendai 980
+Institute for molecular Science, Myodaiji, Okazaki 444

A system for spectroscopy in the far-infrared region at the beam line BL6A1 covers a wavenumber region from 5 to 250 cm^{-1}.

I. Collection of Long Wavelength Light

Figure 1 shows the optical system. The radiation from the orbit is reflected by the plane mirror M_1^p and collected by a spherical mirror M_2^s. The long wavelength radiation diverges considerablly and a large acceptance angle is necessary for the collecting system. The light is reflected by two plane mirrirs M_3^p and M_4^p which are beneath M_1^p and M_2^s. After passing through a Si window, it is guided to the collimating system. A wedge shaped Si window of 2mm thickness separates the high and low vacuum parts. The mirror M_1^p is made of copper and has a small cut through which the short wavelength light within 20×10 $mrad^2$ passes to another system. The surface of the all mirrors are coated with gold.

II. Spectrometer and Sample Chamber

The collected light beam is made parallel by the toroidal mirror M_5^T in Fig.1. The cross sectional size of the parallel beam is about 36×45 mm^2. The horizontally polarized component is selected by the wire grid polarizer WG_1 and lead to a Martin-Puplett interferometer made by Specac Co.

The interferometer is separated from the sample chamber by a polyethylene window of 1 mm thickness. The light is polarized horizontally or vertically according to the direction of a wire grid polarizer WG_2. The light beam is collected by a toroidal mirror M_7^T on a sample S. In the case of the observation of the reflectivity, reflected light from the sample is collected by a spherical mirror M_8^S to a detector D. The angle of incidence is 7.5°. In the case of the transmission measurement, the detector is displaced to a position D' behind the sample as shown by the dashed line in Fig.1.

III. Spectral response

In Fig.2, spectral response is shown from 10 to 250 cm^{-1} detected by a Golay cell at the position D' in Fig.1 without any sample. The current of the UVSOR ring is 45.5 mA. The spectra show the intensities of light passed through different sizes of a diaphram placed at the sample position S. When the diameter of the aperture is larger than 3 mm, the intensity on the high energy region does not decrease. This result shows that owing to the low emittance of the source, an effective size of the beam at the sample position is as small as about 3×3 mm^2. This is a remarkable property because a small spot of slightly convergent light is obtained with a high intensity. The dashed curve in Fig.2 shows the intensity of light from a high pressure mercury lamp through 3 mm aperture. The intensity is much weaker than that of the synchrotron radiation at the current of 45.5 mA. Using this property, we have observed anisotropic reflectivity spectra of a K_2AgI_3 single crystal of 2 mm diameter at 80 K.

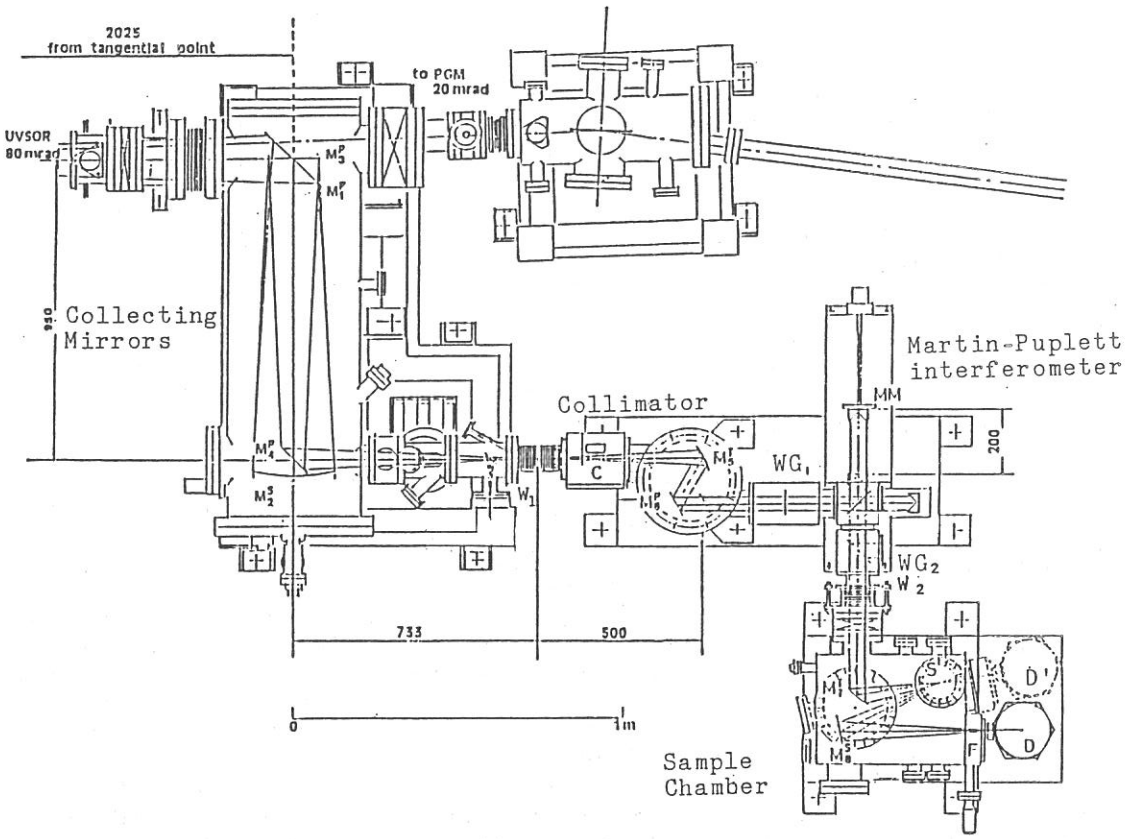

Fig.1 Optical system for far-infrared spectroscopy at BL6A1.

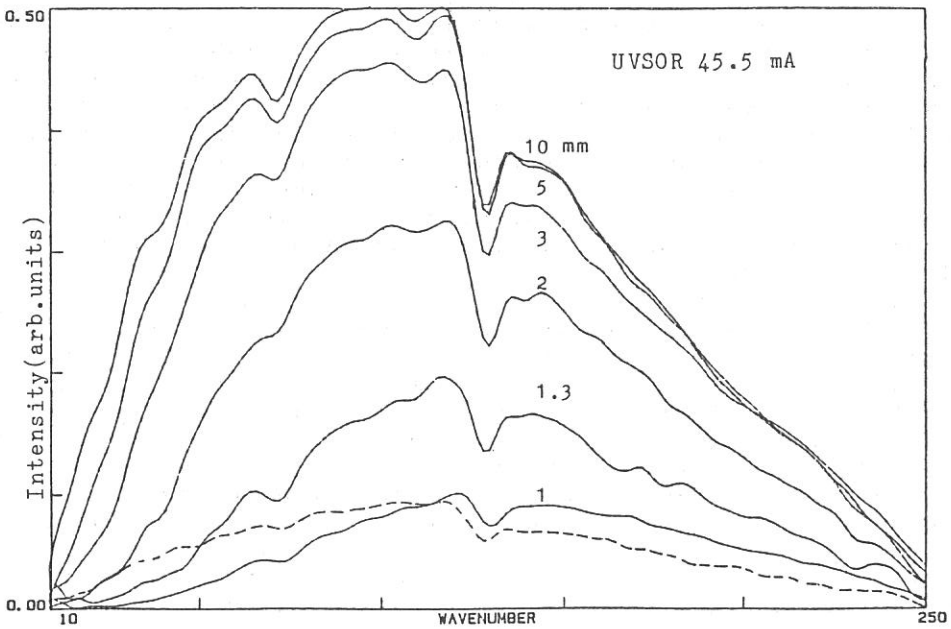

Fig.2 Intensity of spectra detected by Golay cell through apertures of different diameters placed at the sample position. Spectral resolution $\Delta\nu$ is 6 cm^{-1}. The dashed curve is the intensity of a Hg lamp through 3 mm aperture.

PLANE-GRATING MONOCHROMATORS FOR 2 EV < hν < 100 EV AT BL6A2 AND BL8B2

K. Seki, H. Nakagawa,[a] K. Fukui,[b] E. Ihsiguro,[c] R. Kato,[d] T. Mori, K. Sakai, and M. Watanabe

Institute for Molecular Science (IMS), Myodaiji, Okazaki 444

[a]Department of Electronic Engineering, Fukui University, Bunkyo, Fukui 910 and IMS

[b]Department of Applied Physics, Fukui University, Bunkyo, Fukui 910. Now at IMS

[c]Department of Applied Physics, Osaka City University, Sumiyoshi-ku, Osaka 558

[d]Department of Physics, Kyoto University, Sakyo-ku, Kyoto 606

At BL6A2 and BL8B2, we adopt two plane-grating monochromators (PGM) of the same design for studying solids by photoelectron spectroscopy and optical measurements, with moderate energy resolution (0.1 - 0.2 eV) and intensity. PGM can cover a farily wide range of photon energy with a good spectral purity.[1-6] The hν range of the present monochromator covers the whole valence excitations of various solids, and is also sufficient for mapping the energy-band dispersion relation E = E(k) by angle-resolved photoemission technique.

The optical design is illustrated in Fig. 1. Divergent synchrotron radiation is made parallel by two premirrors (M_0 and M_1) and vertically

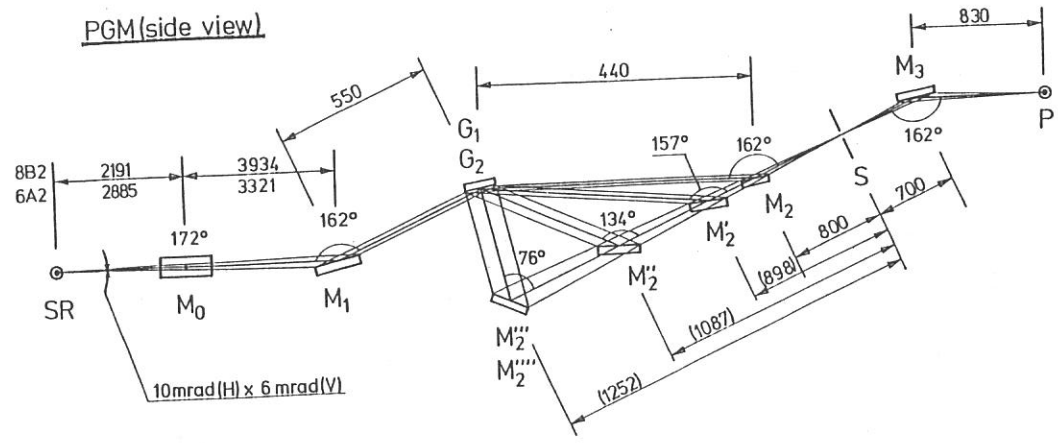

Fig. 1 Schematic of the optical design of the PGM

diffracted by one of the two innterchangeable, mechanically-ruled gratings (G_1; 1200 l/mm, G_2; 450 l/mm). The diffracted light is focused by one of the five cylindrical mirrors (M_2 - M_2'''') onto the exit slit S. Finally, the toroidal mirror M_3 focuses the divergent radiation onto the sample P in the measurement chamber. The deterioration of the resolution by the finite source size is minimized by virture of the small source-size of UVSOR (design values σ_x = 0.3 mm and σ_y = 0.2mm).

Rather similar performances have been observed for the two monochromators. The observed relative intensity distribution, at a slit width of 500 μm, is shown in Fig. 2. It was measured with a photomultiplier with a sodium salicylate energy converter. The unit of the ordinate could be calibrated for an absolute value of ∿2 x 10^{11} photons/s at a ring current of 27 mA, by measuring the photoemission from an Al-foil and using a reported value of photoemission yield.[7] Later, the exchange of a miss-blazed G_1 led to an improvement of this distribution, including the increase of the intensity at 10 eV $h\nu$ < 20 eV. The energy calibration was performed by measuring sharp features in the absorption spectra of rare gases, O_2 gas, CH_3I gas and alkali halide films. The resolution at a slit-width of 300 μm was found to be 0.015 - 0.3 eV in the wavelength range from 230 to 13.5 nm, from the sharpness of the features in these spectra. The spot size of the zeroth-order light at the sample surface (P) is < 1 x 1 mm^2, as designed.

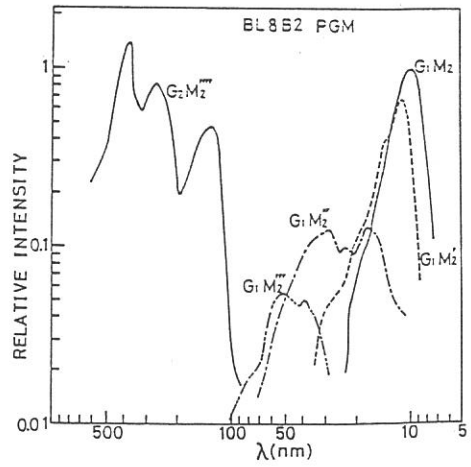

Fig. 2 Spectral intensity distribution of the PGM

References

1. K. P. Miyake, R. Kato, and M. Yamashita, Sci. Light 18 (1969) 39.
2. J. B. West, K. Codling, and G. V. Marr, J. Phys. E7 (1974) 137.
3. M. R. Howells, D. Norman, G. P. Williams, and J. B. West, J. Phys. E11 (1978) 199.
4. W. Eberhardt, G. Kartoffen, and C. Kunz, Nucl. Instrum. Methods, 152 (1978) 81.
5. F. Rieman and R. Torge, Nucl. Instrum. Methods, 208 (1983) 313.
6. S. Suga, M. Taniguchi, S. Shin, H. Sakamoto, M. Yamamoto, M. Seki, Y. Murata, and H. Daimon, Nucl. Instrum. Methods, 222 (1984) 80.
7. E. B. Salomon, Mucl. Instrum. Methods, 172 (1980) 79.

PERFORMANCE OF A DOUBLE CRYSTAL MONOCHROMATOR FOR BL-7A OF UVSOR

Takatoshi MURATA, Tokuo MATSUKAWA*, Masahiro MORI*, Masayoshi OBASHI*, Shun-ichi NAO-E**, Hikaru TERAUCHI***, Yasuo NISHIHATA***, Osamu MATSUDO+, Jun-ichiro YAMAZAKI+

Department of Physics, Kyoto Univ. of Education, Fushimi-ku, Kyoto 612
*Department of Physics, College of General Education, Osaka Univ., Machikaneyama, Toyonaka 560
**Department of Physics, College of General Education, Kanazawa Univ., Kanazawa 920
***Department of Physics, Faculty of Science, Kwansei-Gakuin Univ., Nishinomiya 662
+Institute for Molecular Science, Myodaiji, Okazaki 444

A high vacuum compatible constant offset double crystal monochromator (DXM) was constructed and tested at BL-7A using soft x-ray emitted from a normal bending magnet section of UVSOR. A schematic layout of the beam line of BL-7A is given in Fig. 1. The constant offset during the rotation of crystal plane was realized by a simple linkage of linear motions of the two crystals with two linear guides placed on both imput and output beam levels. The mechanism is similar to that of Cowan et al.[1] and will be described in detail elsewhere. The mechanical movement was found to be very smooth through a full rotation of 60° (between 15° and 75° of Bragg angle), and the constant offset was successfully achieved.

The intensity of the monochromatized light was monitored with Hamamatsu R-595 electron multiplier with a first dinode of Cu-Be or evaporated CuI. The output current was lead into TOA AM-271A digital picoammeter. The control of goniometer and data acquisition were made with NEC PC-9801E microcomputor through digital I/O and/or IEEE-488 standard interface bus.

The monochromator crystals such as KAP(100), mica(001) and beryl(10$\bar{1}$0) whose 2d value is 26.64Å, 19.80Å, and 15.98Å, respectively were tested. In Fig. 2 is shown the throughput transmission spectrum of the DXM for beryl crystal at the operating condition of the ring of 750MeV and about 30 mA. No radiation damage was observed for both beryl and mica crystals. The KAP crystal, however, suffered a serious damage on the surface even in the 600MeV operation.

Fig. 3 shows the Na K-edge near edge absorption spectrum of a thin film of NaCl which was evaporated in situ on a collodion film in the sample chamber. Despite the presence of many structures due to impurities and constituent atoms in the monochromator crystal in the throughput transmission spectrum, no structure appears in the absorption spectra of NaCl. All the structures were eliminated by the division of signals without and with a sample. From the doublet separation of the spectrum in Fig. 3 we can estimate the resolution of about 1eV which is practically sufficient for this energy range.

Further studies of other crystals such as InSb (111) and Quartz (10$\bar{1}$0) along with the spectrum of x-rays emitted from a superconducting horizontal wiggler are also planned.

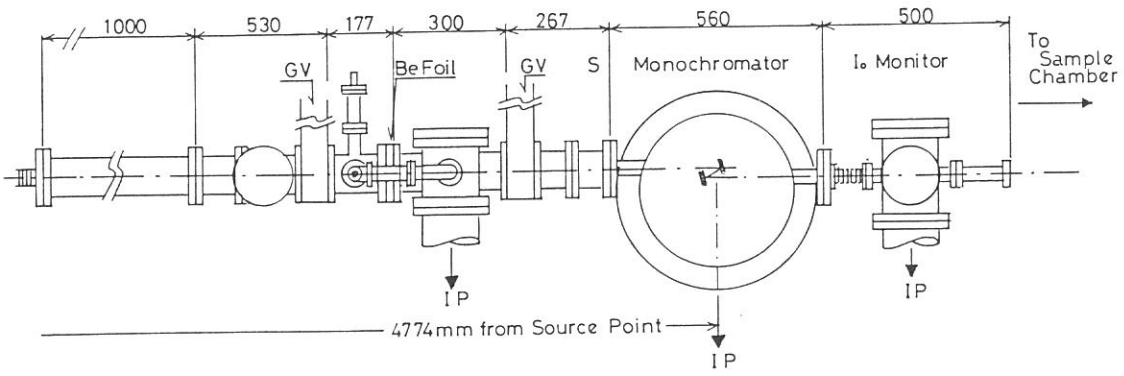

Fig. 1 Schematic layout of BL-7A. GV and IP mean gate valve and ion pump, respectively.

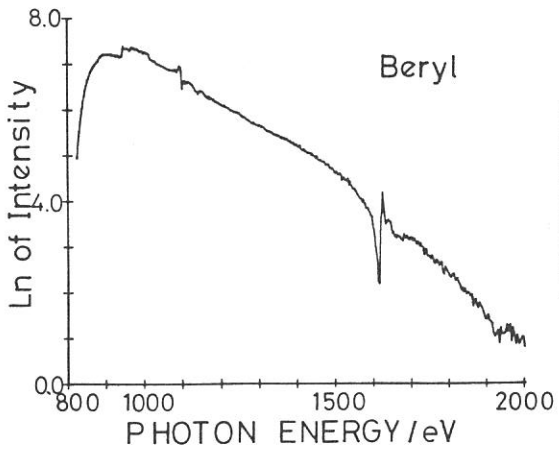

Fig. 2 Throughput transmission spectrum of DXM with beryl monochromator crystal.

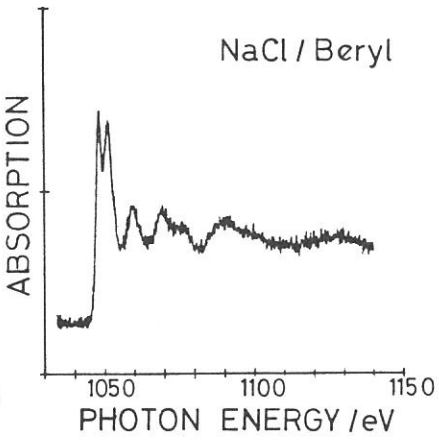

Fig. 3 Na K-edge near edge spectrum of NaCl taken with beryl crystal.

Reference

1) P. L. Cowan, J. B. Hastings, T. Jach, and J. P. Kirkland, Nucl. Instrum. Methods 208, 349 (1983)

The Vacuum-UV Spectrophotometer Installed in the BL-7B Beam Line

Toshio HORIGOME, Mitsukazu SUZUI, Kazuo HAYAKAWA
and Tadaoki MITANI

Institute for Molecular Science, Myodaiji, Okazaki 444

A vacuum-UV spectrophotometer using a improved 1 m Seya-Namioka-type monochromator has been constructed by the members of the Equipment Development Center and installed in the BL-7B beam line. An outline of the spectrophotometer is shown in Fig. 1. In order to achieve a maximum through-put of the monochromatic light, the spectrophotometer was designed on the basis of the results of the ray-trace calculation from the light source to a sample point through two troidal focussing-mirrors. A further improvement was made by employing a new microcomputer-driven mechanism for exchange of two concave gratings (600 or 1200 and 2400 ruled lines per mm with different blaze angles) mounted in the monochromator under an ultra-high vacuum. The expected efficiency of the spectrophotometer has been almost satisfied as follows; the intensity of the monochromatic light is about 10^{10} photon/sec with $\Delta\lambda/\lambda = 1\%$ at 50 nm for the storage ring currents of 40 mA, a maximum resolution of 0.15 nm for 1200 line/mm and a beam size on a sample position of about 1x2 mm^2 with a beam aperture of 26 mrad. In Fig. 2, the relative intensities of the monochromatic light are plotted for two kinds of gratings as a function of photon energy. It is found that that, by exchanging the gratings at 18 eV, this spectrophotometer is available in a wide energy region from 0.2 to 40 eV, being free from mixing with a stray light or the second-order diffracted light. The reproducibilities of exchanging and

scanning motions of the gratings are in a same order accuracy as the maximum resolution.

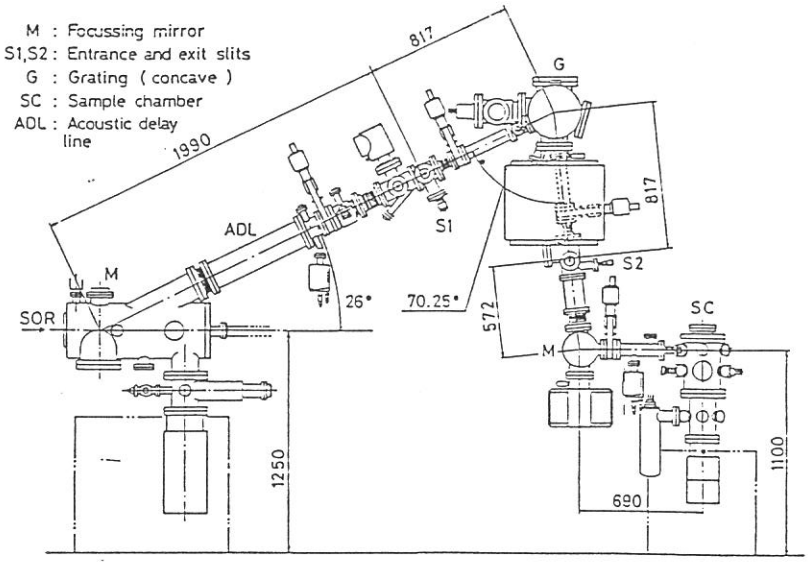

Fig. 1 Schematic diagram of the vacuum-UV spectrophotometer.

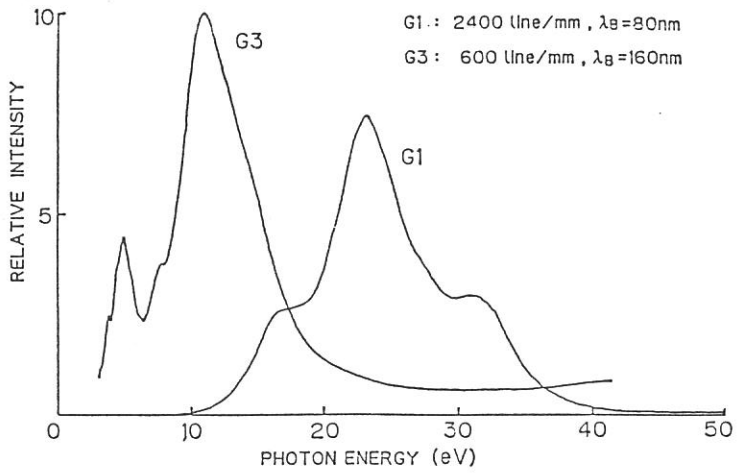

Fig. 2 The intensity of the monochromatic light for two kinds of gratings.

STRUCTURE OF BL8A

Kusuo SAKAI and Makoto WATANABE
Institute for Molecular Science

BL8A is a free port. Its plan and side views are shown in Fig.1 and Fig.2, respectively. It is composed of a front end, an acoustic delay line and a separation chamber. The front end is different a little from common ones described in p. 11. That is, a fast closing valve has a viton gasket so that it can shut out air completely. Its closing time is 20 ms. The acoustic delay line is 1 m long. It has eight diaphragms, the aperture of which is 80 mm x 27 mm, and two ion sputter pumps. It delays propagation time of leakage of 1 atm air by 40 ms. It also acts as a differential pumping system and can keep pressure difference of one order. A pneumatic valve after the acoustic delay line (indicated as 16 in Fig.2) has a glass window. One can aligne instruments by the use of SOR passing through the window. After that, the separation chamber is located. Users can connect their own instruments after this chamber. When users make irradiation experiments, such as lithography, they can use this chamber as a sample chamber.

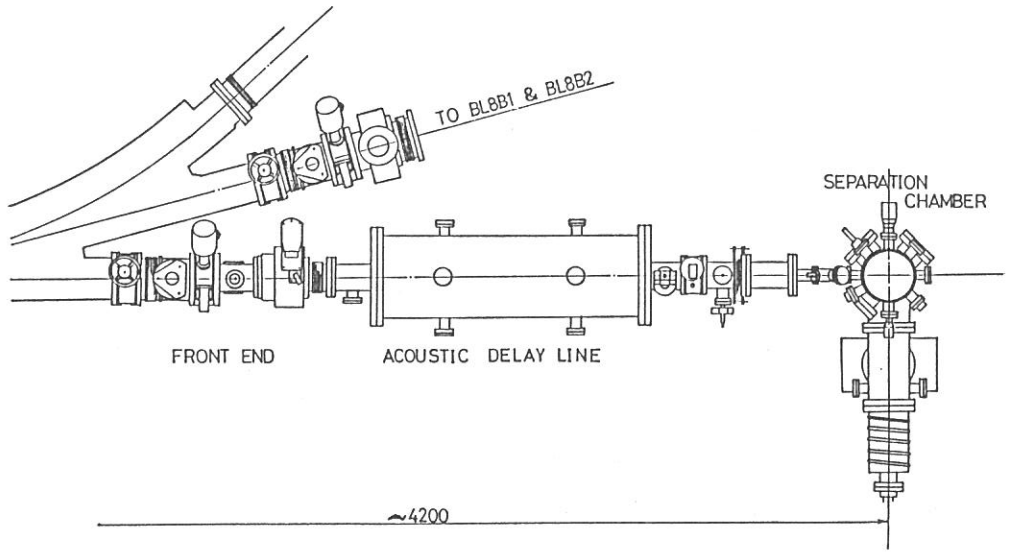

Fig. 1 Plan view of BL8A.

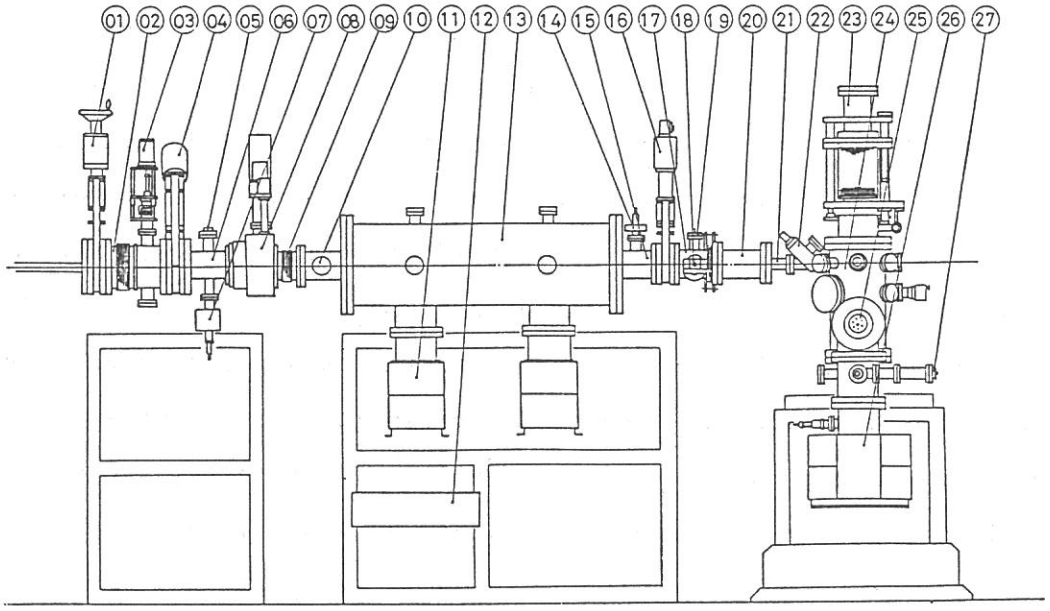

Fig. 2 Side view of BL8A. 01: manual valve, 03: beam shutter, 04 and 16: pneumatic valves, 05 and 27: ion gauges, 07,11 and 26: ion sputter pumps, 08: fast closing valve, 14: sensor for fast closing valve, 18: appendage pump, 19: pirani gauge, 22: straight through valve and 25: titanium sublimation pump.

RESEARCH ACTIVITIES

Isotope Effect on the Fluorescence Cross Section for the Dissociative Exctation Processes. I. CH_3CN and CD_3CN.

A. HIRAYA, S. OHSHIMA*, Y. MATSUMOTO,** K. TABAYASHI, and K. SHOBATAKE
Institute for Molecular Science, Myodaiji, Okazaki, 444 Japan
* Dept. of Chem., Toho Univ., Funabashi, Chiba, 274, Japan
** Inst. of Chem. & Phys. Research, Wako, Saitama, 351, Japan

The relative cross section and quantum yield of fluorescence from the nascent $CN^*(B,A)$ formed by photodissociative excitation of acetonitrile-h_3 and -d_3 were determined in the wave length region of exciting photon between 105 and 150 nm on the fluorescence apparatus for vapor phase photochemistry using UVSOR synchrotron radiation as a light source. Figure 1a and 1b show the absortion and the fluorescence cross section againt the excitation photon wave length for CD_3CN and CH_3CN, respectively. The quantum yield for emission from the excited photofragment $CN^*(B,A)$ formed by the reaction:[1,2]

$$CX_3CN + h\nu \longrightarrow CX_3CN^{**}$$
$$\longrightarrow CX_3 + CN^*(B,A) \quad (X = H, D)$$

has been found to increase gradually with photon energy. We have also found that the fluorescence quantum yields for two isotopic compounds are almost identical in the valence band region above 130 nm, while that for the CD_3CN is about a factor of two larger than the one for CH_3CN in the Rydberg transition region below 125 nm. The present findings are explained in light of the isotope effect of competing dissociation channels involving the motion of hydrogen atoms in the methyl group, such as formation of CH_2CN + H, CHCN + H_2, CH_2 + HCN. Preliminary measurements of the fluorescence excitation spectra of HCN and DCN show that the quantum yields for $CN^*(B\longrightarrow X)$ emission from the photofragments are almost identical for two hydrogen isotopic compunds except for some isotopic shifts in vibrational frequencies, which makes a contrast to the findings on the CX_3CN system.

1) H. Okabe and V. H. Dibeler, J. Chem. Phys. 59, 2430 (1973).
2) M. N. R. Ashfold and J. P. Simons, J. Chem. Soc. Faraday II74, 1263 (1978).

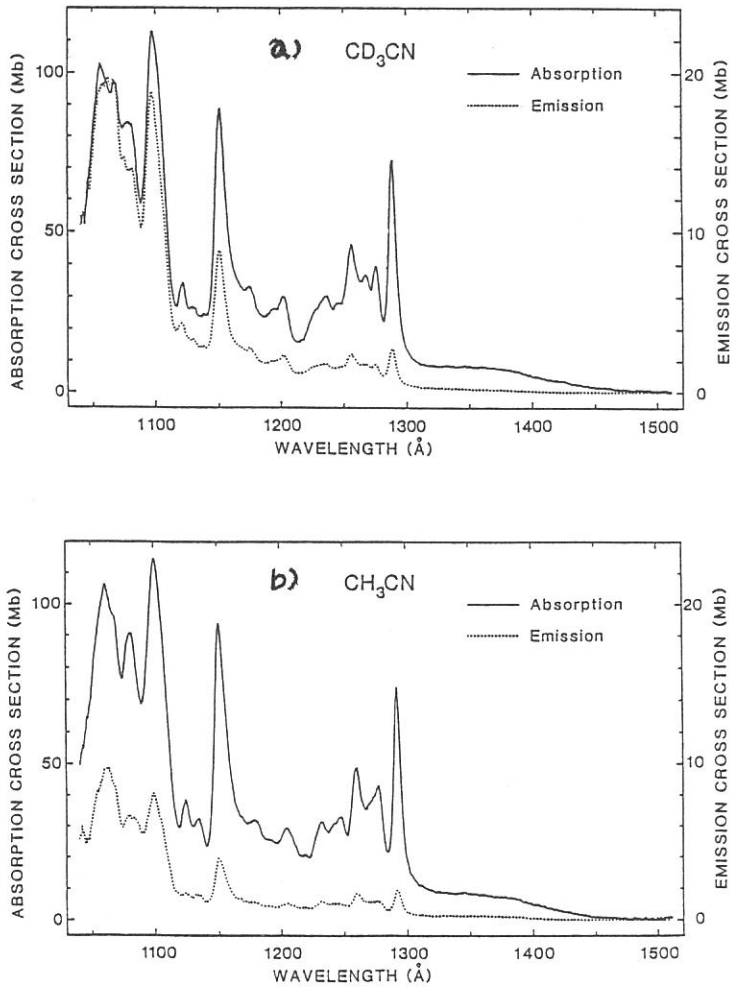

Figure 1. Absorption and fluorescence cross section versus wave length of the exciting photons for CD_3CN (upper) and CH_3CN (lower) in the gas phase. The fluorescence cross section was put on an absolute scale by scaling the fluorescence intensity to that of H_2O whose absolute fluorescence cross section is determined by Lee et al. (J. Phys. B 11,47 (1978)). The resolution of the dispersed synchrotron light was about 5.0 Å.

FLUORESCENCE FROM ION-PAIR AND RYDBERG STATES OF I_2

R.J. DONOVAN*, B.V. O'GRADY*,
Kosuke SHOBATAKE and Atsunari HIRAYA

*Department of Chemistry, University of Edinburgh,
West Mains Road, Edinburgh EH9 3JJ, U.K.
Institute for Molecular Science, Myodaiji, Okazaki 444, Japan.

Absorption and emission excitation spectra of I_2 vapor have been recorded in the wavelength region 105-210 nm using synchrotron radiation from UVSOR. Transparent light intensity was measured by a combination of a sodium salicylate coated window and a photomultiplier. The absorption cross section was determined from the attenuation of light intensity in a cell with an optical path length of 10.9 cm. Fluorescence was viewed at right angle to the incident light and observed at wavelengths longer than the air cut-off (ca. 180 nm).

The measured absorption cross section as a function of wavelength, in the region 105-210 nm, is shown in figure 1. Three broadly different regions in the absorption spectrum are distinguished: the broad feature between 173-205 nm is due to ion-pair absorption assigned as $D(0_u^+) \leftarrow X(0_g^+)$[1], and the sharp bands between 132-176 nm are due mainly to Rydberg transitions, and the broad continuous absorption is due to photoionization.

As shown in figure 1, the strongest fluorescence band is observed in the region 173-205 nm associated with the $D(0_u^+)$ ion-pair state. It is striking that fluorescence is not observed from the C_6 Rydberg system (175 nm)[2]. Because of low sensitivity of the fluorescence measurement system in this wavelength region, it can not be said whether C_6 Rydberg state fluoresce or not. But, it was strongly suggested[3] that there is a fast dissociation channel from C_6 Rydberg system.

An interesting feature of this band is the structure observed 175-182 nm, composed of several dips. The location of the first member of these dips in 173-178 nm coincides with those of the strong C_6 Rydberg absorption system. From the appearance of these dips in the fluorescence band associated with the $D(0_u^+)$ ion-pair state, it is concluded that this ion-

pair state is strongly mixed with sparse vibrational levels of non-fluorescent C_6 Rydberg state. Another strong fluorescence dip is observed at 182nm. Although no assignment is attempted here for the state which is responsible for this dip, it would appear that the $D(0_u^+)$ ion-pair state is strongly perturbed in this region and is probably predissociated.

Intense fluorescence is again observed for shorter wavelength than 151 nm. From the dispersed fluorescence spectra[3], it is found that the excitation to the C_7 Rydberg system (150 nm) gives rise to the emission from an ion-pair state. This is another evidence for perturbation between the Rydberg and ion-pair states. Below 149 nm, predissociation can yield electronically excited iodine atom. Actually, emission from both 6s $^4P_{5/2}$ and 6s $^2P_{3/2}$ states of atomic iodine have been observed[3].

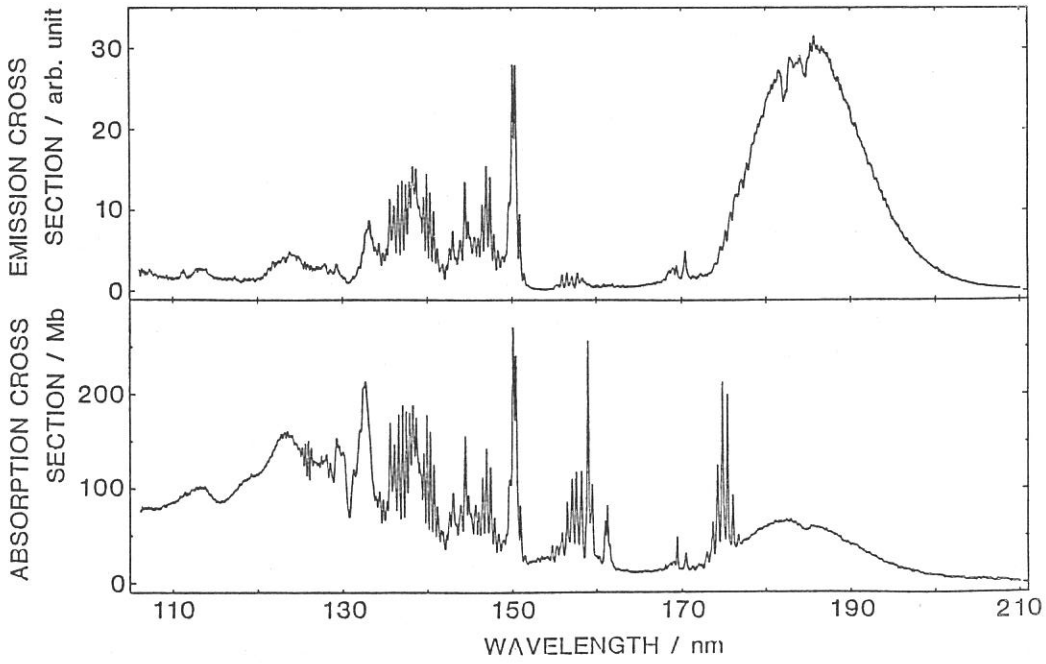

Fig. 1. Absorption (lower) and fluorescence excitation (upper) spectra of I_2 vapor (11 mtorr).

1. R.S. Mulliken, J.Chem.Phys., 55, 288 (1971)
2. P. Venkateswarlu, Can. J.Phys., 48 1055 (1970)
3. Emission spectra of I_2 excited in Rydberg region, next paper.

EMISSION SPECTRA OF I_2 EXCITED IN RYDBERG REGION

Atsunari HIRAYA, Kosuke SHOBATAKE and R.J. DONOVAN*

Institute for Molecular Science, Myodaiji, Okazaki 444, Japan
*Department of Chemistry, University of Edinburgh,
West Mains Road, Edinburgh EH9 3JJ, U.K.

From the fluorescence excitation spectrum of I_2 vapor (105-210 nm) obtained by monitoring longer wavelengths than ca. 180 nm, it was suggested that some emitting states other than optically prepared state are formed following the excitation to the Rydberg systems higher than the C_7 Rydberg system. In an attempt to identify such emitting states, emission spectra of I_2 vapor have been measured in the region above 180 nm.

The emission spectrum excited at the peak position (150 nm) of the C_7 Rydberg absorption system is shown in figure 1(a). The strongest emission band is observed at 183 nm. Following this band at longer wavelength region weak continuous emission band system with maxima at 216, 236, and 270 nm is observed. Further weak bands are also observed at 304, 323, and 340 nm. In the emission spectrum excited at 137 nm, where several Rydberg absorption systems are overlapped, is shown in figure 1(b). Two strong emission bands at 183 and 206 nm, and very weak bands at 323 and 340 nm are observed. The general feature of the emission spectra excited in the Rydberg systems higher than the C_7 Rydberg system is the same as that excited at 137 nm. In these emission bands, two emission bands at 323 and 340 nm appear more prominently under higher pressure conditions. These two emission bands can be assigned as the D → X (323nm)[1] and D' → A' (340nm)[2] ion-pair

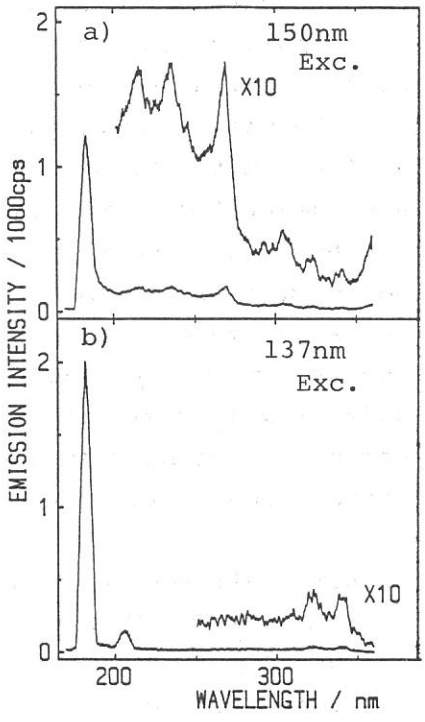

Figure. 1. Emission spectra of I_2

emission bands in which the emitting states are formed by collisions.

On the other hand, five emission bands located at shorter wavelength than 310 nm are not affected by the sample gas pressure. Two of these primary emission bands, 183 and 206 nm, can be assigned as the 6s $^4P_{5/2} \rightarrow 5p^5\ ^2P_{3/2}$ and 6s $^2P_{3/2} \rightarrow 5p^5\ ^2P_{1/2}$ transitions of iodine atom, respectively. From the excitation spectra monitored at both 183 and 206 nm emission, the onset for the formation of 6s $^4P_{5/2}$ and that of 6s $^2P_{3/2}$ states were found to lie at 150 ± 0.5 nm and 146 ± 1 nm, respectively.

The 270 nm band was observed in the emission spectrum under high pressure conditions, and assigned as the emission from the F ion-pair state[3] formed by collisions to the ground state of I_2. It should be noted that the 270 nm band observed here, following the excitation to the C_7 Rydberg system, is not the collision induced emission band. And it has been suggested from the absorption spectrum that the C_7 Rydberg system is quite strongly perturbed[4]. From these observations, it is concluded that the C_7 Rydberg system is strongly mixed with the F ion-pair state and thus the excitation to the C_7 Rydberg state results in the emission from F ion-pair state.

So far the emitting states produced following the excitation to the Rydberg states under low pressure condition are identified as two excited states of iodine atom (6s $P_{5/2}$ and 6s $^2P_{3/2}$) and the F ion-pair state. When Xe is added as a buffer gas, emission from XeI^* excimer become dominant irrespective of excitation wavelengths shorter than 192 nm, except for the C_6 Rydberg state which does not fluoresce even under low I_2 pressure without Xe. From these results, it is strongly suggested that a very fast dissociation to the ground state atoms takes place from the C_6 Rydberg state.

1. R.S. Mulliken, J.Chem.Phys., 55, 288 (1971).
2. K.P. Lawley, M.A. MacDonald, R.J. Donovan and Agust Kvaran, Chem.Phys.Lett., 92, 322 (1982).
3. H.Hemmati and G.J. Collins, Chem.Phys.Lett., 75, 488 (1980)
4. R.J. Donovan, B.V.O'grady, K.Shobatake and A.Hiraya, Chem.Phys.Lett., 122, 612 (1985).

$CCl_2(\tilde{A}^1B_1)$ RADICAL FORMATION IN THE VUV PHOTOLYSES OF CCl_4 AND $CBrCl_3$

Toshio IBUKI, Atsunari HIRAYA* and Kosuke SHOBATAKE*

Institute for Chemical Reserach, Kyoto University, Uji, Kyoto 611
*Institute for Molecular Science, Myodaiji, Okazaki 444

Gas-phase CCl_2 radical has been generated in various ways. Laser induced fluorescence(LIF) bands have been detected in the 500-560 nm range[1] and band structures have been partially resolved.[2] The LIF method also has shown that the radiative lifetime of the electronically excited $\tilde{A}^1B_1$ state is 3.81 ± 0.30 μsec.[3] In the present work $CCl_2(\tilde{A}^1B_1)$ radical is formed by the direct photodecomposition of CCl_4 and $CBrCl_3$ molecules using Lyman-α or Ar I resonance lines. The absorption and fluorescence excitation spectra of CCl_4 and $CBrCl_3$ are measured on a fluorescence apparatus at the BL-2A station of UVSOR.

Fig. 1 shows the emission observed when CCl_4 was photolyzed by a H Lyman-α lamp. Quite similar spectrum devoid of structure was found in the case of $CBrCl_3$ photoexcitation. The time dependence of the fluorescence decay was found to be expressed by a superposition of two lifetime components of 1.9 and 3.2 μsec at the extrapolated zero pressure by using a pulser which emits about 10 nsec(FWHM) light of 121.6 nm.

The observed emission was assigned as the $CCl_2(\tilde{A}^1B_1 \rightarrow \tilde{X}^1A_1)$ transition based on the following observations:

(1) Absorption bands of CCl_2 ($\tilde{A} \leftarrow \tilde{X}$) transition appear in the 440-560 nm range,[4] which overlaps with the present emission wavelength region.

(2) The spectral feature in Fig. 1 resembles well to the chemiluminescence spectrum(diffuse band in the 400-800 nm range) observed in a Ba + CCl_4 reaction,[5] in which the emitter has been assigned as $CCl_2(\tilde{A}^1B_1)$ radical.

(3) The long lifetime component of 3.2 μsec is close to the value of 3.8 μsec in Ref. 3.

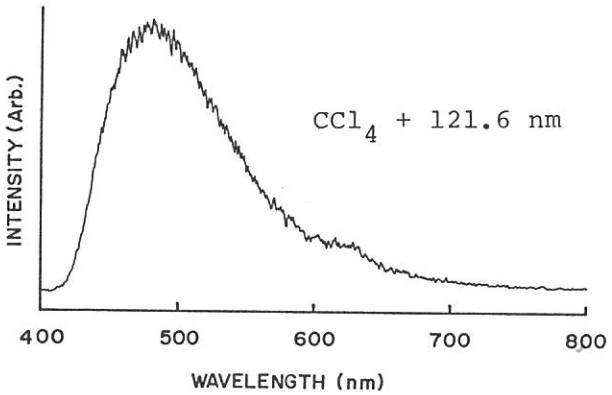

Fig. 1. Dispersed fluorescence.

Absorption and fluorescence excitation spectra of CCl_4 and $CBrCl_3$ are shown in Figs. 2 and 3, respectively. Although quite weak fluorescence can be observed at the beginning of the first excited states of CCl_4 and $CBrCl_3$, sharp increases of emission intensities at around 143 nm(8.7 eV) in Figs. 2 and 3 indicate the following decomposition processes:

$$CCl_4 + h\nu \rightarrow CCl_2(\tilde{A}^1B_1) + 2Cl \qquad \Delta H \simeq 8.9 \text{ eV}$$

$$CBrCl_3 + h\nu \rightarrow CCl_2(\tilde{A}^1B_1) + Br + Cl \qquad \Delta H \simeq 8.3 \text{ eV}$$

where ΔH values were calculated by the observation that the emissions are found at $\lambda > 405$ nm.

Assignments of the absorption peaks of CCl_4 have been given by Causley and Russell.[6] However, we have found no previous study on the quantitative absorption spectrum of $CBrCl_3$ in the VUV range. The valence configuration of $CBrCl_3$ is $(3a_1)^2(4e)^4(1a_2)^2(5e)^4$.[7] We tentatively assign the Rydberg bands in Fig. 3 as follows:

nm	Transition
185.0	$5e \rightarrow \sigma^*$
157.5	$5e \rightarrow ns(3/2)$
152.0	$5e \rightarrow ns(1/2)$
145.5	$4e \rightarrow ns$
136.7	$5e \rightarrow np(3/2)$
134.7	$1a_2 \rightarrow np$
133.0	$5e \rightarrow np(1/2)$
130.0	$4e \rightarrow np$
115.5	$3a_1 \rightarrow np$
113.5	$(5e)^{-1}$ (3/2)
111.0	$(5e)^{-1}$ (1/2)

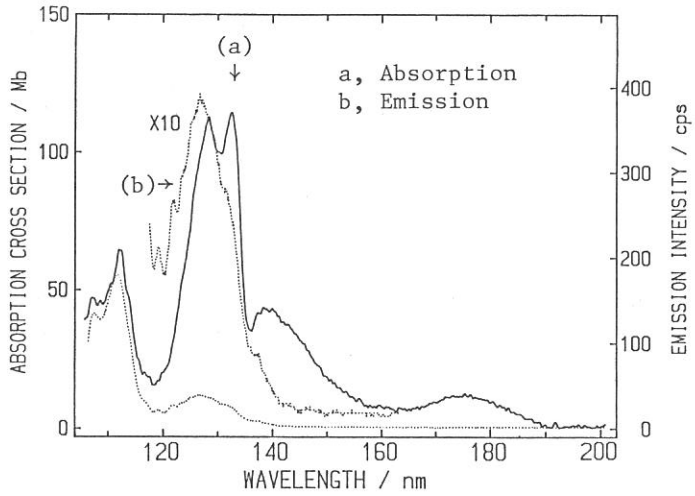

Fig. 2. Absorption and fluorescence excitation spectra of CCl_4.

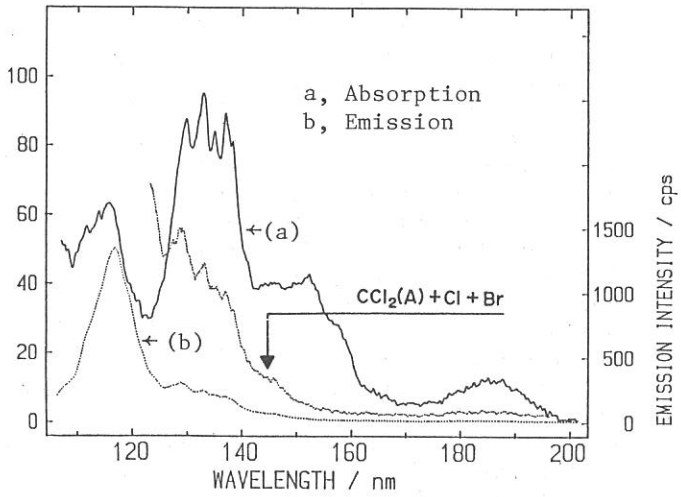

Fig. 3. Absorption and fluorescence excitation spectra of $CBrCl_3$.

References

1) J. J. Tiee, F. B. Wampler and W. W. Price, Chem. Phys. Lett., 65, 425 (1979).
2) D. A. Predmore, A. M. Murray and M. D. Harmony, Chem. Phys. Lett., 110, 173 (1984).
3) R. E. Huie, N. J. T. Long and B. A. Thrush, Chem. Phys. Lett., 51, 197 (1977).
4) D. E. Milligan and M. E. Jacox, J. Chem. Phys., 47, 703 (1967).
5) R. Kiefer, A. Siegel and A. Schultz, Chem. Phys. Lett., 59, 298 (1977).
6) G. C. Causley and B. R. Russell, J. Electron Spectrosc. Relat. Phenom., 11, 383 (1977).
7) I. Novak, T. Cvitas and L. Klamsinc, J. Chem. Soc., Faraday Trans. 2, 77, 2049 (1981).

ABSORPTION AND FLUORESCENCE SPECTRA OF CH_3SCN AND RELATED MOLECULES

Ikuo TOKUE, Atsunari HIRAYA*, and Kosuke SHOBATAKE*

Department of Chemistry, Niigata University, Niigata 950-21
*Institute for Molecular Science, Myodaiji, Okazaki 444

Vacuum UV photolysis of CH_3SCN and CH_3NCS produces fluorescence attributed to SCN(A, B) radicals[1]. The emission spectra of the CH_3S radicals is obtained in the photolysis of $(CH_3)_2S$[2]. In this study, the photoabsorption and fluorescence cross sections of CH_3SCN, CH_3NCS, CH_3NCO, and $(CH_3)_2S$ were measured in the 105-210 nm region and the emission spectra from the excited fragments were observed in the 300-500 nm region.

Synchrotron radiation dispersed by a 1 m Seya-Namioka monochromator was used as the light source. The dispersed photon flux entered the gas cell (10.9 cm long) through LiF window. The photon flux was measured by using a combination of sodium salicylate coated LiF window and a photomultiplier. The total fluorescence in the 160-650 nm region was observed at right angle to the primary photon beam. The emission from the excited photofragments dispersed by a Nikon P250 monochromator was observed in the 300-500 nm region. The sample vapor was continuously introduced into the gas cell and slowly pumped by a rotary pump. All chemicals were degassed at 77 K.

In the absorption of CH_3NCS, several valence-type transitions are very intense, while no Rydberg progression is observed. On the other hand, for CH_3SCN, CH_3NCO, and $(CH_3)_2S$, a number of absorption were found to fit Rydberg progressions of the form, $\nu_n = IP - R/(n-\delta)^2$, where IP and R are the ionization potential and the Rydberg constant, respectively. In all three spectra, the initial member of each series is assigned an n of 4, which restricts δ (the quantum defect) to 1-2. Three Rydberg series constructed for each molecule are, according to convention, the s, p, and d Rydberg series, respectively. The values of δ and IP are listed in Table 1. The values for $(CH_3)_2S$ are in good agreement with those in the literature[3]. The absorption and fluorescence cross sections(c.s.) of CH_3SCN are shown in Fig. 1 with three Rydberg progressions indicated. The fluorescence c.s. shows structure corresponding to the absorption c.s.

The emission spectra observed from excitation of CH_3SCN at 152.6 ± 1 and 125.6 ± 1 nm are shown in Fig. 2. The emission spectrum obtained at 152.6 nm is assigned to the SCN(A-X) and SCN(B-X) bands, while that obtained at 125.6 nm is mainly attributed to the CN(B-X) band. The photodissociation pro-

cesses that produce these excited photofragments are

$$CH_3 \begin{cases} \rightarrow CH_3(X^2A_2'') + SCN(A^2\Pi/B^2\Sigma^+), & \Delta H=6.39/6.49 \text{ eV}, \quad (1) \\ \rightarrow CH_3S(X^2E) + CN(B^2\Sigma^+), & \Delta H=7.45 \text{ eV}, \quad (2) \end{cases}$$

where the ΔH values represent the enthalpy of dissociation. The threshold wavelength for Reaction 2 is $\approx$166 nm. The CN(B) species seems to have a little contribution to the fluorescence produced at 152.6 nm.

The emission spectrum observed from excitation of CH_3NCS at 153.5±1 nm is identical with that from CH_3SCN at 152.6 nm excitation and is assigned to the NCS band. The emission spectra observed from CH_3NCO (λ_{exc}=138±1 nm) and $(CH_3)_2S$ (λ_{exc}=152±1 nm) are assigned to the NCO(A-X) and CH_3S(A-X) bands, respectively.

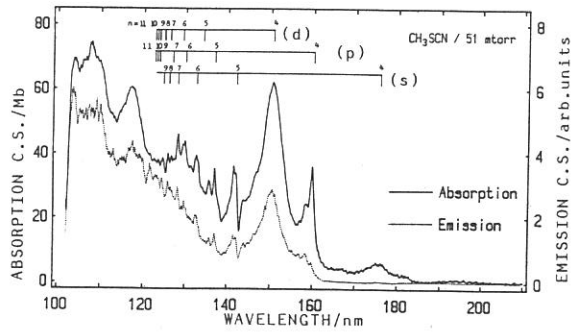

Fig. 1. The absorption and total fluorescence c.s. of CH_3SCN

Table I IP and δ of CH_3SCN, CH_3NCO, and $(CH_3)_2S$

Molecule	series	δ	IP/cm^{-1}
CH_3SCN	s (n=4-10)	1.92	80727
	p (n=4-11)	1.58	81071
	d (n=4-11)	1.20	80995
CH_3NCO	s (n=4-11)	1.98	86050
	p (n=4-11)	1.58	86030
	d (n=4-10)	1.23	86217
$(CH_3)_2S$	s (n=4-12)	2.00	70006
	p (n=4-11)	1.60	70236
	d (n=4-11)	1.19	70073

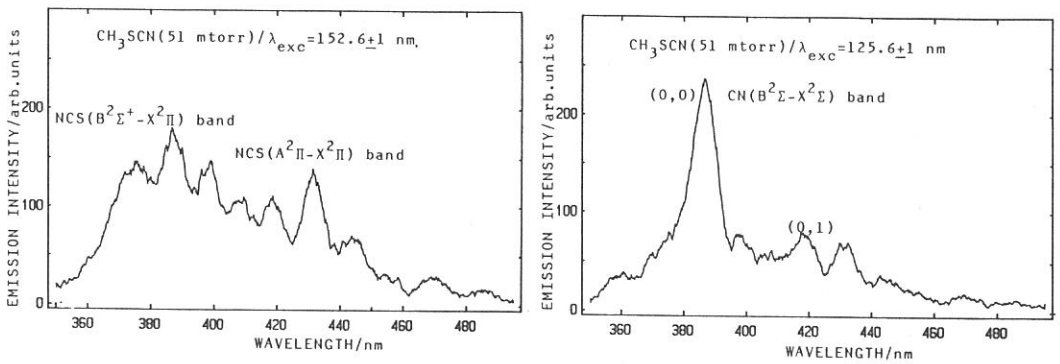

Fig. 2. Emission spectra produced from CH_3SCN at 152.6 nm and 125.6 nm excitation

References: [1] P.D'amario et al., JCS Faraday Trans.I, 68(1972)940. [2] K.Ohbayashi et al., Chem. Phys. Lett., 52(1977)47. [3] J.D.Scott et al., J. Chem. Phys., 59(1973)6577; R. McDiarmid, J. Chem. Phys., 61(1974)274.

DIRECT VUV ABSORPTION MEASUREMENTS OF SUPERSONIC COOLED MOLECULES AND MOLECULAR CLUSTERS

Yohji ACHIBA, Haruo SHIROMARU, and Katsumi KIMURA
Institute for Molecular Science, Myodaiji, Okazaki 444

Investigations of excited state structure and dynamics of molecules are often hindered by limited spectroscopic information available concerning their higher electronic states. Thermal inhomogeneous broadening effects, including sequence band congestion and the overlap of vibronic band rotational envelope, combined with rapid photochemical and photophysical relaxation channels, frequently result in diffuse gas phase absorption spectra displacing little or no vibrational structure.

The technique of supersonic cooling provides a means of producing rotationally and vibrationally cold molecules in the gas phase. Furthermore, recent experimental results have definitely shown that this method is quite useful for producing a large amount of molecular clusters under a collision-free condition.

In this project we have constructed an experimental setup for direct VUV absorption measurements of jet-cooled molecules and molecular clusters. A synchrotron radiation at UVSOR is used as an VUV light source by a 1-m seya monochromator (see also the description on the BL2B2 in the previous section). A gaseous sample is expanded through a pulsed supersonic nozzle ,and then introduced through a skimmer into a photon-melecule interaction region. The SR light is crossed with the supersonic beam, and then detected by a photomultiplier operated at the pulsed frequency. Absorption measurements are performed by operating two pulse counters in our microcomputer system. One of the counters is synchronized with an open phase of the pulsed nozzle, and the other one with closed phase. Such a situation is shown in Figure 1 as a timing chart of the counters. The light intensities of I and I_0 are measured by counters A and B, respectively.

A preliminary experimental result obtained by the present

system is shown in Figure 2. A transmission curve shown in this figure is attributed to the Rydberg series converging to the third ionic state of N_2.

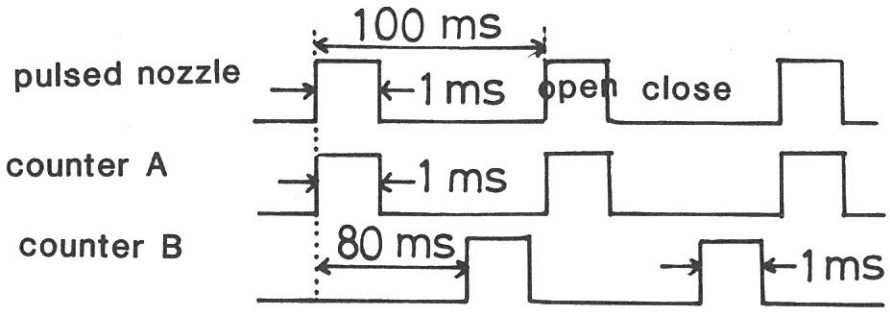

Figure 1 A timing chart of counters A and B as well as a pulsed nozzle.

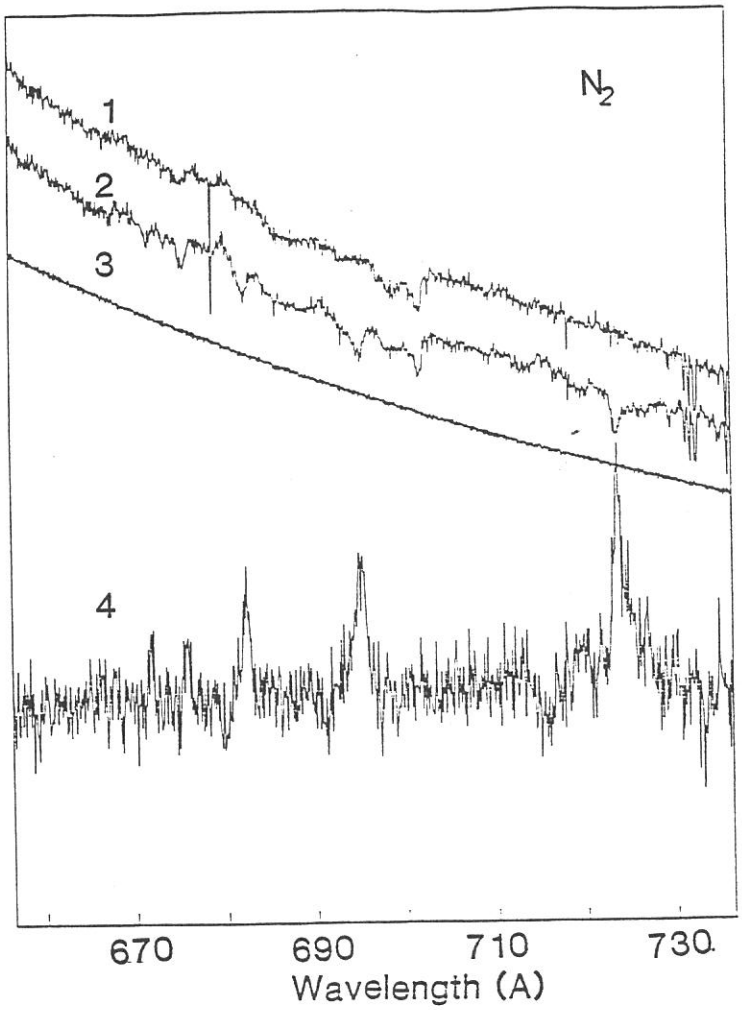

Figure 2

Light intensity curves and a transmission curve of N_2 molecule: Curves 1 and 2 indicate light intensity changes as a function of SR wavelength, where the curve 1 (I_0) is obtained by a counter B, and the curve 2 (I) by a counter B. Curve 3 means an intensity change of an electron beam current. Curve 4 indicates a transmission curve obtained by dividing the curve 2 by the curve 1.

PHOTOIONIZATION OF METHANOL CLUSTERS

Nobuaki WASHIDA*, Yohji ACHIBA, Haruo SHIROMARU, and Katsumi KIMURA

Institute for Molecular Science, Myodaiji, Okazaki 444
*Division of Atmospheric Environment, National Institute for Environmental Studies, Tsukuba-gakuen, Ibaraki 305

The ion molecule reactions of CD_3OH are known to produce ions of $(CD_3OH)H^+$ and $(CD_3OH)D^+$:

$$CD_3OH^+ + CD_3OH \rightarrow (CD_3OH)H^+ + CD_3O \qquad (1a)$$

$$\rightarrow (CD_3OH)D^+ + CD_2OH \qquad (1b)$$

In the present study, Reactions (1a) and (1b) were studied by photoionization of neutral CD_3OH dimer. Fig.1b represents the mass spectrum of CD_3OH clusters photoionized by an Ar resonance lamp (11.83 and 11.62 eV). Signals at m/e=35 and 36 from $(CD_3OH)H^+$ and $(CD_3OH)D^+$, respectively, were observed. Fig.2 summarizes the results of a reduced intensity, $(CD_3OH)_{n-1}D^+/(CD_3OH)_{n-1}H^+$, distributions relative to the cluster size n. In the case of the dimer, the ratio of (1a)/(1b) is 1.2. A question of interest is that the $(CD_3OH)D^+$ is produced from a familiar hydrogen bonded dimer of CD_3OH (A) or another type of dimer (B).

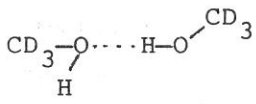

(A)

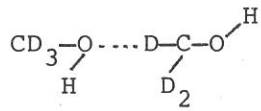

(B)

In order to get an answer, the appearance potentials of $(CD_3OH)H^+$ and $(CD_3OH)D^+$ were measured by using synchrotron orbital radiation. Results are shown in Figs 3 and 4. No significant difference was observed in the photoionization efficiency curves for the $(CD_3OH)H^+$ and $(CD_3OH)D^+$ ions. The results suggest that the precursory dimer of the $(CD_3OH)D^+$ ion is the same as that of the $(CD_3OH)H^+$, probably type A. The deuterium migration may occur in the dimer (A) after ionization.

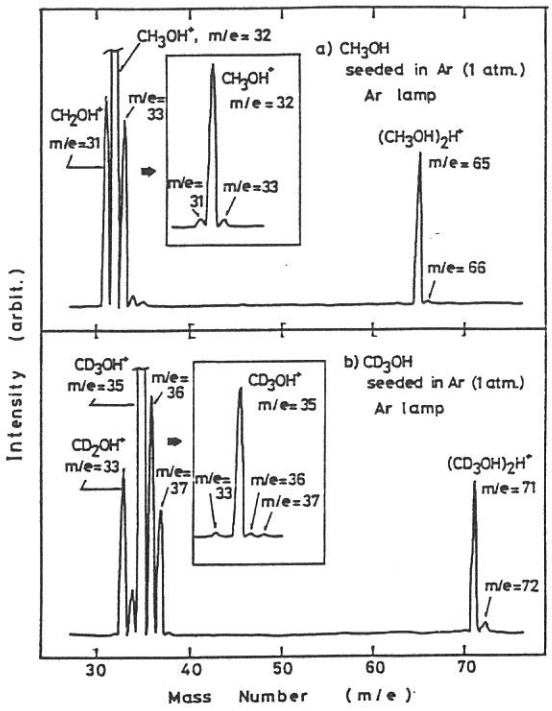

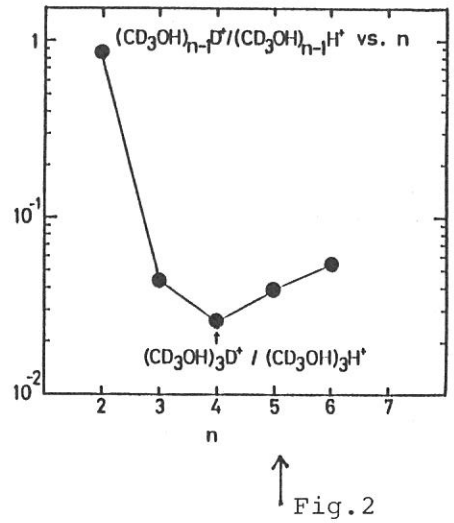

Fig.2

Fig.1

Fig.3

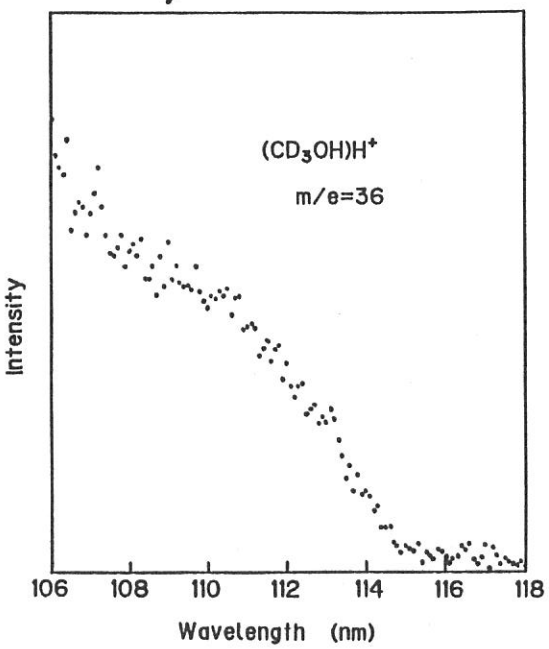

Fig.4

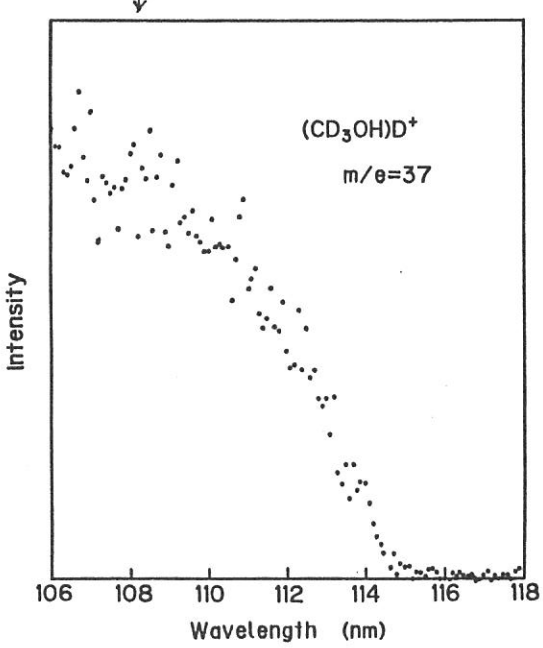

THRESHOLD ELECTRON SPECTRUM AND PHOTOIONIZATION EFFICIENCY CURVE OF CH_3Cl

Shinzo SUZUKI and Inosuke KOYANO

Institute for Molecular Science, Myodaiji, Okazaki 444

Using the TEPSICO-II apparatus described elsewhere,[1,2] we have investigated the threshold electron spectrum (TES) and photoionization efficiency curve (PIEC) of CH_3Cl over the wavelength range from 40 to 120 nm. The ultimate goal here is the state- or internal energy-selected studies of unimolecular and bimolecular processes of molecular ions, utilizing a coincidence measurements of various ions with threshold electrons.

Figure 1 shows the threshold electron spectrum of CH_3Cl taken with the incident photon resolution of about 0.02 nm. Four major bands are clearly seen; the complex first band which is assigned to the ^2E ground state of the ion, the broad structureless second and third bands which respectively correspond to the removal of a σa_1 and π_e electron, and the weak fourth band which has not been observed in the He I photoelectron spectra because of its energy. Compared with the He I spectra,[3] the second and third bands are seen to be relatively much stronger in the TES.

Ions observed in the wavelength range studied are parent ion CH_3Cl^+ and two fragment ions CH_3^+ and CH_2Cl^+. In Fig. 2 we present an ionization efficiency curve for the CH_3^+ fragment. The weak broad peak above 900 nm

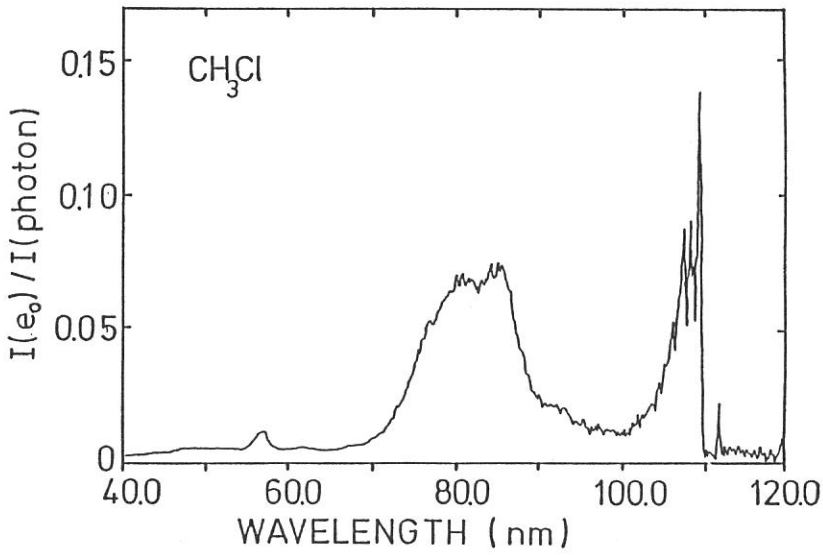

Fig. 1 Threshold electron spectrum of CH_3Cl

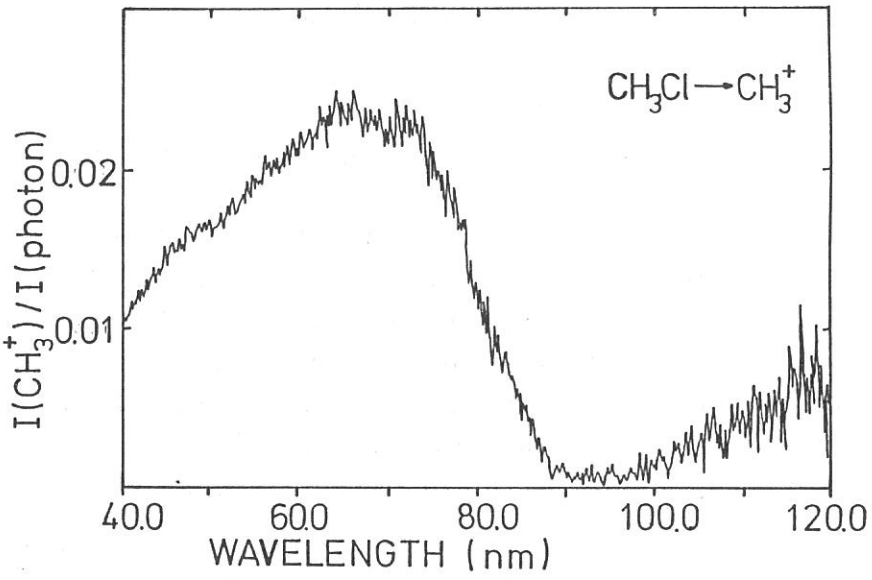

Fig. 2 Photoionization efficiency curve for CH_3^+ from CH_3Cl

corresponds to the ion - pair process $CH_3Cl + h\nu \rightarrow CH_3^+ + Cl^-$, whose cross section decreases monotonically toward the first ionization onset of the molecule. No rise in the CH_3^+ efficiency is seen at the ionization onset nor at any wavelength in the range corresponding to the formation of the ground state ions, indicating that ions in this state are nondissociative. The second huge peak in the PIEC starts to rise at about 90 nm , the wavelength that exactly coincides with the onset of the second band in the TES, and keeps rising throughout the region of the second and third TES bands, until it reaches a maximum at 65 - 70 nm where no threshold electrons are observed. All these facts indicate that CH_3^+ is produced through excitation to the second and/or third electronic state(s) of the parent ion and that this excitation is most efficiently accomplished by photons of somewhat shorter wavelengths than the thresholds. It is not certain, on the other hand, whether the fourth state is dissociated to give CH_3^+ or not. The coincidence experiments with these threshold electrons would shed light to these problems.

References

1 I. Koyano, K. Tanaka, T. Kato, and E. Ishiguro, in this Report.
2 I. Koyano, K. Tanaka, T. Kato, S. Suzuki, and E. Ishiguro, Nucl. Instr. Meth., in print (1986).
3 D. W. Turner, C. Baker, A. D. Baker,and C. R. Brundle, Molecular Photoelectron Spectroscopy (Wiley - Interscience, New York, 1970); K. Kimura, S. Katsumata, Y. Achiba, T. Yamazaki, and S. Iwata, Handbook of He I Photoelectron Spectra of Fundamental Organic Molecules (Japan Scientific Society, Tokyo, 1981).

INVESTIGATION OF DEEP VALENCE AND CORE LEVEL EXCITATION IN VOLATILE COMPOUNDS WITH GROUP IV ELEMENTS USING UVSOR

Shin-ichi NAGAOKA, Shinzo SUZUKI and Inosuke KOYANO

Institute for Molecular Science, Myodaiji, Okazaki 444

Shallow valence level excitation and the subsequent fragmentation of many molecules have been studied extensively using several kinds of light sources in recent years. However, the processes following deep valence and core level excitation have not been investigated in detail so far, because, for the purposes of such investigations, the conventional light sources are insufficient in both photon energy and intensity. The synchrotron radiation is expected to provide a powerful means to obtain information about the deep level excitation. Volatile compounds with group IV elements are particularly suitable for detailed investigations of the above-mentioned processes in the vapor phase, because the rather small binding energies of the d core levels allow the studies in the normal incidence region. Accordingly, we have initiated the studies of the deep valence and core level excitation and the subsequent fragmentation in such compounds, using UVSOR. Here, we report preliminary observations of threshold electron spectra of $Sn(CH_3)_4$ and $GeCl_4$ in the wavelength range between 30 and 65 nm.

The experiments were performed using the TEPSICO-II apparatus at BL3B, which has a 3m normal incidence monochromator. The threshold electron spectra were obtained by dividing the threshold electron intensity by that of the exciting light. Experimental results are shown in Fig. 1.

In Fig. 1 the solid line represents the threshold electron spectrum of $Sn(CH_3)_4$, which was taken with the slit width of 0.2 mm. The bands located at 40.0 and 42.4 nm (31.0 and 29.2 eV, respectively) are assigned to the $4d_{3/2}$ and $4d_{5/2}$ core levels, respectively. The 4d core binding energy obtained is in good agreement with that estimated by X-ray

photoelectron spectroscopy (30.4 eV).[1] The band at 58.7 nm (21.1 eV) is considered to be related to the a_1 and/or t_2 molecular orbital(s).

In Fig. 1 the dotted line represents the threshold electron spectrum of $GeCl_4$, which was taken with the slit width of 0.3 mm. The band located at 33.9 nm (36.6 eV) is tentatively assigned to the $3d_{5/2}$ core level. Since the photon intensity of the monochromatized light is weak in the wavelength range below 35 nm, we cannot determine the 3d core binding energy unambiguously. The bands at 51.9 and 59.8 nm (23.9 and 20.7 eV, respectively) are considered to be related to the a_1 and t_2 molecular orbital(s), respectively.

Further investigations, including the threshold electron - fragment ion coincidence measurement, are in progress.

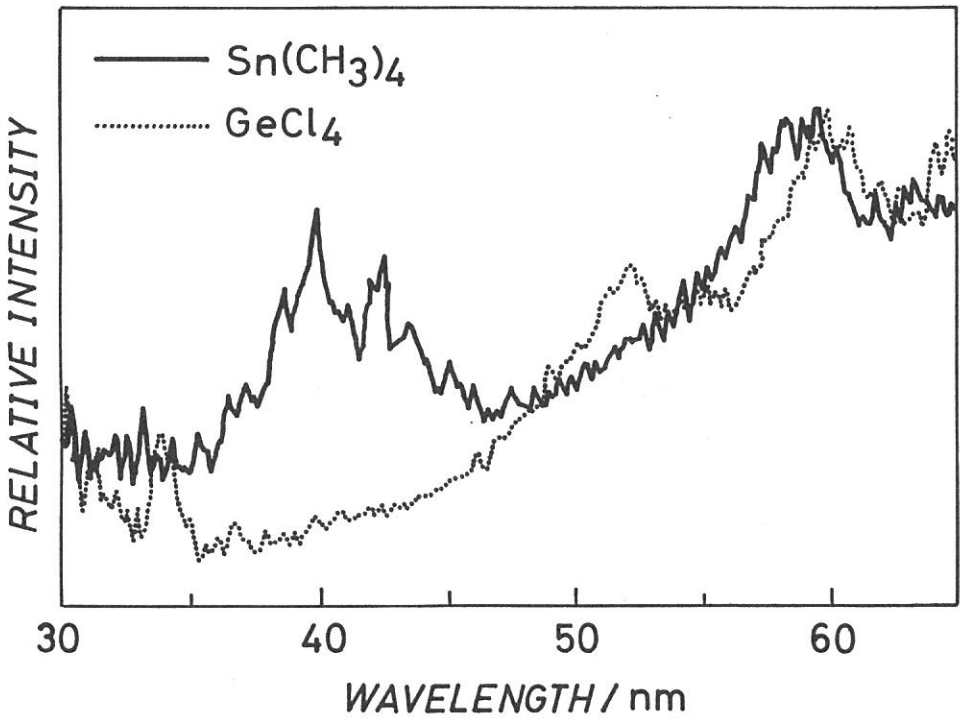

Fig. 1 Threshold electron spectra of $Sn(CH_3)_4$ and $GeCl_4$

Reference

1. S. C. Avanzino and W. L. Jolly, J. Electron Spectrosc. Relat. Phenom., 8 (1976) 15.

Polarized Reflection Spectra of Orthorhombic Indium Bromide in 2 - 100 eV Region

Kaizo NAKAMURA, Yasuo SASAKI, Makoto WATANABE* and Masami FUJITA+

Department of Physics, Kyoto University, Kyoto 606
*Institute for Molecular Science, Okazaki 444
+Maritime Safety Academy, Kure 737

Reflection spectra of orthorhombic indium bromide crystal (InBr: space group D_{2h}^{17}) have been investigated at LHeT by using synchrotron radiation and its polarization characteristics in the energy region between 2 and 100 eV. Single crystal of InBr was grown by Bridgman method which was cleaved into thin slabs with ac-surface. Two platelets of InBr were mounted on the sample holder of cryostat to get polarized reflection spectra. Light from 600 MeV storage ring was monochromatized with the plane grating monochromator (PGM) at BL6A2. Energy range 2 - 100 eV can be covered with five spectral ranges with the combination of two gratings and five mirrors. Vacuum in the sample chamber was kept less than 10^{-9} Torr. Incident and reflected light was detected with a photomultiplier coated with sodium salicylate, which is rotatable around the specimen.

Figure 1(a) shows the spectra for polarization parallel to the c-axis (E//c) and (b) for the a-axis (E//a). They are highly dichroic reflecting the anisotropy of the crystal.

In the low energy region (2 - 4 eV), both spectra are consistent with the previous results.[1] The first exciton peak at 2.33 eV is due to the transition from the top valence band, which consists mainly of In 5s orbital, to In 5p conduction band bottom. This transition is allowed for E//c.

Structure between 3 and 15 eV is classified into 2 groups: One from Br 4p valence band, lying in the lower energy region, and the other from In 5s valence band. Identification of each fine structure rests much upon the development of the band structure

calculation involving the spin-orbit interaction. Above 10 eV intensity begins to diminish.

At about 20 eV sharp doublet structure with the separation of 0.8 eV are observed in both spectra. These are identified as In 4d core exciton (In N_V and N_{IV}).[2] These are also dichroic and composed of 5 components altogether. Possible transitions inferred from the atomic picture of In^+ in the C_{2v} environment cannot explain the dichroic nature clearly. It is necessary to get more detailed information of the covalent character of the In in the TlI crystal structure. At about 75 eV a broad structure is observed resulting possibly from core levels of both In and Br.

References

1) M. Yoshida, N. Ohno, H. Watanabe, K. Nakamura and Y. Nakai: J. Phys. Soc. Jpn 53 (1984) 408.
2) J. A. Bearden and A. F. Burr: Rev. Mod. Phys. 39 (1967) 125.

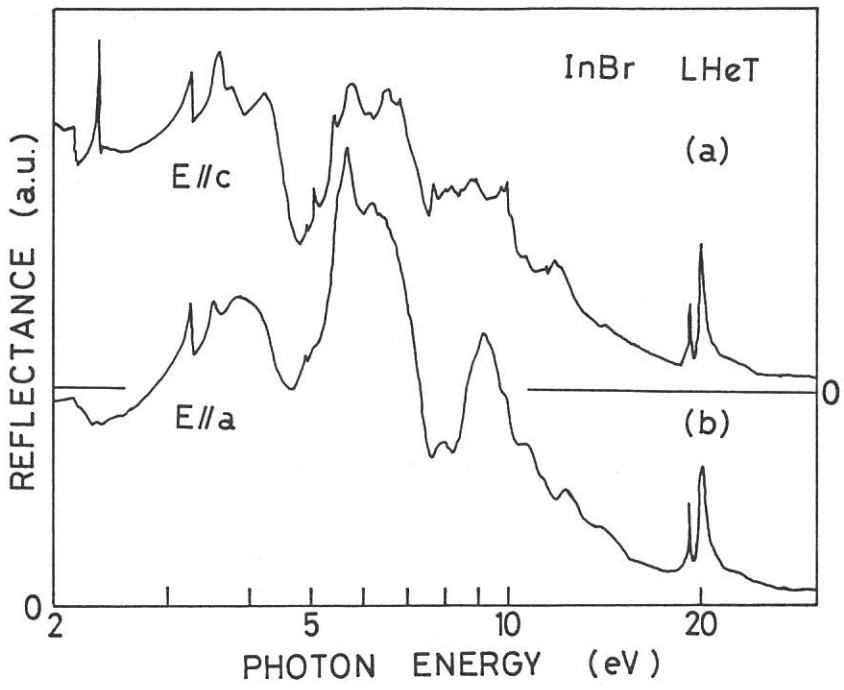

Fig. 1. Reflection spectra of InBr at liquid helium temperature. (a) for E//c and (b) for E//a.

Reflection and Luminescence Excitation Spectra of Cadmium Halide Crystals

Hideyuki NAKAGAWA, Yukio SHIMAMOTO*, Hiroaki MATSUMOTO*, Masami FUJITA**, Takeshi MIYANAGA***, Kazutishi FUKUI and Makoto WATANABE

Institute for Molecular Science, Myodaiji, Okazaki 444
* Department of Electronics, Fukui University, Bunkyo, Fukui 910
** Maritime Safety Academy, Wakaba, Kure 737
*** Department of Physics, Faculty of Education, Wakayama University, Sakaedani, Wakayama 640

Reflection and luminescence excitation spectra in cadmium bromide and iodide crystals were measured at 5 K and 78 K using synchrotron radiation from SOR-RING of IMS as a light source for the energy range up to 100 eV. The SR was monochromatized with a plane grating monochromator and was incident on the crystal nearly along the crystal c-axis.

Two groups of well resolved structures are observed at 5 K in the reflection spectra below 10 eV as shown in Fig. 1. These structures are almost the same as those previously reported by Kondo et al.(1) and by Lemonnier et al.(2). They are interpreted as due to the excitonic transitions associated with those from the upper valence band of halogen p-like character to the lowest conduction band of cadmium s-like character. Structures in the low and the high energy groups are connected to the excitonic transitions at the Γ point and at the Z ($CdBr_2$) or A (CdI_2) point in the BZ, respectively.

In the higher energy region from 10 to 15 eV appear several less pronounced structures, the origins of which are not clear at present. The excitonic and the band-to-band transitions from the halogen s-like states to the higher p-like conduction states may be related to these structures.

Doublet structures are observed clearly at 15.67 and 16.35 eV in $CdBr_2$ and at 15.13 and 15.83 eV in CdI_2 as shown in Fig. 2. These structures are connected to the Cd^{2+} $N_{IV,V}$ core excitonic transitions, that is, the optical excitation from the Cd^{2+} $4d_{5/2}$ and $4d_{3/2}$ states to the upper conduction states of cadmium 5p-like character. The splitting energies of the doublets are 0.68 eV in $CdBr_2$ and 0.70 eV in CdI_2 and are considered to correspond to the $N_{IV,V}$ splitting energy of the cadmium atom, ~1.0 eV. The chemical shift

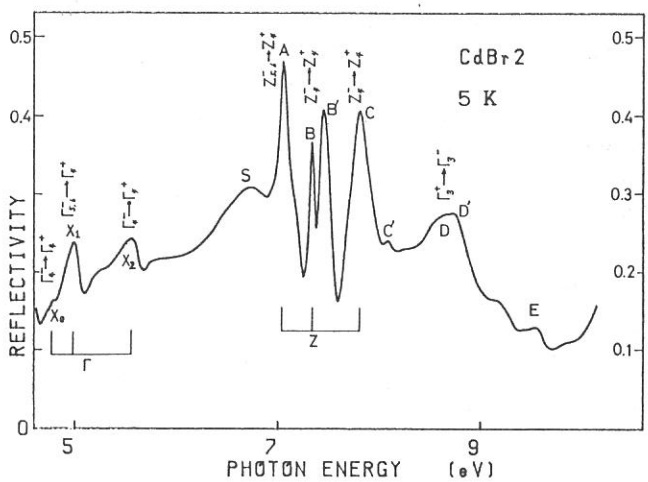

Fig.1 Nearly normal incidence optical reflectivity spectrum of the cleaved surface of $CdBr_2$ single crystals measured at 5 K in the energy region below 10 eV.

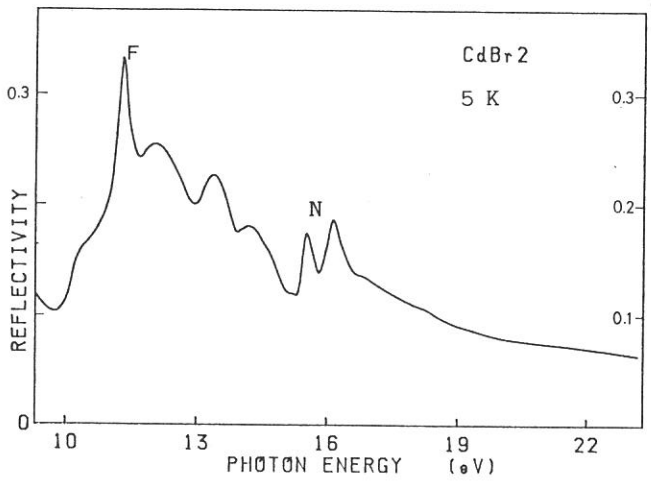

Fig.2 Nearly normal incidence optical reflectivity spectrum of the cleaved surface of $CdBr_2$ single crystals measured at 5 K in the energy region from 10 to 22 eV. The doublet structure indicated by the label N is considered to be due to the cadmium d-core excitons.

of the structures between bromide and iodide are likely to be due to the mixing of the halogen p-orbitals to the upper conduction states. Several substructures are also discernible on and around the doublets. They are attributed to the crystal field splitting arising from the axial symmetry of the cadmium halide crystals. Dichroic measurements will reveal more detailed structures of the core excitons.

It was not possible in the present experiments to resolve reliable structures due to the halogen inner core excitonic transitions which are expected to appear in the energy region from 30 to 100 eV.

Luminescence excitation spectra were measured at 5 K in the direction perpendicular to the crystal c-axis. At this temperature, it is well known that the only one emission band appears in the near ultraviolet region; at 3.30 eV in $CdBr_2$ and at 3.36 eV in CdI_2. In the excitation spectra below 20 eV are observed sharp dips corresponding to the peaks in the reflection spectra. Relative intensity of luminescence is enhanced with increase of the excitation energy in the region from 10 to 20 eV. The first stage of the increase begins at about 9.8 eV which corresponds to the double energy of the lowest excitons. The onset of the second stage is observed as a rapid increase in the intensity at around 13 eV which is over double the energy of the band-to-band gap. The abrupt increase of the luminescence intensity suggests the existence of multiple exciton production processes (3). More quantitative experiments on luminescence yield are nescessary to make further discussions on these processes.

In the higher energy regions up to 100 eV, no clear structures are observed and the luminescence intensity is almost independent of the excitation energy. Irradiation in these regions produces a new emission band at 1.5 eV in the CdI_2 crystal, which may be connected to the defect production caused by the high energy light irradiation.

References

(1) S.Kondo and H.Matsumoto: J.Phys.Soc.Jpn. 51 (1982) 1441.
(2) J.C.Lemonnier, I.Pollini, J.Thomas and A.Lenselink: 7-th International Conference on VUV, p252.
(3) M.Yanagihara, Y.Kondo and H.Kanzaki: J.Phys.Soc.Jpn. 52 (1983) 4397.

RARE-EARTH $N_{4,5}$ ABSORPTION SPECTRA OF SOME RARE-EARTH COMPOUNDS

Kenjiro TSUTSUMI, Osamu AITA, Kouichi ICHIKAWA,
Masao KAMADA, and Makoto OKUSAWA

College of Engineering, University of Osaka Prefecture,
Mozu, Sakai, Osaka 591

The electronic property of rare-earth compounds and alloys containing a partially filled 4f shell has been a subject of theoretical and experimental studies because the rare-earth ions in some of these substances are in a homogeneous mixed-valence state. Among these substances SmB_6 is known to be a typical example, and the investigation of mixed-valence system of this substance has been performed by many experimental methods such as x-ray photoelectron spectroscopy (XPS)[1] and Sm L absorption spectroscopy.[2]

In the $N_{4,5}$ absorption spectra of rare earths sharp structures appear near the threshold. These structures are interpreted as originating from the electronic transition of the 4d electron to the localized unoccupied 4f level. Because of a strong exchange interaction between the $4f^{n+1}$ electrons and the 4d hole, the resultant multiplet levels of the $4d^9 4f^{n+1}$ configuration spread over several tens of electron volts. The purpose of the present study is to investigate whether the Sm $N_{4,5}$ absorption spectrum of a mixed-valence compound SmB_6 represents the multiplet structures originating from the Sm^{2+} and Sm^{3+} ions or not. Also, the $N_{4,5}$ absorption spectra of rare-earth compounds, LaB_6, $LaCl_3$, $CeCl_3$, $SmCl_3$, $EuCl_3$, and $GdCl_3$, were measured for references.

A grazing incidence vacuum spectrometer equipped with a concave grating with the radius of 2 m and the grooves of 1200/mm was used for the measurement. The synchrotron radiation from the storage ring at the Institute for Molecular Science was used as a light source.

Fine structures of the Sm $N_{4,5}$ absorption spectrum of a mixed-valence compound SmB_6 are shown in the figure together with those of $SmCl_3$ which is

believed to be a trivalent substance. The constant-initial-state(CIS) spectra measured by Allen et al.[3] with the initial states at the $4f^6(Sm^{2+})$ and $4f^5(Sm^{3+})$ peaks in the valence band of SmB_6 are also shown by dotted lines. These CIS spectra are believed to represent the 4d photoabsorption structures of the Sm^{2+} and Sm^{3+} ions. The arrows show the 4d ionization thresholds of the Sm^{2+} and Sm^{3+} ions determined by XPS data. As seen from this figure the gross features of the Sm $N_{4,5}$ absorption spectra of SmB_6 and $SmCl_3$ and the CIS spectrum for the Sm^{3+} ion are quite similar one another. This fact suggests that the absorption spectrum of SmB_6 is dominantly attributed to the 4d excitation of the Sm^{3+} ion.

In the case of Sm^{2+} ion the $4d^9 4f^7$ final state caused by the 4d photoabsorption is clearly above the 4d threshold of the Sm^{2+} ion as seen from the CIS spectrum for the Sm^{2+} ion. Therefore, since the final state of the absorption process in the Sm^{2+} ion might involve the $4d^9 4f^n$+(unbound electron in the continuum) state, the structure due to the $4d^9 4f^{n+1}$ excited state is buried in the broad background and this prevents the spectrum from appearing as distinct peaks. While, the CIS spectrum provides the structure only due to the decay, $4d^9 4f^{n+1} \rightarrow 4d^{10} 4f^{n-1}$ + (ejected electron), among the various final states caused by the photoabsorption, and thus the structure due to the Sm^{2+} ion is clearly seen in the CIS spectrum.

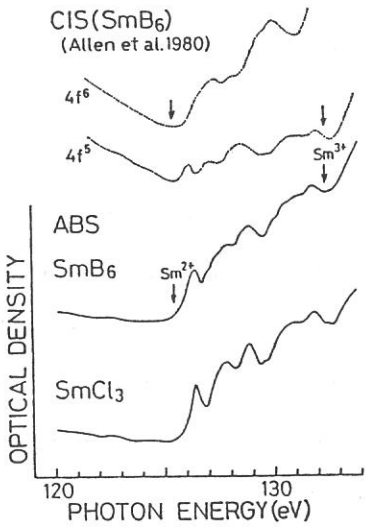

Fig. Fine structures of the Sm $N_{4,5}$ absorption spectra of SmB_6 and $SmCl_3$ and the CIS spectra of SmB_6. Arrows show the 4d ionization thresholds of the Sm^{2+} and Sm^{3+} ions.

References

1) J. -N. Chazalviel, M. Campagna, G. K. Wertheim, and P. H. Schmidt: Phys. Rev. B 14, 4586(1978).
2) M. Okusawa, Y. Iwasaki, K. Tsutsumi, M. Aono, and S. Kawai: Jpn. J. Appl. Phys. 17, Suppl. 17-2, 161(1978).
3) J. W. Allen, L. I. Johansson, I. Lindau, and S. B. Hagstrom: Phys. Rev. B 21, 1335(1980).

Time-Resolved Fluorescence Spectroscopy of Molecular Exciton in Anthracene Single Crystals

Tadaoki MITANI, Takaya YAMANAKA and Iwao YAMAZAKI

Institute for Molecular Science, Myodaiji, Okazaki 444, Japan

Synchrotron radiation from storage ring has a number of advantages as a light source for time-resolved fluorescence and excitation spectroscopies. A high repetition rate of the pulsed time structure enables us to measure a precise subnanosecond time decay by using a time-correlated single-photon counting system. By using an improved 1 m Seya-Namioka type monochromator (see the BI-7B report), we have constructed a computer-aided spectrophotometer available for time-dependent fluorescence and excitation measurements in an energy region of 2-40 eV. The block diagram of this apparatus is shown in Fig. 1. The application of this system to the spectral analysis of fluorescence in anthracene single crystals have been successfully made.

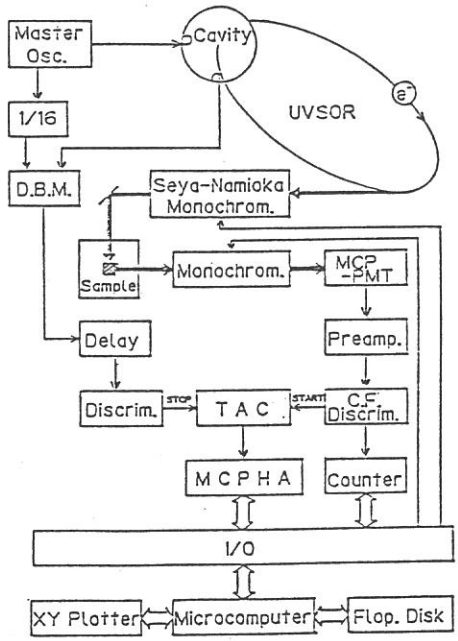

Fig. 1

The time decay of the fluorescence of the singlet exciton in anthracene single crystals exhibits a characteristic dependence on wavelength of the excited light pulse as shown in Fig. 2. For an excitation at a relatively long wavelength, the time decay follows a single-exponential function in more than 3 orders. The life time of the singlet exciton is definitly determined to be 8.6 nsec at 77 K, which is agreement with the previous data. Whereas, by scanning excitation photons to much shorter wavelength, the time decay is remarkably changed and its profile can not be expressed by a single-exponential curve. In addition, the rise time of the emission becomes much faster than the time resolution of the instruments (< 100 psec). Such a characteristic feature of the time decay is clearly reflected in the time-resolved fluorescence spectra in a short time-domain of a few nanosecond as presented in Fig. 3. The spectra of the prompt emission observed within about 300 psec have a simple structure having a tail in a lower energy side. As time going on, the spectrum has more clearly vibrational structures. Then the pectra after about 100 psec are almost independent on time and closely resemble the stationary fluorescence. Thus, the radiative process of the prompt emission is considered to be essentially

different from thcse of the delayed fluorescence in a thermally equilibrium. This implies the presence of an additional radiative-decay channel fcr the higher energy excitations above the threshcld energy of about twice of the excitcn energy.

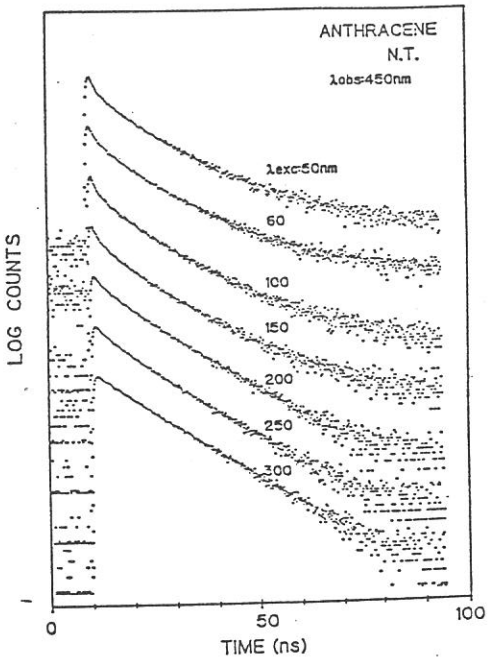

Fig. 2 The time decays of the flucrescence of anthracene crystals at 77 K as a function of excitation wavelength.

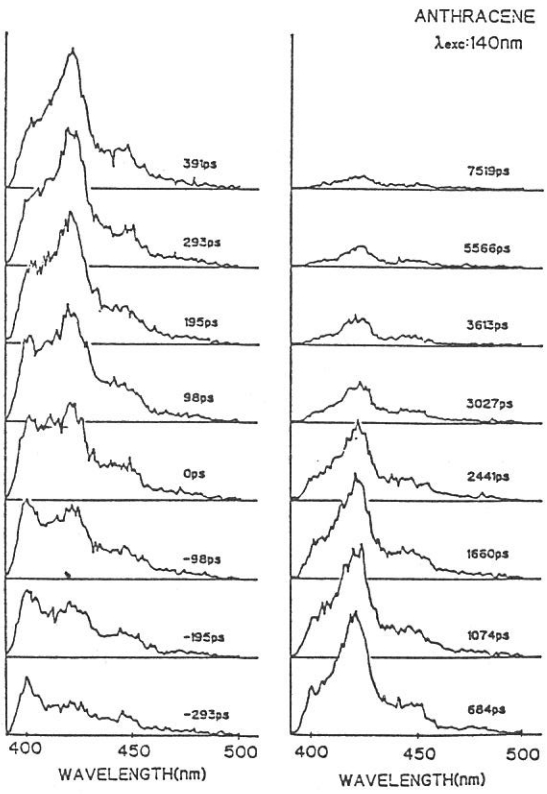

Fig. 3 The time-resclved fluorescence spectra of anthracene crystal at 77 K.

MEASUREMENT OF THE FLUORESCENCE DECAY CURVE USING UVSOR LIGHT PULSE

Tadashi OKADA, Kiyoharu NAKATANI, and Tadaoki MITANI*

Department of Chemistry, Faculty of Engineering Science,
Osaka University, Toyonaka 560
*Institute for Molecular Science, Myodaiji, Okazaki 444

One of the target of interest in photochemical primary processes in condensed phase is to know the dynamical behavior and the relaxation pathways of highly excited molecules in solution which is also studied in the field of radiation chemistry as well as multiphoton laser chemistry.

For the developments of the time resolved detection system using synchrotron radiation in the UV and VUV region, the fluorescence lifetime of the standard compounds were measured by using a time correlated single photon counting electronics coupled with a micro-channel-plate photomultiplier as a detector. Measurements were carried out under the condition of multi-bunch operation of storage ring. An example of the decay curve is illustrated in Figure 1. The time resolution obtained using this system is about 100 ps and has been limited by the walk of timing.

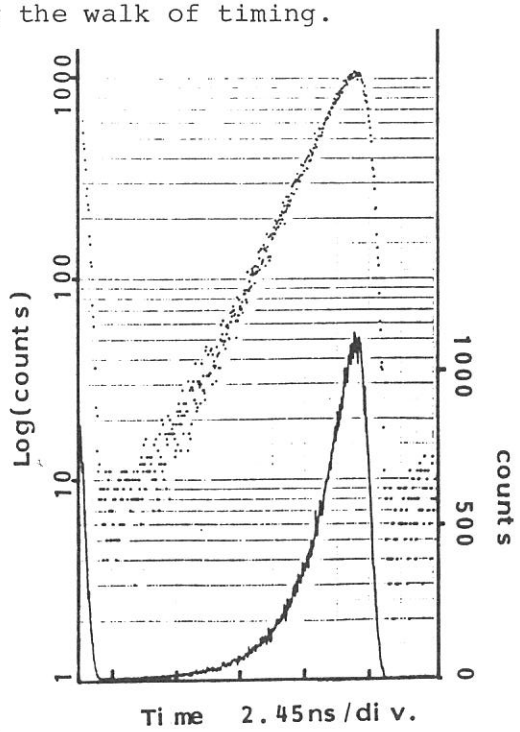

Figure 1. Decay curve of Rhodamine B in aqueous solution. The obtained lifetime was 1.56 ns without deconvolution.

As an application of time resolved spectroscopy to the study of the photoinduced intramolecular electron transfer process in fixed donor-acceptor system, the temperature dependence of the fluorescence decay curve of 4-(N,N-dimethyl aminophenyl)$(CH_2)_2$(9-anthryl) (A_2) in cellulose acetate film has been measured (Figure 2). The results are compared with those obtained by using a streak camera under excitation with picosecond laser pulse.

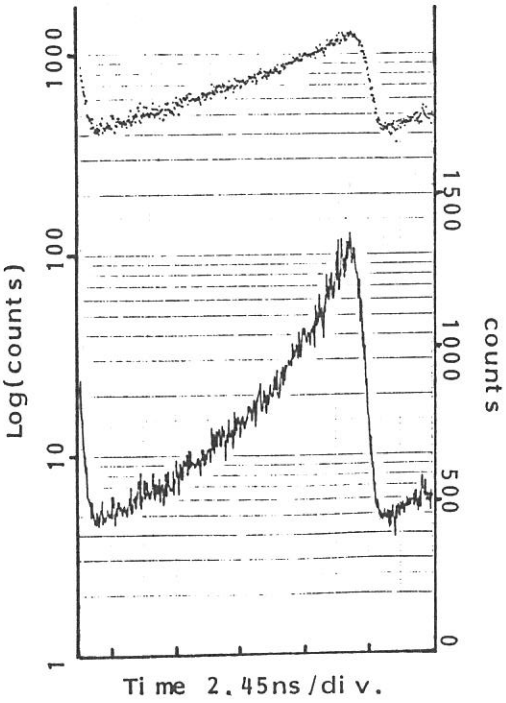

Figure 2. Non-exponential decay curve of the fluorescence of anthracene part of A_2 in cellulose acetate film at 300K.

MEASUREMENTS OF TIME BEHAVIOR OF TRYPTOPHYL FLUORESCENCE BY TIME-CORRELATED SINGLE-PHOTON COUNTING

Atusi KURITA, Shuichi KINOSHITA, Takashi KUSHIDA,
Yuji GOTO, Kozo HAMAGUCHI, and Tadaoki MITANI*

Faculty of Science, Osaka University, Toyonaka 560
* Institute for Molecular Science, Okazaki 444

The combination of highly sensitive single-photon counting and synchrotron radiation pulses having short duration, stable intensity and high repetition rate is considered to be very suitable for the UV spectroscopy with high time resolution and high precision. In order to confirm this, we performed measurements of the decay characteristics of tryptophyl fluorescence by combining UVSOR with our time-correlated single-photon counting system. It is known to be possible with this system to determine a fluorescence decay time as short as several picoseconds by using a CW mode-locked laser as the exciting source.

First, the time profile of the synchrotron radiation pulse was determined. The pulse duration was found to be about 400 ps, which is much narrower than that reported for the Stanford positron-electron accelerator ring of 650 ps. Next, we measured the time behavior of tryptophyl fluorescence around 340 nm in N acetyl-L-tryptophanamide and the constant (C_L) fragments of the immunoglobulin light chain. It was found that the fluorescence intensity shows a single exponential decay in the former, while it has two decay components in the type λ fragment (Figs.1 and 2). The fluorescence time behavior did not change appreciably in both materials, when the excitation wavelength was varied between 220 and 300 nm. The time characteristics of fluorescence depolarization was also obtained successfully.

The constant fragment of immunoglobulin is an interesting material, because it shows no great conformational change on reduction of the only intrachain disulfide bond, which is buried in the interior hydrophobic region. As shown in Fig.3, the fluorescence decay time was found to be lengthened by the reduction of the type λ fragment. This fragment contains two tryptophan residues: one locating close to the disulfide bond, and the other near or on the surface of the protein molecule. On the other hand, the intact type κ fragment, which has only one

tryptophan residue deep inside the molecule, is almost nonfluorescent. When the disulfide bond is reduced, it fluoresces, and its time behavior was found to be very similar to that of the reduced type λ fragment (Fig.4). These results are well explained by the removal of the fluorescence quenching effect of the energy-accepting intrachain disulfide bond.

Although the detailed analysis has not been made yet, the comparison of the time characteristics of the fluorescence anisotropy between the intact and reduced fragments will give valuable information on the internal rotational motions within these macromolecules. Besides the knowledge on the time behavior of tryptophyl fluorescence in proteins, the present experiment demonstrated various advatages of the fluorescence spectroscopy by the combination of UVSOR and the time-correlated single-photon counting technique, such as the high sensitivity, high time resolution, high precision, promptness of the measurement, and tunability of the exciting wavelength.

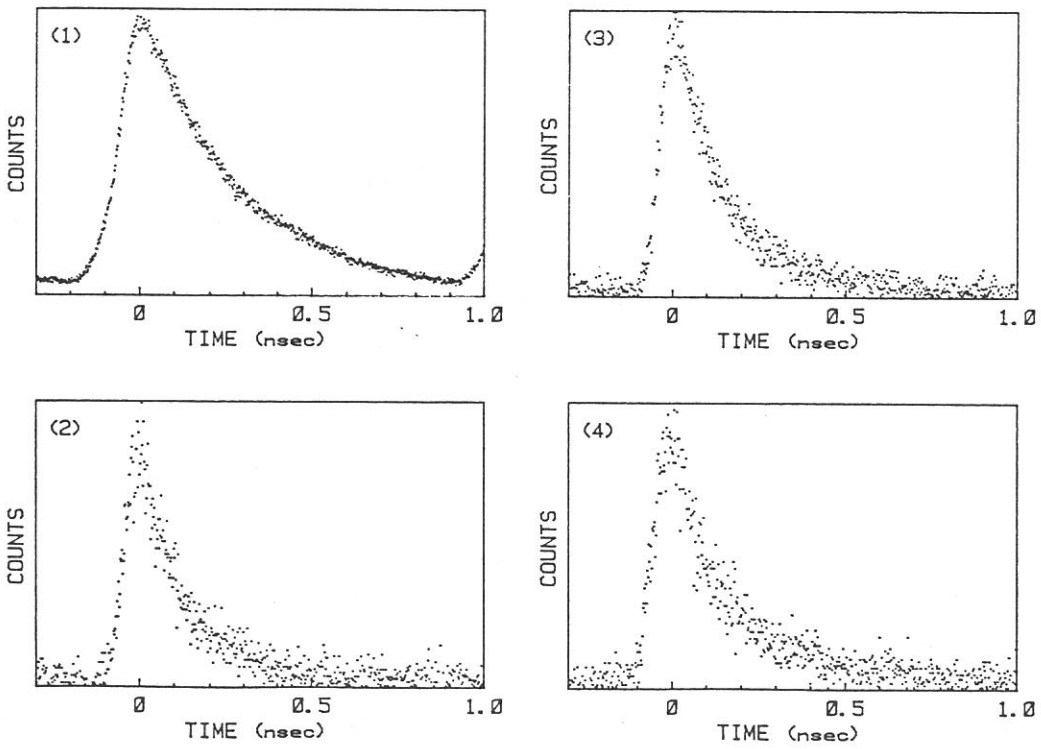

Time behavior of tryptophyl fluorescence of (1) N acetyl-L-tryptophanamide, (2) intact type λ C_L fragment, (3) reduced type λ fragment, and (4) reduced type κ fragment.

PHOTON STIMULATED DESORPTION OF POSITIVE IONS FROM LIF

Tsuneo YASUE, Tetsuji GOTOH*, Ayahiko ICHIMIYA, Yoichi KAWAGUCHI*, Masahiro KOTANI*, Shunsuke OHTANI*, Yukichi SHIGETA*, Shoji TAKAGI*, Yuji TAZAWA* and Goroh TOMINAGA*

Department of Applied Physics, Nagoya University, Nagoya 464
*Institute of Plasma Physics, Nagoya University, Nagoya 464

Resently several observations of photon stimulated desorption (PSD) from alkali halides have been carried out[1-3]. In this paper, we report on the measurements of positive ion yields from LiF as a function of the incident photon energy (the ion yield spectrum), and discuss the mechanism of PSD from LiF.

The experiments were carried out on BL8B2 of UVSOR. LiF (100) surface was cleaved in the air, and the specimen was mounted in a UHV chamber. The sample was heated to about 150 °C to avoid electronic charging during the measurements. The relative photon intensity was measured by the photoelectron ejection from Au. The relative ion yield was normalized with the relative photon intensity.

Figures 1(a) and 1(b) show the relative ion yield spectra of Li^+ and F^+ ions. In Fig. 1(a) there is a rapid rise of ion yield at about 56 eV, and is a weak peak at 58.4 eV. The ion yield increases above 59 eV, and is almost constant up to 67 eV. The spectrum of F^+ ions is similar to that of Li^+ ions below 60 eV. However the considerable difference in the yield spectra is observed above 60 eV. There are a sharp peak at 60.2 eV and a deep valley at 63.5 eV in the F^+ yield spectrum.

In order to consider the mechanism of PSD from LiF, we compare the yield spectra with the photoabsorption spectrum[4]. The rapid rise at about 56 eV and the structure at 58.4 eV is also seen in the photoabsorption spectrum. Those structures are ascribed the core excitation of $Li^+(1s)$ state. Then following two different interatomic transitions are considered;

$$Li^{+*} + F^- \longrightarrow Li^{0*} + F^+ + e^- \qquad (1)$$

and

$$Li^{+*} + F^{-} \longrightarrow Li^{+} + F^{0} + e^{-}, \qquad (2)$$

where asterisks indicate the core-excited states. The Madelung constant for the final state of eq. (1) is negative and that of eq. (2) is positive. Therefore the process of eq. (1) is dominant for PSD of positive ions from LiF. Either Li^{+} or F^{+} ions can desorb from the surface by the Coulomb repulsive force between a F^{+} ion and the first nearest Li^{+} ions. Since the residence time near the surface of Li^{+} ions is shorter than that of F^{+} ions, the difference in the spectra might be explained due to the re-neutralization probability of Li^{+} and F^{+} ions. However it is difficult to explain the structure of the F^{+} yield spectrum above 60 eV, since this probability should not depend on the photon energy.

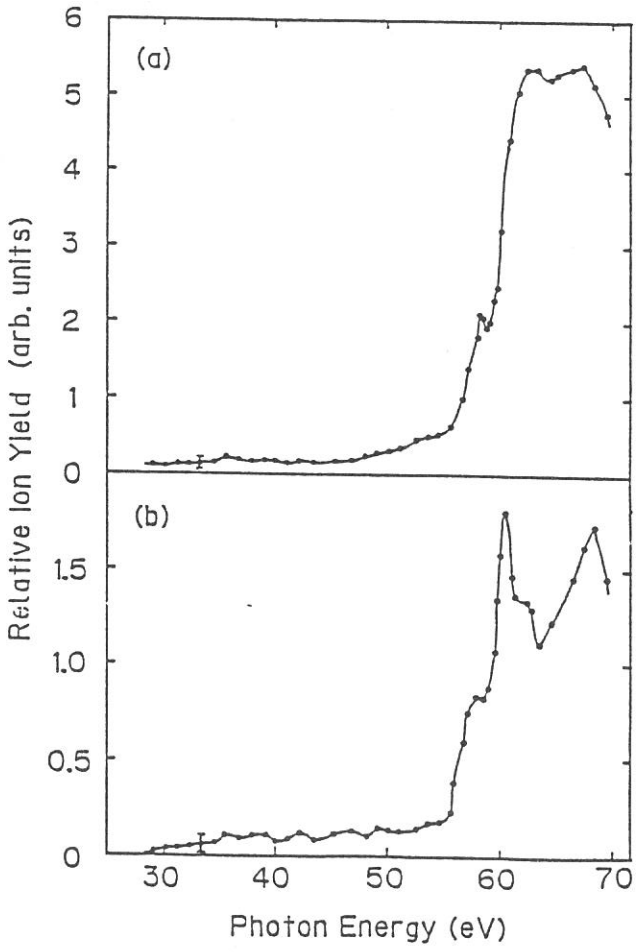

Fig. 1. Relative ion yield spectra. (a): Li^{+}, (b): F^{+}.

References

1) T.R. Pian et al., Surf. Sci. 128 (1983) 13.
2) C.C. Parks et al., Phys. Rev. B28 (1983) 4793.
3) C.C. Parks et al., Phys. Rev. B29 (1984) 4709.
4) B.F. Sonntag, Phys. Rev. B9 (1974) 3601.

FABRICATION OF X-RAY OPTICAL ELEMENTS BY SYNCHROTRON RADIATION X-RAY LITHOGRAPHY

Hiroaki ARITOME

Faculty of Engineering Science, Osaka University
Toyonaka, Osaka 560

I. Introduction

The advantage of synchrotron radiation as a source for x-ray lithography for LSI production is now well established. Synchrotron radiation x-ray lithography (abbreviated here as SR lithography) is a powerful tool also for fabricating x-ray optical elements such as transmission gratings and zone plates.

Elements of present interests are:

1) Transmission gratings for diagnostics of plasma of the laser nuclear fusion, space telescopes and synchrotron radiation spectroscopy.
2) Zone plates for diagnostics of plasma of the laser nuclear fusion, x-ray microscopes, synchrotron radiation spectroscopy and projection type x-ray lithography.

A pattern with a high aspect ratio (height/width) can be easily obtained by SR lithography even when the width is in the range of 20-100 nm. This is a very useful advantage from the point of application of synchrotron radiation to fabricate x-ray optical elements.

SR lithography is also applicable to fabricate the electronic devices of the next generation, the physical principles of which are different of those conventional. Conventionally, x-ray lithography means the proximity printing which is a way of pattern fabrication without optical lenses. This is due to the fact that it was difficult to get the x-ray lenses. In the case of fabricating patterns with 20-100 nm range, the projection type x-ray lithography with x-ray imaging elements should be preferable from the point of x-ray lithography as a mass production of future nanometer electronic devices. For this purpose, the optical system using layered synthetic materials (LSM) will be most promising. But, in special cases, zone plates can be also used. Those experiments are interesting because the spatial resolution of zone plates (20-50 nm) is better than the LSM according to the present technology.

From the above points, exposure characteristics of various x-ray resists such as PMMA (poly(methyl methacrylate)), FBM (poly(hexafluorobutyl methacrylate)), CMS (chloromethylated polystyrene) and CPMS (chloromethylated polymethylstylene) were investigated at the beam line BL-8A. The zone plates for synchrotron radiation spectroscopy of undulator radiation was succesfully fabricated by SR lithography and gold plating. The x-ray mask was fabricated by electron beam lithography and reactive ion ething or ion beam etching (1,2).

II) X-ray exposure experiments

The x-ray mask used was the free-standing zone plate with 250 zones, the focal length:200 mm (at the wavelength of 4.5 nm), a minimum zone width:0.97 um and 3 um thick gold. As a filter, 2 um-thick polyimide (Toray SP171) or 2 um-thick SiNx was used to cut off the long wavelength components. The energy of electrons in the ring was 600 MeV or 750 MeV. The energy of 600 MeV was mainly used. At the energy of 600 MeV, in the case of 2 um-thick SiNx, the wavelength range of 0.7-2.0 nm is effective for exposure and in the case of 2 um-thick polyimide the range of 0.7-2.7 and 4.5-8 nm is effective.

In the direct exposure of PMMA and CMS without a mask and a filter, the exposure time was 30 s for PMMA and 1 s for CMS at the beam current of 60 mA. This corresponds to the sensitivity of about 3000 mJ/cm^2 and 100 mJ/cm^2, respectively. Those values are close to the values reported.

For PMMA, the exposure time was 1 m for a 2 um-thick polyimide filter and 8 m for a 2 um-thick SiNx filter.

For FBM, the values were 30 s and 3 s, respectively. Those values are in reasonable agreement with calculated values assuming the absorption coefficient of the filter.

Figure 1 shows an example of the fabricated resit pattern of the above zone plate. From this resist pattern, the gold zone plate was succesfully fabricated by the gold plating. Those zone plates are especially useful for the linear monochromator for spectroscopy by the undulator radiation where the beam profile is nearly circular. The experiments of the linear monochromator is now under progress.

References

1) H.Aritome, H.Aoki, and S.Namba:J.Vac.Sci.Technol. B3 (1985) 265.
2) H.Aritome, K.Nagata, and S.Namba:in "Microcircuit Engineering 85" (K.D.van der Mast and S.Radelaar, Eds., North-Holland, 1985) p.459.

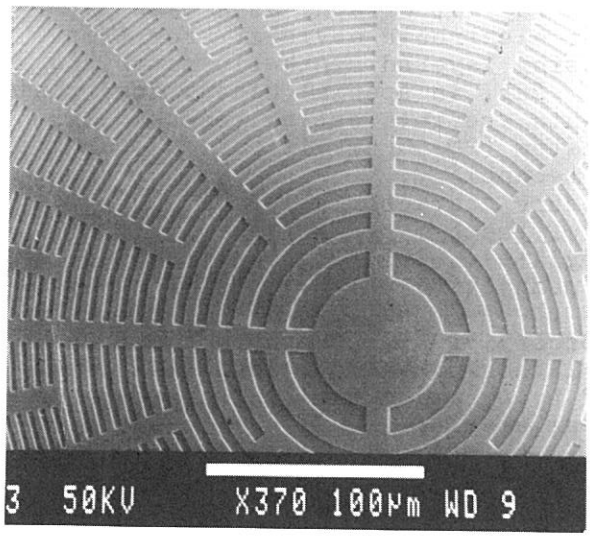

Fig. 1
PMMA resist pattern of a zone plate.

X-RAY VACUUM LITHOGRAPHY

Masaru HORI, Hitomi YAMADA, Takashi YONEDA*, Shinzo MORITA* and Shuzo HATTORI

Department of Electronics, Nagoya University, Chikusaku, Nagoya 464
*Department of Electrical Engineering, Meijo University, Tenpakuku, Nagoya 468

Synchrotron radiation (SR) was successfully applied to vacuum lithography with using plasma polymerizedd resist and plasma development, as shown in Fig. 1. Plasma polymerized methyl methacrylate (PPMMA) and the plasma copolymerized methyl methacrylate with tetramethyltin (TMT), SF_6, I_2 or styrene were prepared by using an inductively coupled gas flow type reactor. The polymer structures of these resists were investigasted by ESCA. ESCA results showed that a small amount of S, F, Sn and I were incorporated into the polymer matrix.

The plasma polymerized resists were exposed to SR under the conditions of 600 MeV and a current of 30 mA directly or through an X-ray mask made of polyimide menbrane and Ta absorbent in a vacuum chamber. SR irradiated resists showed the self development phenomenon. The self developed resists depth by SR exposure without the mask was measured as a function of exposure duration. The results are shown in Fig. 2. It was found that the removed thickness of all resists increased linearly with increasing dose in the low doses region, while it was saturated completely at the high doses region. The self development was enhanced significantly by doping Sn, S and I. In order to confirm the fine pattern fabrication by this method, duplication of mask pattern was examined on the PP(MMA+TMT) resist. The mask pattern of linres and spaces with 1 um width was replicated faithfully on the resists.

The hollowed patterns by self developmenbt were served to O_2 plasma etching in the apparatus with parallel plate electrodes at a gas pressure of 0.5 Pa and a discharged power of 50 W. The results of plasma etching on PPMMA exposed to SR is shown in Fig. 3. The enhancement of differential thickness was observed on the film exposed for 10 min that the self development characteristic altered from increasing to saturating at the duration in Fig. 2. However, the differential thickness decreased with increasing etching duration on exposed 30 min, that the self development was completely saturated at the duration as shown in Fig. 2.

In order to investigate the reaction mechanism of above mentioned self development and plasma development characteristics, IR and ESCA were performed on the same film before and after SR exposure. Also the gas fragments generated from the resists during SR exposure were detected by mass spectroscopy.

From these analyses , it was concluded that PPMMA and its plasma copolymerized resists undergo the elimination of ester structure as the primary degrading reaction by SR exposure and at high doses, the recombination of the dissociated groups have been proceeding, resulting in resist carbonization involving C=C bond,

which was hard enough to withstand the furthermore SR exposure and also retarded the etching rate for oxygen plasma.

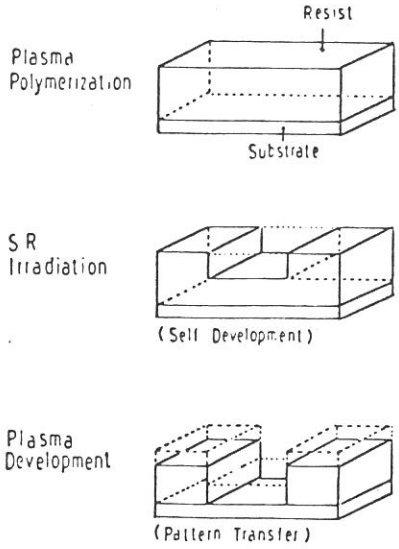

Fig. 1 Process steps

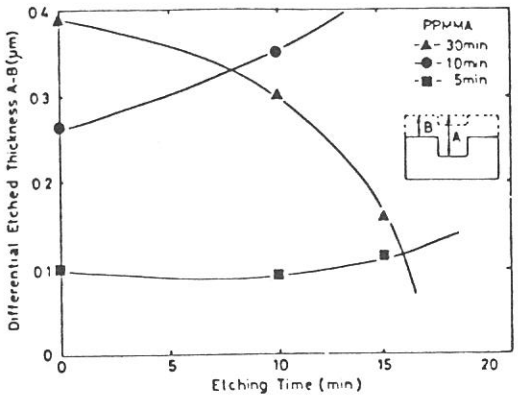

Fig. 3 Plasma etching characteristic in PPMMA.

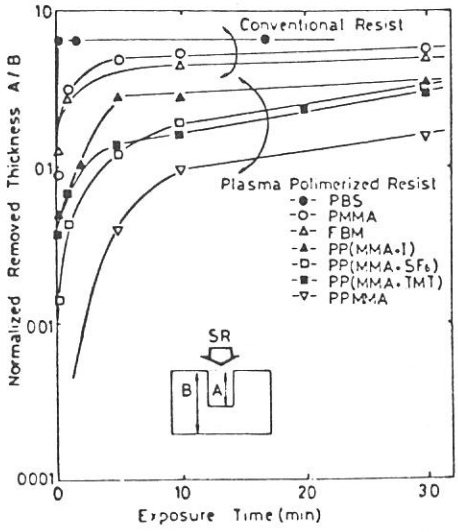

Fig. 2 Self development characteristics.

X-RAY TOPOGRAPHIC STUDY OF *p*-CHLOROBENZAMIDE SINGLE CRYSTAL

Masahiro MORI, Tokuo MATSUKAWA, Masayoshi OBASHI, Takatoshi MURATA*, Shun-ichi NAOE** and Yasuo NISHIHATA***

College of General Education, Osaka University, Toyonaka, Osaka 560
*Kyoto University of Education, Kyoto 612
**College of Liberal Arts, Kanazawa University, Kanazawa, Ishikawa 920
***Department of Physics, Kwansei-Gakuin University, Nishinomiya, Hyogo 662

Introduction

Synchrotron radiation light source has very good directionality. Recently, x-ray topography technique develops rapidly using this character of the synchrotron radiation. It is interesting to apply this technique to the phase transition phenomena (reference 1). It is probable that superlattice reflections are more influenced by the phase transition than the main Bragg reflections, as they only appear under the transition temperature. Our aim is the study of the difference between both refrections.

This experiment is the first step of this aim. At first, we have to take into consideration that the shortest wavelength is 9Å when UVSOR operates at 600MeV and 100mA.

Experimental

Triclinic *p*-chlorobenzamide was chosen for the sample. The transition temperature of this sample is about 40°C. Crystal data are a=15.027, b=5.481, c=14.486, α=97.84, β=111.99, and γ=95.17 from reference 2. Crystals obtained from an ethanol solution had a shape elongated along b axis. The typical size of these samples is about 10x40x3 mm^3. It has previously been ascertained that they are triclinic structures with photographic methods. The other main aim of this time experiment is the estimation of the practical intensitiy of UVSOR.

We took the diffraction photographs putting white synchrotron radiation beam on the single crystal with Back Laue Photographic method. X-ray films were covered with 15μm-thick aluminium foil to be prevented from visible light. The experiment was done as follow conditions:

synchrotron energy	600MeV
synchrotron current	80mA
exposed time	6.0minutes
observed diffraction angles	from 110° to 172°
slit	full open
temperature	room temperature

Results and discussions

Superlattice reflections could not be ascertained as these intensities are not strong. Four Bragg spots were observed on x-ray films. The figure is the picture of one of them at about 168 diffraction angles. The outlook of defects is reflected in such a kind of photograph. But this figure is too complicated to understand it. It is seemed that this shows the behavior

of crystal growth in an ethanol solution. Further discussions can not be done to see it of such complicated materials. It is necessary to do such a kind of experiment to choose and use more simple crystals. It is more important to use shorter wavelength x-ray source. In the case that synchrotron operates at 750 MeV, the shortest wavelength is 5Å. When the wiggler apparatus operates, it is only 2Å.

References

1) S. Suzuki, H.Kawata and M. Ando ; Photon Factory Activity Report 1983/84 page VI-135
2) T. Taniguchi, K. Nakata, Y. Takaki and K. Sakurai ; Acta Cryst. B34 (1978) 2574

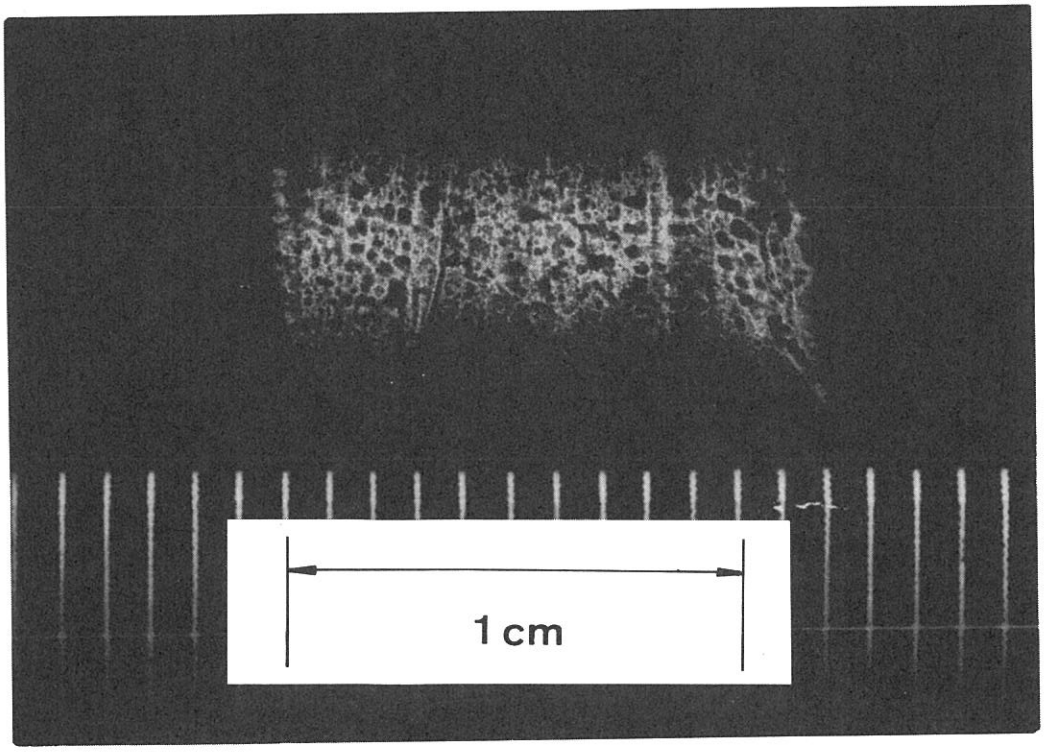

APPENDIX

ORGANIZATION

Staff

Director	Hiroo INOKUCHI	Professor
Light Source Group		
	Toshio KASUGA	Associate Professor
	Hiroto YONEHARA	Research Associate
	Toshio KINOSHITA	Engineer
	Masami HASUMOTO	Engineer
Measurement Systems Group		
	Makoto WATANABE	Associate Professor
	Kazutoshi FUKUI	Research Associate
	Kusuo SAKAI	Section Chief Engineer
	Osamu MATSUDO	Unit Chief Engineer
	Jun-ichiro YAMAZAKI	Engineer
	Eiken NAKAMURA	Engineer
Secretary	Takayo OHTE	
Guest Scientists		
	Katsumi YOSHIDA	Adjunct Associate Professor from Univ. of Tokyo (April 1980 - March 1981)
	Motohiro KIHARA	Adjunct Professor from National Lab. High Enegy Phys. (April 1981 - March 1983)
	Takatoshi MURATA	Adjunct Associate Professor from Kyoto Univ. of Education (May 1982 - March 1984)
	Hideyuki NAKAGAWA	Adjunct Associate Professor from Fukui Univ. (April 1984 - March 1986)
	Godfrey SAXON	Foreign Visiting Professor from Daresbury Lab. (October 1983 - March 1984)
	Kaizo NAKAMURA	Visiting Scientist from Kyoto Univ., JSPS (April 1985 - March 1986)
	Teruo HOSOKAWA	Visiting Research Fellow from NTT (April 1985 -)

Representative of Beam Lines

BL2A	Kosuke SHOBATAKE	Dept. Molecular Assemblies
BL2B2	Katsumi KIMURA	Dept. Molecular Assemblies
BL3B	Inosuke KOYANO	Dept. Molecular Assemblies
BL8B2	Hiroo INOKUCHI	UVSOR and Dept. Molecular Assemblies
Others	Makoto WATANABE	UVSOR

Steering Committee (June 1984 - May 1986)

Hiroo INOKUCHI	IMS	Chairman
Toshio KASUGA	IMS	
Katsumi KIMURA	IMS	
Nobuyuki NISHI	IMS	
Kosuke SHOBATAKE	IMS	
Yasuo UDAGAWA	IMS	
Makoto WATANABE	IMS	
Hideyuki NAKAGAWA	IMS and Fukui Univ.	
Takehiko ISHII	Univ. of Tokyo	
Kozo KUCHITSU	Univ. of Tokyo	
Takeshi NAMIOKA	Tohoku Univ.	
Takanori OSHIO	Ashiya Univ.	
Shunsuke OHTANI	Nagoya Univ.	
Taizo SASAKI	Osaka Univ.	
Tadamasa SHIDA	Kyoto Univ.	

LIST OF PUBLICATIONS (1981-1985)

1) "Design of UVSOR Light Source"
M.Watanabe, A. Uchida, O. Matsudo, K. Sakai, K. Takami, T. Katayama, K. Yoshida and M. Kihara : IEEE Trans. Nucl. Sci. NS-28, (1981) 3175.

2) "The UVSOR Facility at IMS"
I. Koyano, Y. Achiba, H. Inokuchi, E. Ishiguro, R. Kato, K. Kimura, K. Seki, K. Shobatake, K. Tabayashi, Y. Takagi, K. Tanaka, A. Uchida and M. Watanabe : Nucl. Instr. Meth. 195 (1982) 273.

3) "Ion-Trapping Effect in UVSOR Storage Ring"
T. Kasuga, H. Yonehara, T. Kinoshita and M. Hasumoto: Jpn. J. Appl. Phys. 24 (1985) 1212.

4) "Beam Properties of UVSOR Storage Ring"
T. Kasuga, H. Yonehara, T. Kinoshita and M. Hasumoto: IEEE Trans. Nucl. Sci. NS-32 (1985) 2550.

5) "Present Status of UVSOR"
T. Kasuga, H. Yonehara, T. Kinoshita and M. Hasumoto: IEEE Trans. Nucl. Sci. NS-32 (1985) 3409.

6) "Undulator and Wiggler of UVSOR"
H. Yonehara, T. Kasuga, O. Matsudo, T. Kinoshita, M. Hasumoto, J. Yamazaki, T. Kato and T. Yamakawa: IEEE Trans. Nucl. Sci. NS-32 (1985) 3412.

7) "Emission Spectra SiH ($A^2\Delta \rightarrow X^2\Pi$) and $SiCl_2$ ($\tilde{A}^1B_1 \rightarrow \tilde{X}^1A_1$) in the VUV Photolyses of Silane and Chlorinated Silanes"
N. Washida, Y. Matsumi, T. Hayashi, T. Ibuki, A. Hiraya and K. Shobatake: J. Chem. Phys. 83 (1985) 2769.

8) "Fluorescene from Ion-Pair and Rydberg States of I_2"
R.J. Donovan, B.V.O' Grady, K. Shobatake and A. Hiraya : Chem. Phys. Lett. 122 (1985) 612.

LOCATION

Ultraviolet Synchrotron Orbital Radiation (UVSOR) Facility, Institute for Molecular Science (IMS) is located at Okazaki. Okazaki (population 280,000) is 260 km southwest of Tokyo, and can be reached by train in about 3 hours from Tokyo via New Tokaido Line (Shinkansen) and Meitetsu Line.

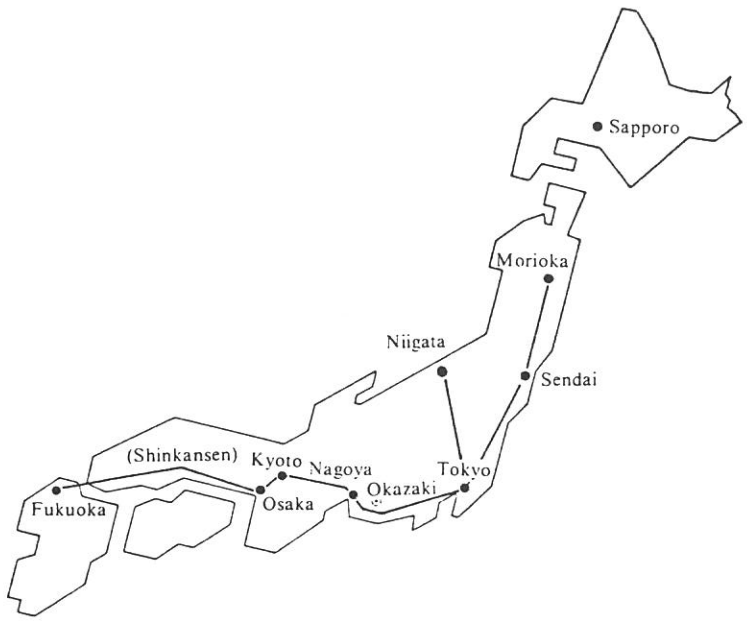

Address is as follows.
UVSOR Facility
Institute for Molecular Science
Myodaiji, Okazaki 444, JAPAN

Telephone : 0564-54-1111(IMS), ex. 400-409 (UVSOR)
Fax : 0564-52-9649 (IMS)
Telex : 4537475 KOKKEN J (IMS)